AUTOMATION OF A THREAD ROLLING MACHINE FOR USE IN A FLEXIBLE WORKCELL

A Thesis
Presented to
The Academic Faculty

By

Matthew Wagner

In Partial Fulfillment
Of the Requirements for the Degree
Master of Science in Mechanical Engineering

Georgia Institute of Technology

August, 2007

AUTOMATION OF A THREAD ROLLING MACHINE FOR USE IN A FLEXIBLE WORKCELL

Approved by:

Dr. Shreyes Melkote, Advisor
School of Mechanical Engineering
Georgia Institute of Technology

Dr. Steven Danyluk
School of Mechanical Engineering
Georgia Institute of Technology

Dr. Steve Dickerson
Professor Emeritus
School of Mechanical Engineering
Georgia Institute of Technology

Date Approved: July 6, 2007

ACKNOWLEDGEMENTS

I would like to take this opportunity to thank a number of persons who made this thesis and project possible. First, my advisor Dr. Shreyes Melkote, provided unwavering support, through many changes in this project's focus. His constant guidance and encouragement provided direction and mentorship for which I am grateful. My sincere thanks also go to John Morehouse for his contractual work and negotiation that made this project a reality.

I also thank Alcoa Fastening Systems for funding this project and providing me with this tremendous opportunity. Special thanks go to Curtis Lea, Luke Haylock and Martin Ryan for supporting this project. Also, I thank everyone at Alcoa Fastening Systems City of Industry whom which I had the pleasure of working.

My most sincere gratitude goes to Dr. Steve Dickerson and the staff at CAMotion robotics. Their trust in me as a designer and adopted employee took this project from drawing board to reality, and provided me with an incredible learning opportunity.

Finally I thank my family for their constant support throughout this process. My mother Barbara provided countless words of encouragement when I needed them, her constant support made the impossible seem possible. My father Eugene provided me with the skills to solve countless design problems through many late nights in our garage, and participated in many design discussions via telephone when I needed the opinion of a fellow "hot rodder".

TABLE OF CONTENTS

LIST OF TABLES

LIST OF FIGURES

LIST OF SYMBOLS

t_{batch}	time to process a batch of parts
n_{parts}	number of parts in a batch
t_{slow}	slowest cycle time in the overall process
$t_{part,avg}$	average time to produce one part
$t_{inprocess}$	time a piece or batch spends in production
$t_{cycle,n}$	cycle time of process n
t_{move}	time to complete an end effector move
d_{move}	length of an end effector move
v_{max}	maximum end effector velocity
a_{move}	end effector acceleration / deceleration
α	part angular error in 2-D analysis
h	part head height in 2-D analysis
d	part head diameter in 2-D analysis
l_x / l_y	moment lengths for 2-D analysis
d_g	gripper opening distance
R_g	gripper face radius
$x_c / y_c / z_c$	potential contact point on gripping face
$x_p / y_p / z_p$	discrete point in contact with gripping face
o_x / o_y	X/Y part offset in gripper

SUMMARY

Aerospace fastener production contains many machining and forming operations, such as heading, centerless grinding and thread rolling. Typically many of these processes have been hand fed, especially for large diameter parts. This thesis presents a general automation plan, based on the concept of a workcell, by which large diameter fastener production processes can be automated. Specifically, an automatic loading and unloading system for a thread rolling machine is developed and prototyped to prove the overall workcell concept.

The workcell plan developed is based on a workpiece-rack style transport method, which is shown to be an effective means of transporting fasteners in a fully oriented state throughout the production process. The transport method designed also eliminates problems associated with part-to-part contact during transport, which is often a concern for large diameter workpieces subject to stringent quality control.

With respect to the overall plan developed, an automatic part loading and unloading system is developed for a thread rolling process. Within this system design a universal fastener gripping system is developed, which has potential application to any process in which headed parts need to be grasped. The gripping system is designed to accommodate a large range of fastener sizes and styles with a minimum of tooling changeover.

In order to predict the performance of the proposed gripper design, a unique grasping model is developed. The concept of an error boundary is introduced as a metric

for predicting the error tolerance of a gripping system. The model results are verified by testing the prototyped gripping system's error tolerance under a number of conditions.

The automation system is prototyped and assembled, and shown to be a viable means of loading and unloading large diameter parts to a thread rolling machine. The grasping system is also tested with a full range of fastener styles and sizes, and shown to produce a stable grasp on all parts considered. The gripping fingers are also shown to be resilient to contact degradation after repeated grasps of sharp edged parts.

CHAPTER 1
INTRODUCTION

In today's competitive global economy, manufacturers are experiencing more pressure than ever to automate their production processes. As a result, designers of automation systems face many challenges during system development, some with far reaching consequences that may not initially be realized. The aim of this thesis is to evaluate these design decisions and present them in a general way which can be applied to other systems and applications. Specifically this thesis addresses the design of an automatic loading and unloading system for a thread rolling machine, used in producing aerospace fasteners. A typical fastener can be seen in Figure 1.1.

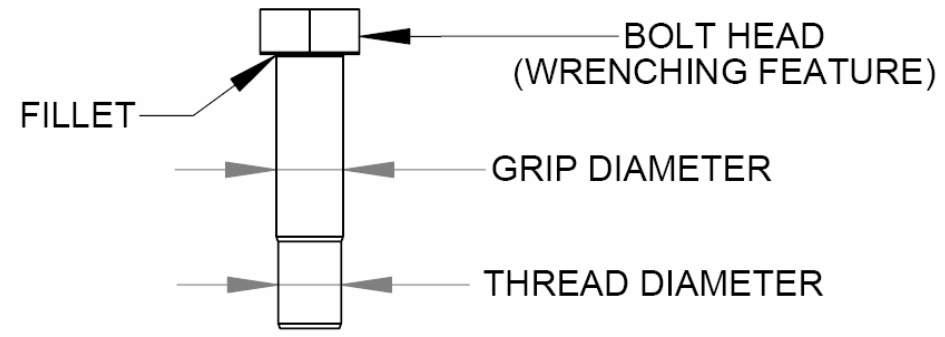

Figure 1.1 Typical aerospace fastener

The design of any automation system should begin on the macro scale. Issues such as the system's role in the overall manufacturing process and material flow through

the plant should be addressed before considering any specific mechanical designs. In this specific case, it is desired to use the concept of a workcell to plan the overall process in an effort to maximize productivity and minimize costs. Evaluating design concepts such as these need not be arbitrary. Tools such as discrete time analysis will be shown to be useful in evaluating proposed ideas.

Moving inward toward the micro scale, each machine in the process should be automated with respect to the overall plan. Prior to developing any mechanical designs, the timing of each individual process should be optimized. The thread rolling process is selected in this thesis, and timing issues within the thread rolling process are addressed before mechanical design begins by modifying the associated induction heating process. This planning maximizes productivity and simplifies the mechanical design to follow.

Finally, the micro scale of detailed component design can be addressed. It is this phase of design which requires analysis and performance prediction, which can be accomplished by a number of approaches. Often existing methods are suitable to predict the performance of the system, such as simple kinematic timing analysis or finite element analysis. However, the designer must sometimes develop new methods to predict component performance by creatively combining existing fundamental methods. In this thesis it is desired to predict the performance of a qualitatively designed robotic end effector used in an automatic part loading system for a thread rolling machine, which is accomplished by developing a new method of grasp analysis. This grasping analysis offers a fresh perspective to existing methods in that it is practical rather than theoretical, and its direct benefit to the design of the automation system at hand shown.

1.1 Background

Aerospace fastener manufacturers have historically hand fed many fastener forming and machining processes, especially with large diameter workpieces. Trends in manufacturing toward more highly automated processes are leading many facilities toward automatic machine loading and unloading. This trend is a direct result of increasing competition requiring more productivity while simultaneously reducing operating costs. Also, ever tightening safety regulations are limiting the extent to which operators can hand feed parts to potentially hazardous processes. It is desirable for manufacturers to remain ahead of the curve on safety, such that new regulations do not result in costly downtime.

The concept of a workcell has long been used as a blueprint for machine automation. It was desired to establish an overall standard by which all machines in a fastener manufacturing facility could be automated, such that the overall process would function as efficiently as its individual parts. Many practicalities need to be considered in development of this plan, such as ease of changeover between batches, effect of machine downtime on production, and ease of implementation into the facility.

Upon development of a workcell plan, it was desired to automate one machine to prove the overall concept. Thread rolling is common process for producing threads on fasteners, it is superior to thread cutting and used in production of almost all externally threaded fasteners (Kalpakjian and Schmid 2003). Many large size thread rolling operations are hand fed, thus the thread rolling process was selected to prove the automation concept.

On a general level, many situations arise where fasteners must be handled by an end effector. A universal gripping system which can easily accommodate various fastener head styles and sizes is essential to the development of this project, but also easily applicable to future automation projects.

1.2 Problem Statement

The objective of this thesis is to develop an automated part loading and unloading system for a typical fastener manufacturing thread rolling process. First, a workcell automation plan which will serve as a blueprint for this and future automation projects. Second, mechanical design of an automatic loading system for a thread rolling machine is to be developed with respect to the workcell plan. Within development of the thread rolling automation system, a universal gripping system is to be developed which can grasp a variety of part styles and sizes typical to this thread rolling process. Modeling techniques are desired to predict the gripper's performance and error tolerance, and the results of this model are to be used to verify the functionality of the automation system proposed. The objectives of this research are summarized as follows:

1. Develop a broad scale automation plan for aerospace fastener production. This plan should consist of a set of standards by which existing and future machines can be automated, and should be based on the concept of a workcell.

2. Prove the concept developed in step 1 by automating the loading and unloading of parts from a thread rolling process with respect to the broad scale workcell plan.
3. Within the development of the thread rolling automation system, develop a universal gripping system which can be used to grasp a wide variety of fastener styles and sizes.
4. Predict the performance of the error tolerance of the developed gripping system by using models based on fundamental engineering principles.
5. Prototype and test both the automation system and gripping system, comparing expected results with experimental data.

1.3 Motivation

On a general level, this thesis aims to address a number of issues. Clearly, the design of this automation system will benefit the production process in which it is implemented, in terms of both productivity and operator safety. However, many concepts and analyses will be presented in a general manner such that application to other areas is easily achieved.

The workcell development will lead to prototyping of a part transport system, which can be used in any facility fasteners are produced. The assumptions used to develop the workcell plan will show, based on production needs, what level of automation is appropriate for a certain application.

The design of the automation system will facilitate the development of a universal fastener gripping system, which can be used in any application where fasteners are handled automatically. Research in literature and contact with industry showed that very little information is available regarding grasping headed fasteners, although the problem is very common.

Lastly, this thesis will present a new approach to grasp modeling. While a majority of the work in grasping and automated fixture planning is theoretical rather than applied, this model is developed with the machine design engineer in mind. The direct application to this case will be shown, and the model will be developed in a general way which facilitates adaptation to other grasping cases.

1.4 Outline

The general structure of the thesis is as follows. Chapter 2 presents a review of literature relevant to thread rolling, fastener feeding methods, and research in the areas of grasping and part orienting. Chapter 3 analyzes the production needs at a typical aerospace fastener manufacturing facility and develops a workcell automation plan, and also develops a novel method for transporting parts within the workcell. Chapter 4 follows the mechanical design of the automatic loading system for the thread rolling machine and associated part grasping system. The loading system is designed to utilize the part transport method developed in the Chapter 3. Chapter 5 models the fastener grasping process and aims to predict what types of errors the proposed gripping system

can tolerate. Chapter 6 compares the result of the grasping model to experimental data recorded, and Chapter 7 reviews results of the prototyped automation system's testing.

CHAPTER 2
LITERATURE REVIEW

Since much of this thesis will deal with automation of a thread rolling machine, the rolling process itself needs to be understood. Also, prior to developing any specific mechanical designs, a survey of current thread rolling technology is conducted. Automated thread rolling is quite common, and this chapter provides an overview of a few systems of this nature. Recent advances in thread rolling machine development are also discussed, including different styles of rolling machines and developments in process monitoring technology. Since the latter portion of this thesis deals with development of a gripping model, a survey of research in the area of robotic grasping is presented. Much work has been performed in the areas of grasping and fixturing, with the majority of efforts concerned with automated grasp / fixture planning. This chapter will first provide a general overview of the thread rolling process, and secondly survey technologies available in the thread rolling industry. The state of the art in fastener handling in automated processes will be examined. Lastly, an overview of research in the areas of grasping and parts orienting will be presented.

2.1 The Thread Rolling Process

Thread rolling is a commonly used manufacturing process for threading round workpieces, illustrated in Figure 2.1. It is by nature a forming process, thus no material is removed during threading of the blank. Production rates can be high, approaching 8

pieces per second for smaller diameter parts, with slower cycle times for large diameter pieces (Kalpakjian and Schmid 2003).

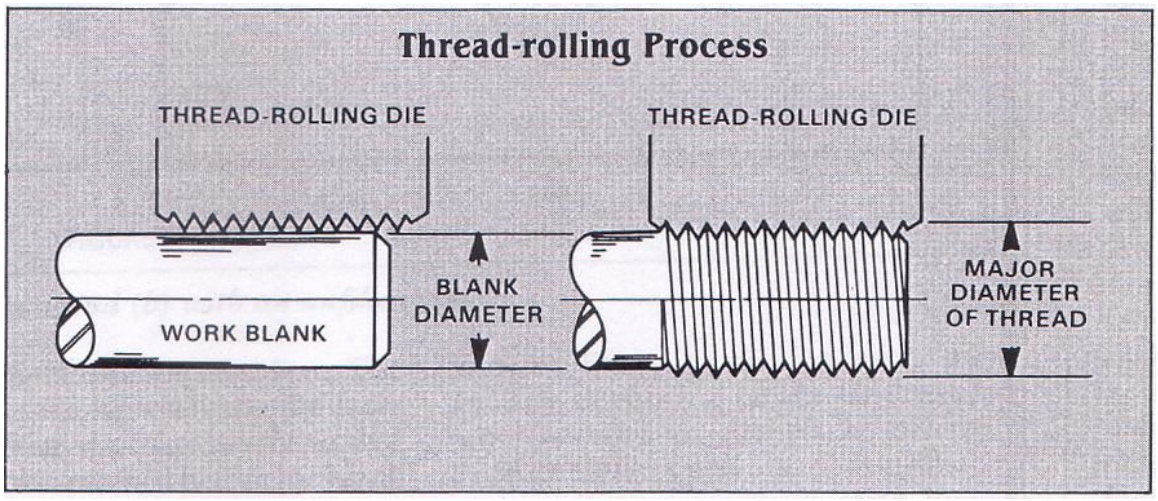

Figure 2.1 Typical thread rolling process (Anon 1987)

Multiple styles of machines are available, with the differences resulting from the types of dies and die motion used. The underlying process is the same for all machines; a blank is passed through moving dies, and the thread shaped dies progressively intrude on the workpiece to be formed. Flat die rolling is common, especially in smaller diameter fasteners, shown in Figure 2.2. In this process, the blank is rolled across the face of a stationary die with a reciprocating opposing die. Cylindrical die thread rolling is also used, shown in Figure 2.3. In this process two or three rotating cylindrical dies are fed into a centrally located part (Anon 1987). Planetary die thread rolling is becoming more common, this system resembles a planetary gear in its configuration. A central round

rotating die is analogous to the sun gear, and parts rolled around it periphery resemble the planet gears, illustrated in Figure 2.4. An outer fixed concave die is similar to the ring gear. The output of a planetary machine can be as much as two times higher than that of a flat die machine (Wiesenfeld 1998).

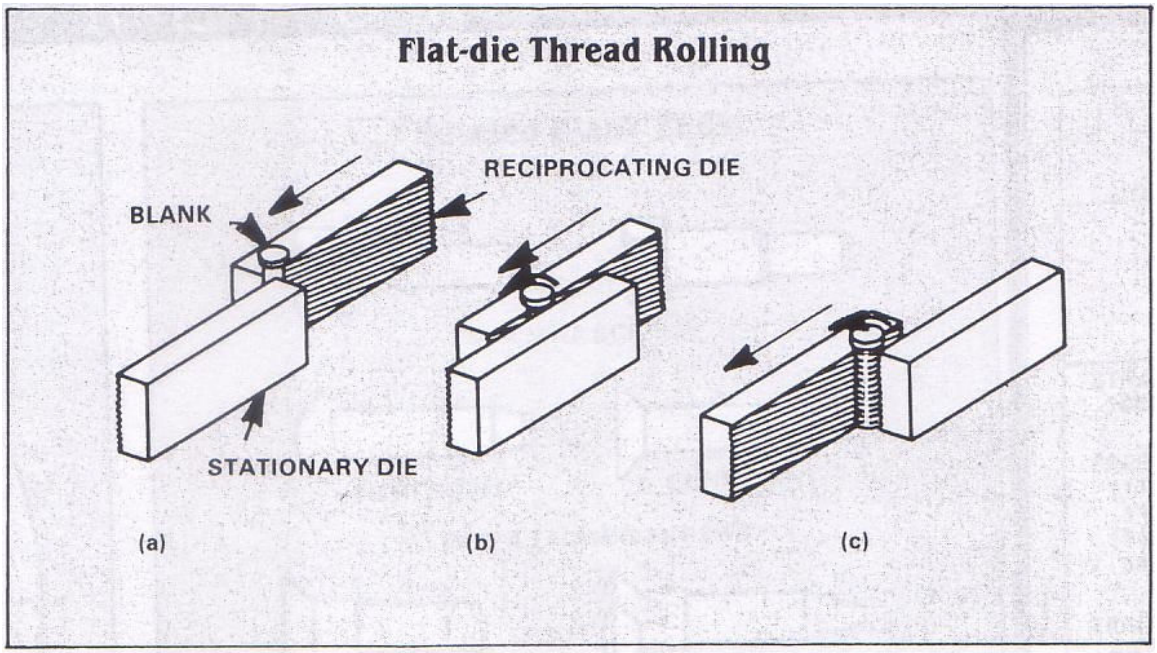

Flat-die thread-rolling process: (a) start of thread-rolling cycle, (b) relation of dies after completing half of stroke, and (c) completion of thread-rolling stroke.

Figure 2.2 Flat die thread rolling process (Anon 1987)

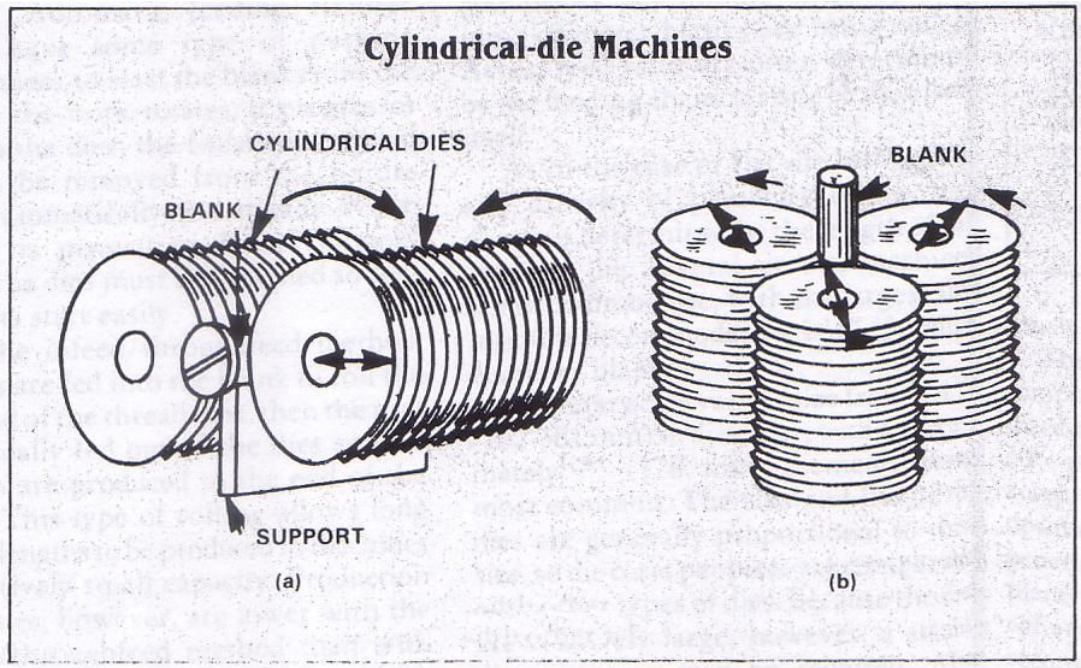

Types of cylindrical-die thread-rolling machines: (a) two die and (b) three die.

Figure 2.3 Cylindrical die thread rolling process (Anon 1987)

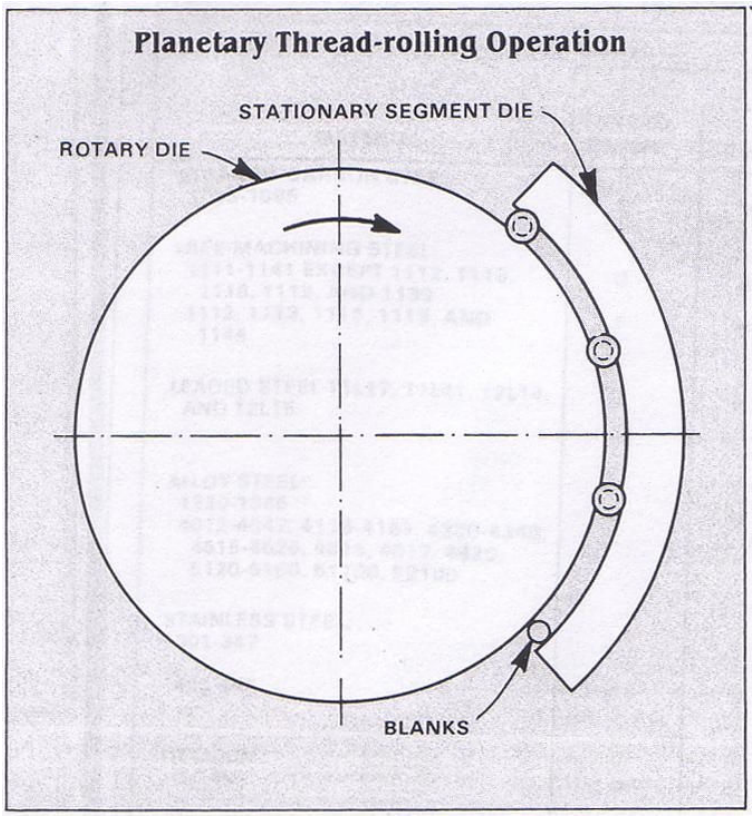

Figure 2.4 Planetary die thread rolling process (Anon 1987)

An important note is that the fastener rotates during thread forming, regardless of the style of machine used. The number of rotations the workpiece makes during threading depends on the die size and also the diameter of the threads, 5 to 10 revolutions is common. Usually more revolutions are used in harder materials, to achieve a more gradual material penetration rate (Anon 1987).

Thread rolling has numerous benefits over thread cutting. Since no material is removed, forming is a more efficient process, provided the blanks are formed to near net shape early in the manufacturing process. Superior surface finish is also possible with rolling, and is much more controllable than if threads were cut. Lastly, rather than cut threads across the grain flow of the material, rolled threads have a grain structure which follows the thread profile. This grain structure, coupled with residual stresses imparted on the surface by rolling, result in a superior product. Rolling is used to produce virtually all externally threaded fasteners (Kalpakjian and Schmid 2003).

Fasteners made of high hardness materials are commonly rolled warm. The blanks are heated to a temperature less than the tempering temperature, usually by means of an induction heating process. Use of this lower than tempering temperature allows the compressive stresses induced by the process to be maintained, thus improving fatigue strength (Anon 1987). All of the fasteners under consideration in this thesis will be rolled warm, heated by means of an induction heater.

2.2 Trends in Thread Rolling Equipment

Modern developments in thread rolling technology include the addition of process monitoring equipment to existing machines. One such system assists the operator during setup, providing information which assists in synchronizing thread alignment between the dies. This allows even an inexperienced operator to achieve an acceptable setup in a short amount of time (Saliger 2006).

Other process monitoring systems monitor the die force produced during the rolling process, and can be useful to the operator in multiple respects. A roll force monitoring system can "learn" what a typical force profile looks like while rolling a properly formed part, and compare real time data to this known curve. If the real time curve exceeds an acceptable error band, parts can be automatically rejected to a scrap bin without stopping the process. Analysis of roll force data at the end of a shift can quickly tell the operator if the dies have been chipped or damaged during the workday (Kopka and Schwer 2003).

Typically before thread rolling, bolts experience a number of operations such as head forming and chamfering. One trend in the development of thread forming machines is to combine as many operations as possible into one system. This could involve a small arrangement of machines with a central part transfer system, similar to a workcell (Eranov and Obukhova 1986). Another approach is to combine multiple operations into one machine, sometimes called a bolt-maker. Machines are available that can cut off slugs, head the slugs, then chamfer and thread roll the part in an effort to reduce work in progress and labor costs (Wiesenfeld 2000).

2.3 Fastener Feeding Technology

In both the manufacture and installation of fasteners, automatically orienting and transporting parts is critical for efficient process operation. The traditional approach to parts handling has been to present parts to each process in a random state, then to orient them by means of a parts feeder. The most versatile and well known feeder of this type is the vibratory bowl feeder, shown in Figure 2.5. Parts placed in a central bowl are made to climb an outer helical track by vibrating the base of the bowl. Features along this track orient the parts, or alternately reject them into the bowl if they are not in the desired state (Boothroyd 1992).

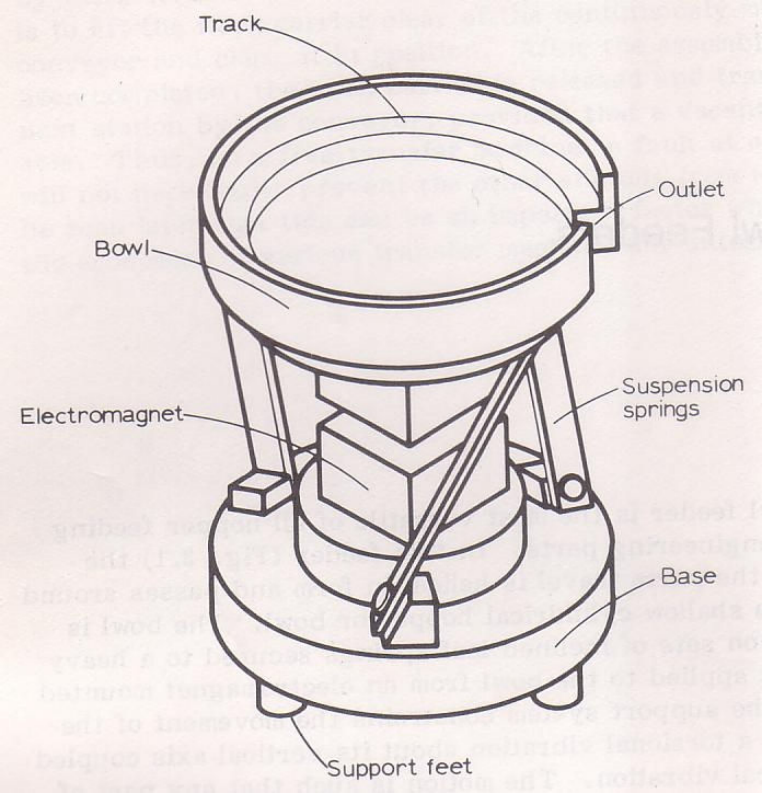

Figure 2.5 Vibratory bowl feeder (Boothroyd 1992)

Despite the vibratory bowl's widespread use, it can be a problematic system. Certain parts can be prone to jamming, and any contaminants on the parts can further complicate this problem (Stancik and Boad 1999). Other methods to feed parts online at a machine tool exist, each with its own strengths and weaknesses. The centerboard hopper feeder, magnetic disc feeder and centrifugal hopper feeder are a few examples, there are many more devices that can be selected based on the type of parts being fed (Boothroyd 1992). These systems are not immune from feeding problems either. In a general sense, fastener feeding jams can idle production machines for as much as 10 minutes for each hour of production (Endres 1998).

A recent trend in automated fastener feeding is to orient the fasteners off-line from the manufacturing process. The oriented parts are then stored in an oriented state in a magazine or cassette, which is presented to the manufacturing process. This completely decouples the feeding process from the manufacturing process. An example of a magazine which uses a coiled tube design is shown in Figure 2.6. Since the magazine or cassette contains pre-oriented fasteners of a known part number, confidence that the correct part can be delivered on demand is greatly increased (Bornes and LeCann 2000). Systems have also been developed that store multiple types of fasteners in one specialized drum. This system can deliver any fastener in storage on demand (Alcombright and Bedwell 1999). The commonality of all of these systems is that they transport parts in an oriented rather than random state, eliminating the need for an orienting system at the machine.

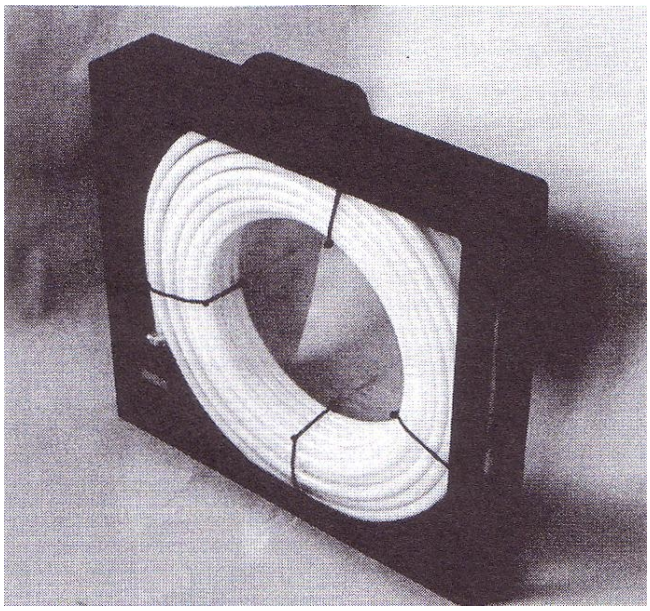

Figure 2.6 Coiled tube magazine storage system

2.4 Overview of Research in Grasping

Much research has been done in the area of robotic grasping and contact. Bicci and Kumar (2000) present an overview of work in the field, presenting a concise summary of a number of areas.

Research in closure properties of grasps aims to define if a rigid body is completely constrained given a certain number of contacts. Within this field, force closure is defined as complete restraint of the body which can resist any external combination of forces, form closure is defined as force close with frictionless contacts. Work in the area of force analysis evaluates what internal forces are necessary in a grasp to prevent motion or slippage. Contact modeling is concerned with the actual gripper-to-part interface, and aims to develop appropriate contact models to represent various physical situations. Efforts in the area of grasp performance assign quantitative measures

to the performance of different grasps. Finally, work in the area of grasp dynamics examines the articulations which are involved in grasping an object.

2.4.1 Optimum Grasps and Grasp Quality

Specific work in the area of grasping which closely resembles this thesis were examined further. The first area of interest was optimum grasp planning, in which algorithms have been developed to automatically determine the best possible mode of gripping a given object. Mirtich and Canny (1994) formulate a grasp algorithm under the assumption of rounded fingertips and contacts with friction, assumptions very applicable in practice. They optimize grasp quality by maximizing the ratio of external wrench applied to finger force developed, since it is desirable to resist an applied force to the part with finger forces as small as possible. The algorithm computes grasps which appear to be optimal by intuition, however they assume there are no space constraints on where the part can be grasped.

Bolvin and Sharf (2004) address the problem of the constraint of gripper geometry. Their work acknowledges the fact that most gripping systems are limited in the direction that forces can be applied, and that only a certain range of motion may be possible. A two dimensional method is discussed, and grasp optimality is based on finger extension and distance from the line of action to the object centroid. While the results are favorable, the method is acknowledged to be somewhat complex for real time implementation.

This concept is developed further by Morales et al. (2006) in which a vision system is used to plan real time grasps. The issue of constrained hand geometry is included in this analysis as well. The system developed is capable of planning a grasp for an object based on only an acquired image, making it very practical for automated vision based applications. Grasps are planned using a grasp region approach, where the contour of the object is discretized into regions of potential grasping.

Montana (1992) focuses specifically on the issue of grasp stability for two fingered grasps. He identifies six factors that affect grasp stability: local object geometry, local finger geometry, distance between points of contact, finger and object viscoelasticity, applied normal force and object mass. The concept of manipulability is also developed, in which the ease of changing a grasp to a new arbitrary configuration is evaluated. It is also shown that contact grasp stability, the tendency of points of contact to return to their original locations in response to a disturbance, is necessary for full understanding of grasp stability.

The issue of manipulation is further addressed by Harada and Kaneko (2002). The case of an enveloping grasp, such as that applied by a robotic hand, is specifically examined. Parts of the grasp are assigned to either a position controlled chain (the fixed surface), or a torque controlled chain (the fingers of the end effector). Conditions which permit manipulability for a specific object are developed from these assumptions.

2.4.2 Gripper jaw design

Much attention has been given to the shape of the gripper jaws themselves. These efforts aim to design the best possible jaw shape for a given part to be grasped. Zhang and Goldberg (2002; 2001) address this problem, using an extruded *n*-sided polygon as the part to be grasped. They assume a 2-jaw parallel gripper design, and the analysis breaks the grasping process into three phases: pushing, toppling and fixturing. Their early work finds the optimum points of contact on the workpiece, while subsequent work is based on the idea of "trapezoidal modules". These trapezoidal modules are easily machineable shapes which are affixed to the gripper jaws and interact with the workpiece. An algorithm is used to optimize the contact points or jaw shape for each phase of grasping, and the final result is a systematic method of jaw design. The only shortcoming of this analysis is that it assumes ample space on all sides of the workpiece to be grasped, a situation not always present in reality.

Zhang, Cheung and Goldberg (2001) further extend the previous analysis to account for shape uncertainty in the part to be grasped. A tolerance class is proposed which predicts a jaw design's performance in light of uncertainty in part shape. This tolerance class is based on maximal and minimal values of acceptable jaw shape.

Cutkosky and Wright (1986) specifically develop methods used to model jaw to workpiece interaction. Their work compares several models of finger to workpiece contact conditions and evaluates their overall contribution to the grasp strength. Scenarios examined include pointed, curved, flat, soft and soft curved fingertips. It is found that a compliant fingertip can produce a more controllable grasp with less gripping force, however Coulomb's law will not provide an accurate approximation of grasping

forces under these conditions. A shearing model with a maximum shear stress is chosen to more accurately model the compliant finger.

2.4.3 Part orienting by pushing

One possible method of orienting a part during or prior to grasping is by pushing. Mason (1986) provides derivation of the fundamental mechanics of a pushing operation. He assumes a rigid object in motion on the horizontal plane, with a single point of contact to a pusher. Support forces are assumed to obey Coulomb's law, however the locations and magnitudes of the support forces are assumed to be indeterminate. Inertial forces are also assumed to be negligible. It is found that the problem of predicting the motion of the object is indeterminate, but the direction of rotation can easily be found.

Akella and Mason (1995) expand on the pushing concept, and develop methodology to orient a part in an unknown state by a number of pushing operations. A radius function, which gives the distance from a point on the part to the pushing wall, is used to determine the part's orientation. Analysis determines how many pushing operations are needed to orient the part, and means are presented to develop a plan for the orientation operations. Methodology is also discussed as to where the sensing point should be placed on the object.

2.4.4 Fixture planning

Although not directly related to the problem of grasping, work in the area of fixture planning has led to interesting techniques and results worth noting for the development of this thesis. Automated fixture planning is concerned with adaptable workpiece holding techniques for use in manufacturing processes. Although the problem statement is different from that of grasping, the desired result to hold the part securely in the presence of external forces is the same. A large body of work exists concerning fixture planning, however for brevity only the works concerning developments in this thesis are presented here.

Asada and By (1985) present methodology in which an adaptable fixturing system can be automatically configured. A robot reconfigures the fixture layout given the input of a part geometry to be constrained. Accessibility and detachability measures ensure the part can be inserted and removed from the fixture developed. This type of work is typical of efforts seen in automated fixture planning.

Lee and Cutkosky (1991) present analysis which is of more interest to this thesis. Their analysis predicts, under a given set of constraints with friction, what combination of forces can be applied without moving the workpiece undesirably. The result is a three dimensional solution space of acceptable combinations of forces and moments applied to the workpiece. This thesis will aim to develop a similar model, only with a three dimensional solution space of part alignment error from which the gripper can correct. An important assumption used in this paper that will also prove useful, is that once the part starts to slip, the instantaneous velocity and resulting frictional force are related.

2.5 Summary

This chapter provided an overview of a number of areas important to the development of this thesis. An overview of the thread rolling process was first discussed, and developments in thread rolling technology examined. The state of the art in fastener feeding was also reviewed, noting the trend of many manufacturers toward orienting fasteners off-line from the production process. Methods of transporting oriented fasteners were discussed. Finally, an overview of research in the area of grasping was presented. Most importantly, metrics were found which predicted the quality of a grasp, the optimum placement of grasp points, and what combination of forces a fixture could withstand.

Building on these existing works, this thesis will first aim to develop a workcell plan and automation system for a typical aerospace manufacturing thread rolling process. Knowledge of the state of the art in thread rolling and fastener feeding systems will be utilized to create a solution which is both functional and innovative. Secondly, this thesis will develop a model which will predict, given a gripper and part geometry, what combinations of angular errors in part presentation the gripper can counteract and correct. Assumptions used commonly in prior grasping work such as Coulomb friction and negligible dynamic effects will be utilized in this model. The motivation for this work is for a practical model which does not aim to automate the designer's job, but rather to provide him with quantitative information on how a proposed design may function.

CHAPTER 3
WORKCELL CONCEPT SELECTION

As mentioned in the first chapter, one goal of this research project was to provide the framework for an automation plan for typical aerospace manufacturing process. The manufacturer had long been interested in the concept of a workcell, and wished to evaluate the ideal mode of implementation for their processes and products. Products with high production volume and similar size constraints were selected as parts to be manufactured in the cell, and a group of machines was established that should be evaluated for the cell plan.

3.1 Problem Overview

The products under consideration for manufacture in this cell are fasteners from 7/16" to 1" diameter, varying in length from 1" to 10". While the details of processing each particular part can vary, the general process for producing a fastener is fairly standardized. A typical fastener is shown previously in Figure 1.1.

The general process for almost any fastener manufacturer begins with raw material as coils of wire for smaller diameter parts or bar stock for larger parts. The first phase in manufacture is heading, where the bar or wire stock is hot forged to produce the head of the fastener. After this phase, parts are centerless ground, or in some cases turned on a lathe, in a number of operations to establish the thread and grip diameters along the length of the part. After critical dimensions are established, the part is fillet

rolled, which cold works the fillet on the underside of the fastener head. This greatly improves fatigue strength in cyclic loading applications. Finally the workpiece is threaded by a thread rolling process, which has been described in detail in Chapter 2. The processes under consideration for this workcell are shown below in Figure 3.1. Only two centerless grinding processes are shown, however as many as four grinding operations may be performed based on the part being produced.

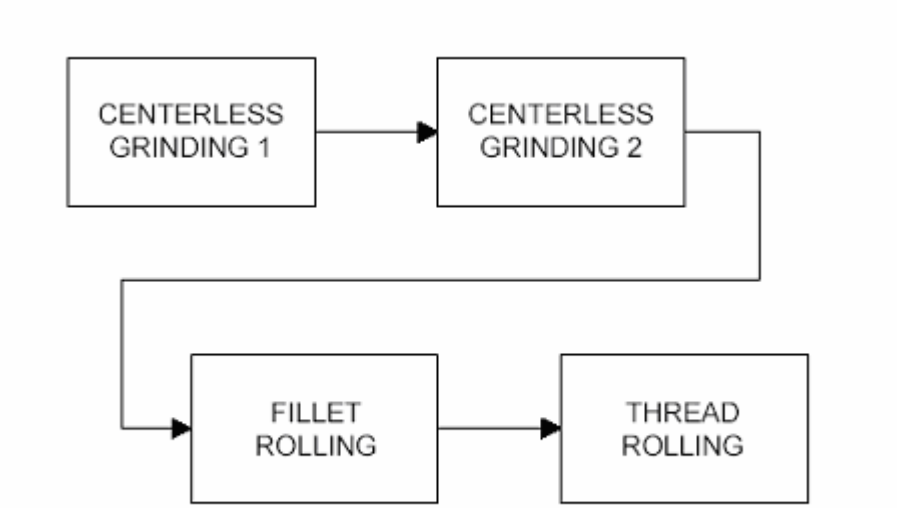

Figure 3.1 Fastener production process considered for workcell

The process described above is a general one, and typically there are many more operations that take place during manufacture. For example, some specialty fasteners must be drilled, broached, stamped with head markings or chamfered on the tip, just to name a few processes.

3.2 Performance Goals for the Cell

An important part of developing and implementing an automation plan is to set goals that can be used as guidelines in the design process (Bothwell 1989). Clearly, the underlying goal of any process improvement is to make more product for less money, however there can be subtleties that must be considered. Here a brief list of goals for the proposed cell is established.

3.2.1 Reduced Labor Costs

A significant portion of the cost of producing a part can often be attributed to paying labor costs for operators to run the necessary equipment in the process. Often times this is unavoidable since skilled operators are needed to set up and monitor machines, a task that is often not easily automated. It is unprofitable to have a skilled operator perform a relatively unskilled job, and as such it is becoming less and less common to hand feed any high volume fastener processing operation (Bothwell 1989).

Aerospace fastener manufacturers often use skilled operators to hand feed parts into various machines. The operator's skill lies in setup and monitoring of the machine, not in loading parts by hand one at a time into a running machine. Part loading can be accomplished by a less experienced operator, or as the goal in this case, by an automation system. This frees the operator to utilize his/her experience in more valuable ways, with ideally one operator setting up another machine while the first machine is running. A one operator per two machine metric is a common goal used in this particular manufacturing facility when designing new equipment.

An added benefit of automating the hand loading process is increased operator safety. Some hand loading processes can bring the operator's fingers dangerously close to moving parts, and fatigue can further endanger the operator. Increasing safety standards are also limiting the extent to which machines can be hand loaded, so it is in the manufacturer's interest to plan for these more stringent standards.

3.2.2 Increased Throughput

A well planned workcell can increase equipment utilization, reduce work in progress, and decrease the time to produce a given run of parts (Vanderspek 1993). The focus on a well planned cell needs to be emphasized; simply automating processes is not a guarantee that the desired goals will be accomplished. For purposes of this discussion, time to produce a batch of parts will be used as a metric for cell evaluation.

3.2.3 Flexibility

The concept of flexibility in a workcell is vital. A cell that performs optimally under the present conditions but is unable to adapt to changes is very undesirable. In the production facility under consideration, flexibility is especially important since the manufacturing process routing for different parts can vary greatly. Also, future efforts to improve the manufacturing process should not be hindered by the fact that the workcell itself is not flexible.

While evaluating this manufacturer's processes and overall goals, flexibility was established as the most important consideration in development of the workcell. Since the facility under consideration typically makes relatively small production runs of highly specialized fasteners, the need for flexibility is paramount. The situation where a facility produces high volume production runs of just a few products would not place such a high value on process adaptability. The varying nature of parts being made in this plant and the uncertainty of the nature of parts to be produced in the future will make flexibility the highest priority in the design of this cell.

Flexibility does not strictly apply to ease of changeover between different parts, it can also refer to the cell's ability to cope with machine downtime (Vanderspek 1993). In reality, the unfortunate fact is that machines can be driven off-line for a number of reasons. This can result from planned occurrences such as parts being sent out for lab inspection, to material problems or difficulty achieving a proper setup. Regardless of the reason, if the entire cell is halted by one machine's downtime, serious losses of production capability can result.

Lastly, flexibility can refer to the ease of adapting and expanding the cell in the future (Vanderspek 1993). This is also very important to the manufacturer under consideration, since the demand for new fastener designs is a constant manufacturing challenge. Also, continual efforts to improve the manufacturing process dictate that the order in which parts are processed may change at some point in the future. The workcell proposed must be adaptable to these circumstances.

3.2.4 Ease of Implementation

A final goal for this cell deals with the realization that implementing the entire plan will be a formidable task. The reality of implementing any process modification in an existing manufacturing facility is that any resulting downtime can be very costly for the manufacturer. The most desirable method of implementation for this particular workcell is a gradual one, a plan that can be implemented in stages with benefit realized at each stage. Implementing each stage should also require a minimum of downtime in production. This will be a final and very important design goal for the cell.

3.3 Proposed Cell Concepts

Two possible workcell concepts are now discussed. The first concept is one which was proposed by the manufacturer, the second is an alternate plan developed upon observing the manufacturing process. Both plans will be evaluated based on the performance criteria established in the previous section.

3.3.1 Highly Automated Sequential Cell

The first workcell concept is that of a highly automated, sequentially operating workcell. This concept was proposed by the manufacturer as their eventual goal for production automation, and a schematic layout can be seen in Figure 3.2. The underlying function of this cell is that machines are collocated, and an automated part transfer mechanism feeds completed parts from process to process. There would be very little

part queue between machines, when a part is completed in one process, it is immediately transferred to the next machine. The part routing from machine to machine would remain fixed, requiring a similar process routing for all parts produced in the cell. The goal of this cell is to require as little operator interaction as possible. It is important to note that this cell transfers individual parts from machine to machine, not batches of completed parts. This will be the primary difference between this cell concept and the second concept introduced in the next section.

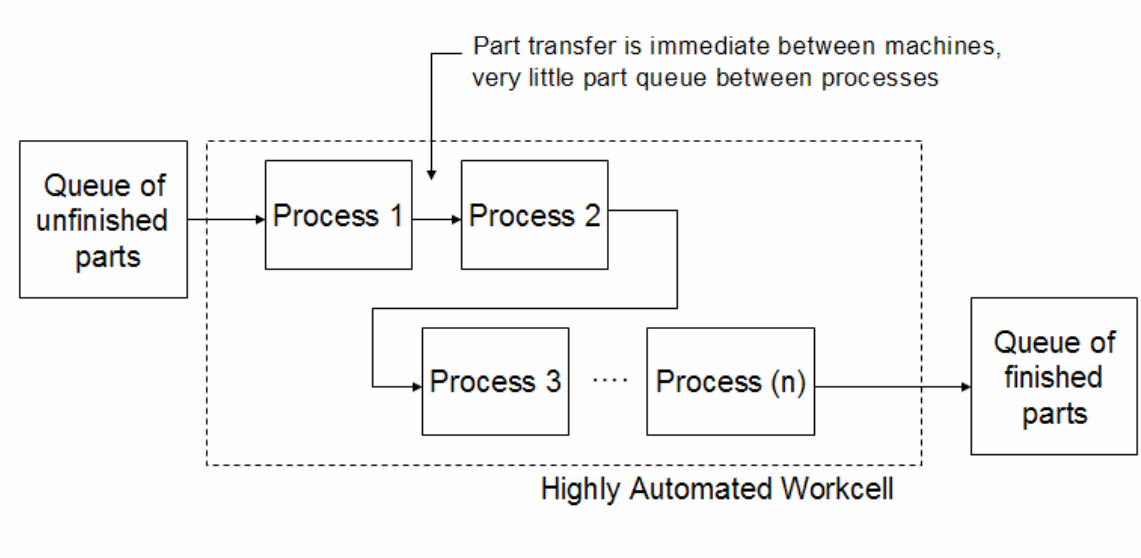

Figure 3.2 Highly automated sequential cell

In terms of satisfying the performance goals set in the previous section, the highly automated sequential cell considerably reduces labor costs. Instead of one operator per machine, one operator could theoretically tend to the whole cell. Setup would require an

operator skilled in all processes of the cell, but once the cell is online very little operator interaction would be required. This methodology reduces operator interaction to the minimum level possible.

The second design goal, time to produce a batch of parts, would not be decreased immediately by implementing this cell concept. As will be shown in later sections, the cell's productivity is still paced by the slowest process, regardless of the other processes in the cycle. Operating under the assumption that a human operator can load parts into a machine as quickly and as reliably as an automation system, this cell layout would not produce parts at a rate any faster than the present hand fed method. As will be discussed later in further detail, the assumption made above may not always be a valid one.

An important design consideration with this sequential layout is that "looping back" should be avoided in order to maximize performance. For example, some parts require as many as four grinding operations. It would be very inefficient to only have two grinders in the cell, since the parts would need to pass through both grinders twice.

A cell of this type would operate in two phases, and would require the entire lot of parts to be queued in-cell. The first phase would involve the first two grinding operations, however since the parts are not ready to be processed further until grinding is complete, the remainder of the cell is idle at this time. The parts would enter a queue at this time, until the entire first grinding phase is complete, as shown in Figure 3.3. This queue could potentially be very large, depending on the batch size. The second phase would involve parts leaving the in-cell queue and completing their second grinding passes, then traveling onward to the remainder of the cell. Only at this time do the remaining processes become active, as illustrated in Figure 3.4. If this type of cell is to

be optimal, “looping back” must be avoided. If four grind operations are required, the cell must contain four grinding machines in sequence.

The problem of looping back is not exclusive to this arrangement of a workcell. Productivity losses are experienced in other configurations as well. However, requiring the automatic transfer mechanisms to be capable of queuing parts and to reroute them to previous machines greatly complicates the design of the system.

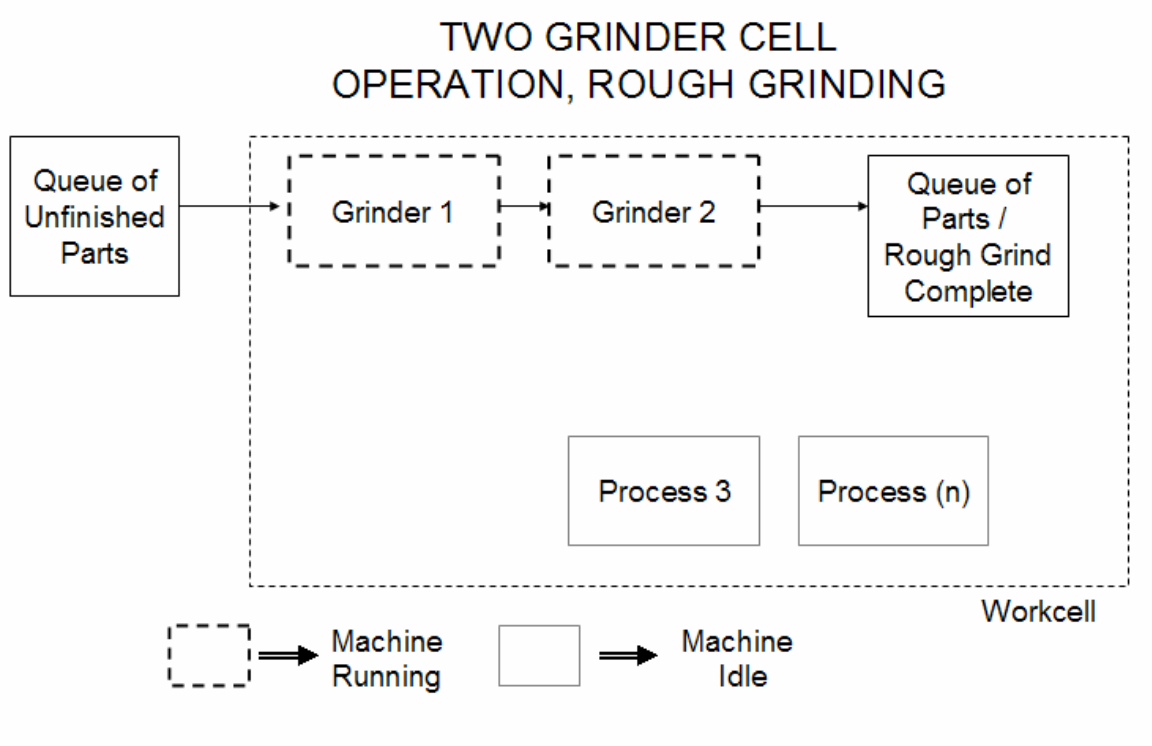

Figure 3.3 Cell with loopback, first phase

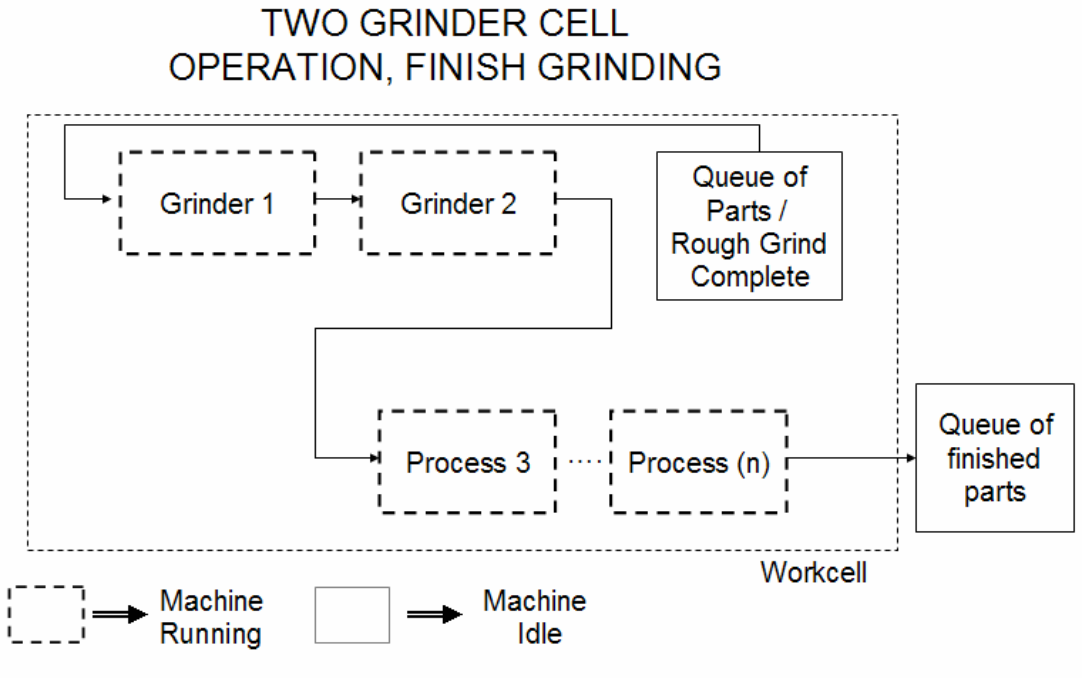

Figure 3.4 Cell with loopback, second phase

The third performance metric, flexibility, is not optimal in this configuration. The part routing among the machines is set in the design of the automation. If a new product requires a completely different part routing, changeover would be difficult. Also, if one machine in the process were to go offline, the whole cell would be brought to a halt. Creative design decisions could overcome some of these problems, however it is clear that in this respect other simpler alternatives should be considered first.

The fourth goal, ease of implementation, is also not optimal in this configuration. First, all machines in this workcell must be collocated. Secondly, each machine must have knowledge of other machines in the process, since cycles times between machines can vary. A machine must not process a part until the next machine inline with it is ready

to accept a part, since there is very little queue to buffer parts between machines. Finally, this design would be difficult to implement in stages, as it is likely that the entire workcell would be designed to function as a unit. This is a large scale project that would require considerable planning and a commitment by the manufacturer to tolerate downtime during implementation.

3.3.2 Reduced Automation Batch Transfer Cell

Upon observing various shortcomings in the highly automated sequential cell, a second design was proposed. This cell is not as highly automated, but places an emphasis on flexibility and ease of implementation. Instead of transferring single parts automatically, this cell will transfer batches of completed parts between machines, as shown in Figure 3.5. The transfer of parts will be done manually by an operator, however automation on each machine will load parts from these batches into the machine automatically.

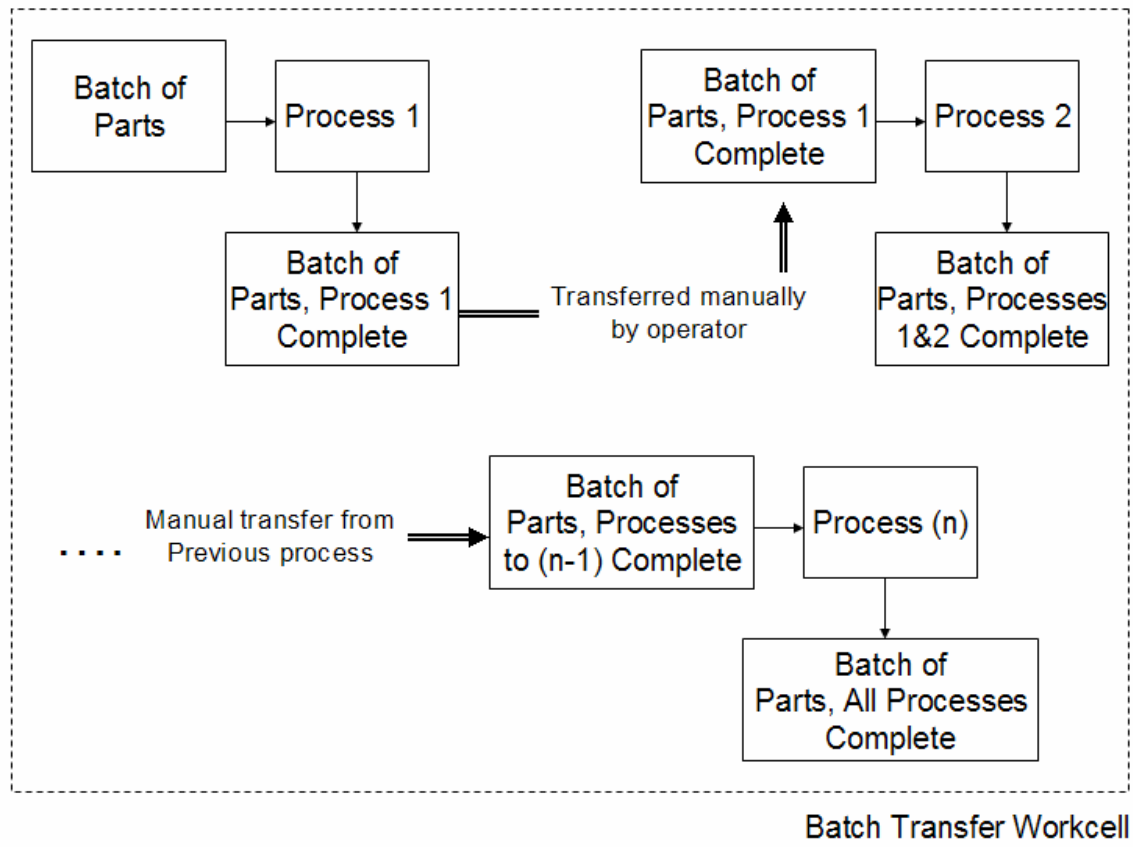

Figure 3.5 Reduced automation batch transfer workcell

In this cell configuration no process routing is permanently fixed, as operators can transfer parts from machine to machine in any manner desired. This workcell configuration could be considered more simply a cluster of machines with similar automation systems, through which products can flow in any manner desired to accommodate various part styles and sizes.

An important aspect of this methodology is that the automation system at each machine will be required to accept batches of parts rather than single pieces. This will likely require each machine's automation system to be somewhat more complex. In this manner, the operator now feeds batches of parts manually to each machine, rather than

individual parts as in the current method. The operator will be free to perform other tasks while the entire batch of parts is being processed, unlike the current method where only 5 to 30 seconds pass before the machine needs to be reloaded with another part. For this methodology to be effective in the current manufacturing environment, the machine must be able to process parts unattended for approximately 30 minutes. If one operator were required to tend to 3-4 machines, this would allow 15-20 minutes per hour to be spent with each machine, which should represent a reasonable amount of time to reload a properly designed automation system twice per hour.

The first design goal of reduced labor costs would be accomplished by this system. While it would require more worker interaction than the highly automated cell concept, a significant improvement over the current method would be possible. One operator could tend to multiple machines, monitoring the process and moving batches of parts between machines when ready. This method would eliminate the need for a dedicated operator at each machine to load parts one at a time to each process.

Per the second design goal of time to produce a batch of parts, as with the highly automated sequential cell, gains in productivity will not be realized simply by automating these processes. The cycle time of each process will still govern the overall cell's productivity, with the slowest process serving as the bottleneck. Increases in productivity would be realized if the automation systems improved cycle times or reliability when compared to a human operator. This will be discussed in more detail in the following section.

The third design goal of flexibility is one of the major benefits of this method. Since operators are manually moving parts from machine to machine, ultimate process

flexibility is maintained. A new production process which skips steps or uses certain machines multiple times will not require any extra hardware to implement. As mentioned in the previous section, "looping back" in the cell and using a particular machine more than once can result in a suboptimal cell, this remains true using this methodology as well. However, using the manual batch transfer method this will not alter the design of the automation system or the part transport systems. Looping back in the batch transfer method has a negative impact on cell cycle times, however does not require complex additional systems to be included in the workcell design. Also, system timing from process to process does not need to be coordinated between machines, since parts are allowed to queue at each station.

The final design goal, ease of implementation, is also a benefit of this method. This concept can easily be implemented in stages, with benefit realized at each stage. If the manufacturer wishes to continue to hand feed a few machines in the overall process, the cell will still function as desired. More labor will be required, but parts can still be moved manually in batches between processes. As more machines are automated, less labor will be required. This approach can be implemented in any manner desired, with added improvement realized for each machine which is automated.

3.3.3 Discrete Time Analysis

In order to gain insight into the expected behavior of the proposed workcell concepts, discrete time simulation was performed using Arena 3.01 (Systems Modeling

Corporaton, 1993-1997). Simulations were run in an effort to find the underlying principles which govern each cell's operation.

Some simplifying assumptions were made in these analyses. First, machine setup time is neglected, since each machine needs to be setup regardless of the workcell method employed. Second, it is assumed that presently an operator can load parts into a machine in a manner which will not limit the machine's cycle time. The machining cycle itself is instead assumed to be the limiting factor. This also includes the assumption that an operator will not need breaks or experience fatigue during the workday, an assumption which is optimistic at best.

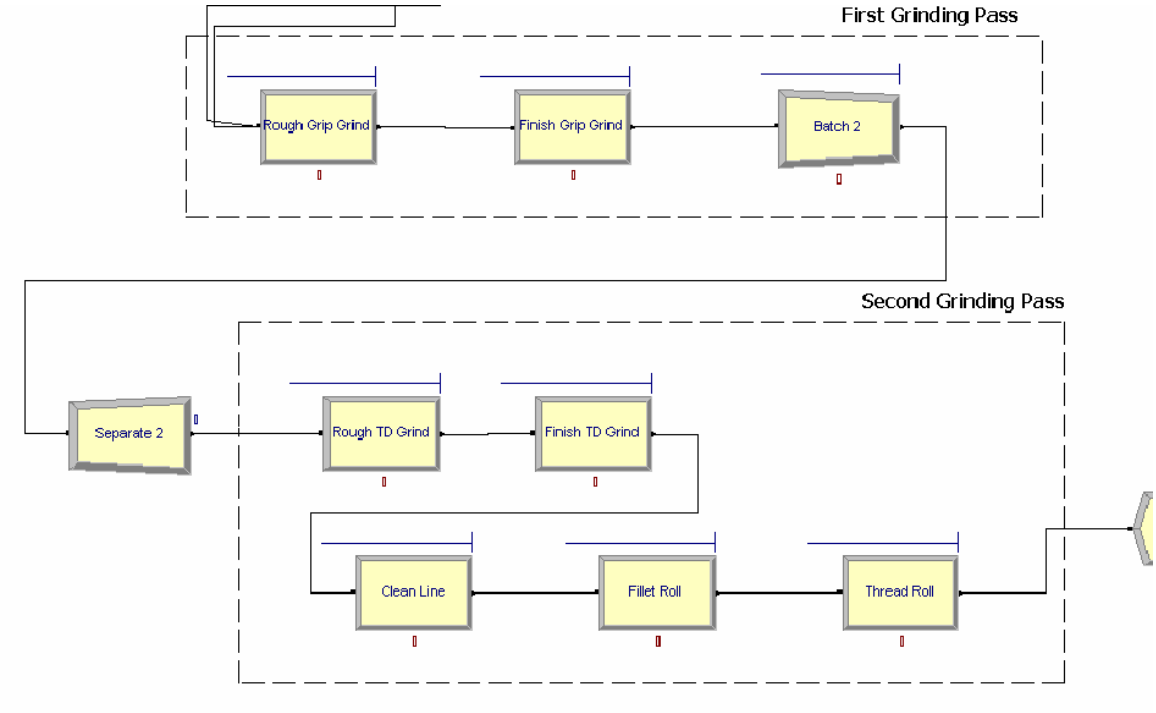

Figure 3.6 Arena discrete time simulation

An example of the Arena simulation program can be seen in Figure 3.6. Each process is represented by a block, which has an associated cycle time. Entities are passed into the cell and are subject to the cycle time of each process, and emerge as "complete" parts. The entities fed into the cell can represent either individual parts or batches of parts, depending on the type of cell under consideration.

3.3.3.1 Discrete Time Analysis of Current Method of Production

The current method of production involves operators hand feeding parts at each station. Parts are processed at each machine until the entire batch is complete, then the parts are transferred to the next machine for continued processing. This method can be somewhat difficult to represent in simulation, since often on the shop floor certain jobs can take precedence over others and batch size can vary with each job. To simplify and simulate this process, assumptions were made that any parts in queue will be treated as first in / first out, that is batches of parts will be processed in the order they are received at each machine. Also, it will be assumed that batch size is constant, which in this manufacturer's case is a reasonable assumption for purposes of an initial analysis.

After running Arena with the cell layout described, it becomes immediately obvious that the governing principles of this method are quite simple. As product enters the processes, there is an initial lag in production while the first batch makes its way through each machine and the cell reaches steady state. After this point, a batch of parts is completed at a regular time interval, governed solely by the slowest cycle time in the process. This is illustrated below in Figure 3.7.

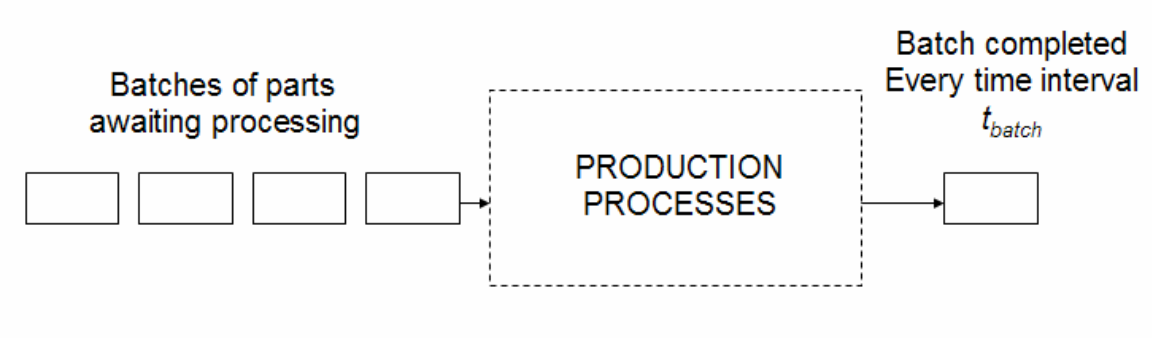

Figure 3.7 Schematic of current method of production

Equations 3.1-3.3 govern the productivity of the cell. A batch of parts is completed every time interval t_{batch}, which is dictated by the slowest cycle time in the process and the batch size. This analysis assumes purely sequential processing with no "looping back" between processes, as discussed in section 3.3.1.

$$t_{batch} = n_{parts} t_{slow} \tag{3.1}$$

t_{batch} = time interval to produce one batch of parts

n_{parts} = number of parts in batch

t_{slow} = slowest cycle time in process

For example, if the slowest machining process in the cycle was grinding, and to grind each part took 20 seconds, this process would pace the flow of material through the

machines. If the batch size was constant at 1000 pieces, a 1000 piece batch would be produced every 20,000 seconds, or 5.55 hours.

On a per part basis, the average time to produce one part can be computed by dividing the time to produce the batch by the batch size in number of pieces. On average, the processes will complete a part every interval equal to the slowest cycle time. In the above example, although it took 5.55 hours to complete a batch, the processes produced a part on an average of one part every 20 seconds.

$$t_{part,avg} = \frac{t_{batch}}{n_{parts}} = t_{slow} \tag{3.2}$$

Although reducing work in progress was not stated as a design goal, it is interesting to observe what effect different cell layouts have on the time a part spends in production. Observing results from Arena, equation 3.3 is found to govern the time a part spends moving through all processes. This assumes that parts are not fed into the process faster than they can exit, as this would result in a queue of parts accumulating at the bottleneck process.

$$t_{inprocess} = n_{parts} \sum_{1}^{n} t_{cycle,n} \tag{3.3}$$

$$t_{inprocess} = \text{work in progress time for one part}$$
$$n_{parts} = \text{number of parts in the batch}$$
$$t_{cycle,n} = \text{cycle time of process } n$$

The total time a part spends in production is a function of all cycle times in the process, as well as the batch size being produced. This is intuitive, as each part must wait for the others it is grouped with to complete to move to the next operation, and the parts must pass through every operation before they are considered complete.

Table 3.1 Simulation results for current production method

Process	Cycle time (sec)
Grind 1	20
Grind 2	20
Grind 3	20
Grind 4	20
Thread Roll	15
Fillet Roll	5
Batch Size	1000 pcs
Steady state batch production time	5.5 hours
Average part production time	20 seconds
In-process time	27.7 hours

Table 3.1 shows simulation results for the current production method using representative cycle times measured for each process. A constant batch size of 1000 pieces is assumed, and four grind operations along with thread rolling and fillet rolling are selected for consideration. A completed batch of 1000 pieces will exit last process every 5.5 hours once steady state operation is reached, with an average part production time of one piece every 20 seconds. A batch of 1000 pieces will remain in-process for 27.7 hours.

3.3.3.2 Sequential Cell Discrete Time Analysis

Next, the sequentially operating highly automated cell model was input into Arena. This model moves individual parts through the process rather than batches, as discussed earlier, and illustrated in Figure 3.8.

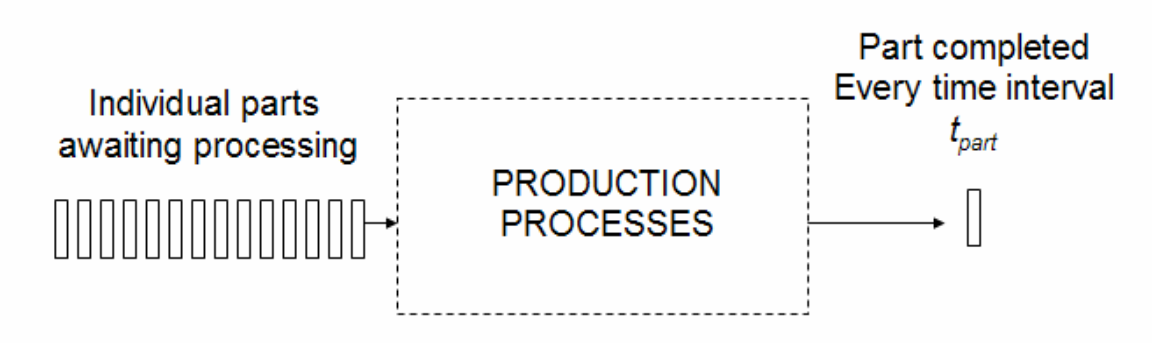

Figure 3.8 Schematic of sequential cell

As with previous analysis, operation is assumed to be sequential with no processes looping back. Equations 3.4 and 3.5 are found to govern productivity and work in progress time, respectively.

$$t_{part} = t_{slow} \tag{3.4}$$

t_{part} = time interval to produce one part

t_{slow} = slowest cycle time in process

Again, the cell's productivity is limited by the slowest operation in the overall process. Since the sequential cell truly processes parts on an individual basis, a part is produced every time interval equal to the slowest cycle time in the process. As in the previous section, if grinding were the slowest operation with a cycle time of 20s, the cell would produce a part every 20s. This differs from the current method of production in that currently, the process produces a batch of parts at a time interval equal to the slowest process time multiplied by the batch size, whereas this cell produces one part every time interval t_{slow}. Over a period of time the average production time of the sequential cell and the highly automated cell would be equal.

Work in progress is however different from the current method. Since parts are being processed on an individual basis rather than a per batch basis, the total time a part spends in process is reduced. This time was multiplied by the lot size in the previous case.

$$t_{inprocess} = \sum_{1}^{n} t_{cycle,n} \tag{3.5}$$

$t_{inprocess}$ = work in progress time for one part

$t_{cycle,n}$ = cycle time of process n

This section illustrates an important point, that productivity will not be automatically increased by automating processes. Work in progress time was shown to be reduced, however the production rate remains the same on average as with the current method. To achieve increases in production rate, an individual machine's cycle time needs to be shortened, or multiple machines need to perform the same process in the situation of an extreme bottleneck resulting from one process.

Table 3.2 Simulation results for sequential cell

Process	Cycle time (sec)
Grind 1	20
Grind 2	20
Grind 3	20
Grind 4	20
Thread Roll	15
Fillet Roll	5
Batch Size	1000 pcs
Steady state part production time	20 seconds
In-process time, one part	100 seconds

Table 3.2 shows the analysis results for the sequential cell. The cycle times are identical to those assumed to analyze the current production method in Table 3.1. This configuration will produce a part every 20 seconds, which is equal to the average production rate for the current production method. In-process time is reduced significantly from 27.7 hours to 100 seconds, due to the immediate part transfer inherent to this cell design.

3.3.3.3 Reduced Automation Batch Cell Discrete Time Analysis

Finally, the reduced automation batch transfer cell is analyzed in Arena. This cell is very similar in analysis to the current method discussed in 3.3.3.1, as batches of parts are moved between machines rather than individual parts. The analysis shows that equations (3.1-3.3) which govern the current process also govern the batch transfer cell, for both production time and work in progress. The results obtained using sample cycle times are also equal to the results of the current method analysis in Table 3.1.

3.3.3.4 Discrete Time Analysis Conclusions

Upon completion of the discrete time analysis, a few conclusions can be drawn. First, simply automating transfer of product between machines will not increase the productivity of the process. The only way to increase productivity is through cycle time reduction of slowest process, or multiple machines performing the slowest process at the same time.

The highly automated sequential cell is shown to reduce work in progress time from the current method of production. If the facility under consideration was expected to make products with extremely short lead times, this measure of cell performance might be given more consideration.

Finally, it is shown that on average, the current method and both cell concepts will produce parts at the same rate. As stated earlier, this operates on the underlying assumption that operators can hand feed processes as quickly and reliably as an automation system can. This assumption is optimistic, as human operators seldom work at 100% efficiency, and must take necessary breaks throughout the work shift. Automating the loading processes in either proposed cell configuration would increase productivity by removing human error from the loading process, thus reducing cycle times at each machine. It is only by these means that either workcell concept will enable the manufacturer to produce parts at a faster rate than is presently seen.

3.4 Selecting a Workcell Concept

After analyzing two overall cell concepts and four design goals, the conclusions are as follows. The manual batch transfer cell is selected, primarily for its flexibility and ease of implementation. These two design goals were decided to be most important in process selection, and the manual batch transfer cell is clearly superior in this respect. Conclusions are summarized below in Table 3.3

Considering productivity and throughput, the manual batch transfer cell does not benefit from the reduced work-in-progress times that the sequential cell has. However, this was not intended as a design goal for the system. Both cells' productivity will still be governed by the slowest process in the cycle, regardless of the method chosen.

The manual batch transfer cell will be more labor intensive than the highly automated cell, but the priorities imposed by other design goals dictate that this compromise must be accepted. While not as minimal as the highly automated cell, operator interaction in the manual batch transfer cell is still a marked improvement over current methods of one operator per machine.

Table 3.3 Comparisons of cell performance criteria

	Highly Automated Sequential Transfer Cell	**Manual Batch Transfer Cell**
Reduced Labor (vs. current one operator per machine)	One operator per workcell	One operator for every 3-4 machines
Increased Throughput / Productivity (vs. current)	Reduced work-in-progress, productivity gains from reduced operator fatigue / breaks needed	Productivity gains from reduced operator fatigue / breaks needed
Flexibility and Adaptability	LOW	HIGH
Ease of Implementation	LOW	HIGH

The manual batch transfer cell will also benefit from reduced human error in loading, and can operate unattended for certain periods of time, which can be scheduled to coincide with break periods for the operators. Also, an added benefit of increased operator safety is realized by removing the operator's hands from the loading and unloading process.

3.5 Selecting a Method of Part Transport

Through analysis in previous sections, it is decided that the workcell will contain a group of automated machines, each of which will accept batches of parts loaded by an operator. The automation systems on each machine should be similar, so that the method used to transport the parts can enable transfer of parts between any two machines in the process at any time. The method of transporting parts chosen should serve as a benchmark for factory automation, any system further developed should both accept parts from and return parts to the chosen transport device.

The only remaining design decision regarding transporting parts is to decide in which state the parts are to be transported. Parts can be transported in both an unoriented or oriented state, with each method providing benefits for particular applications. Any machine, automated or manually fed, will only accept fasteners for processing in a certain orientation. In a manually loaded process, often the operator serves as the orienting device, taking fasteners from a bin and manipulating them into an acceptable position by hand. This act of manual orientation often goes unnoticed, but becomes a formidable task to duplicate when attempting to automate the process.

The following sections will discuss two methodologies used in practice for transporting parts through the production process and orienting the parts for acceptance by each machine in the process, in addition to discussing the details of the methodology used in this effort.

3.5.1 Orienting Fasteners at Each Machine

One orientation methodology suitable for automated fastener production is to orient the parts at each production process. In the author's experience, this is commonly seen in production of smaller fasteners, where a vibratory bowl feeder at each machine accepts a large lot of randomly oriented parts. The vibratory bowl manipulates the parts into an orientation that is required by the automation system, and hands off the properly aligned fastener to the automation. Usually after the fasteners are processed, they return to their randomly oriented state in another bin, and are transported to the next process in this manner.

The benefits of this method are numerous when it is applied to the correct application: 1) it is simple to move large batches of randomly oriented fasteners from machine to machine, 2) any type of bin or container can be used, and 3) the same transport device can be used for a variety of fastener sizes and styles. In addition, the automation system does not need to be overly complex, since a chute and gravity are all that are typically needed to direct the finished parts to their destination transport bin.

This method has certain shortcomings, as well. First of all, a primary requirement is that the parts being produced are easily oriented by a vibratory bowl or a hopper type

orienting device, leading to restrictions on the size and shape of fastener to be successfully oriented. Vibratory bowl feeders are the most common device that are used, and historically they have been known to jam despite the designer's best efforts. Another potential problem relates to parts that may be prone to contact damage, since the reciprocating action of the bowl results in repetitive part-to-part contact. Lastly, this method is redundant, since the same orienting process is repeated numerous times during the production process.

3.5.2 Maintaining Orientation During Transport

Another possible part orientation methodology is to orient the fasteners once at the beginning of the production process, and to keep them in the same oriented state until they are completely processed. This approach involves moving fasteners in an oriented state from machine to machine, so clearly the mode of transport will be more complex than the simple bin of parts referred to earlier.

The benefits of this method are: 1) an orienting device is not necessary at each machine, 2) the problems associated with jamming, or part-to-part contact, in vibratory bowl feeders or hoppers are completely eliminated, 3) this methodology more easily accommodates parts which are difficult to feed via a vibratory bowl or other type of hopper feeder, and 4) it takes advantage of the fastener's oriented state, preserving it throughout the process, unlike the previous approach. The effort to orient the fasteners is only required once at the beginning of the process.

3.5.3 Design for Current Application

Since the fasteners in the application under consideration are large (7/16”-1” diameter), and potentially up to 10” long, they are not likely candidates for automatic orientation in a feeder bowl. The manufacturer has also experienced problems in the past with part-to-part contact damage during transport through the plant, so this is an additional reason to move away from hopper style systems.

These design criteria clearly point to transporting the fasteners in an oriented fashion and maintaining the orientation throughout production. Consequently, it was decided to expand on the current methods already used throughout the plant to develop the part transport device design. Specifically, the new part transport design builds upon a tray and bin type system currently used by the fastener manufacturer.

The current production process uses LewisBins products to transport parts from one process step to the next. These fiberglass-reinforced polyester bins are stackable and can be nested on top of one another. Currently the manufacturer transports fasteners throughout the plant in these bins, moving batches of randomly oriented fasteners from machine to machine. Dollies and hand trucks specifically made to move stacks of bins are seen throughout the facility. Trays are also available which fit the top of each bin as a lid, and the fastener manufacturer has made a limited effort in the past to utilize these trays as a mode of transporting damage prone fasteners.

The design implemented expands on this concept, using a hole pattern machined into the bin lids as a method for transporting fasteners and presenting them to an automation system. The automation systems developed with this concept will pick parts from these trays and return finished parts to the trays. Using this method, operators can

now load trays of parts at a time to a machine, instead of loading only one part at a time. When a tray is finished processing on a particular machine, the tray can easily be moved to any machine in the process, maintaining total process flexibility. Figure 3.9 shows a full transport tray holding 45 hex headed parts.

Figure 3.9 Prototyped transport tray

In order to allow repeatable locating of the tray on the automation system, two locating features are machined into each tray when it is fabricated. To ensure exact relative alignment to the pick and place points, these locating features are machined in the same setup as the part holding holes. In order to address any concerns about locating feature wear over time, and the potential loss of locating reliability, a steel drill jig

bushing with an aluminum press-on retaining ring is used in each locating hole, as shown in Figure 3.10.

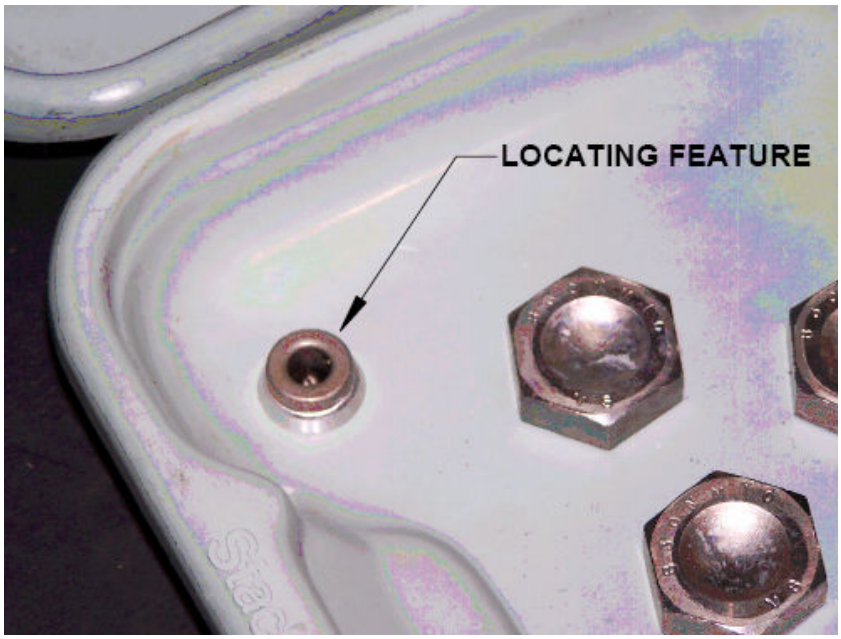

Figure 3.10 Transport tray locating feature

Each part tray is specific to a fastener grip diameter and the hole layout of each tray maximizes the number of fasteners which can be transported per tray. Since the overall size of the tray and the bin are kept constant for all parts under consideration, trays designed for smaller diameter parts hold more parts per tray, and trays designed for larger part sizes hold fewer. The hole diameters are oversized approximately 1/8" from the grip diameter to relax the placement tolerance needed by the automation system. Also, each tray is inscribed with the fastener size it corresponds to, to ensure the operator

selects the correct hole pattern for the part being processed. The complete set of prototyped trays is shown in Figure 3.11.

Figure 3.11 Complete set of prototyped transport trays

3.6 Summary

This chapter presented two possible workcell concepts which will serve as the basis for development of an automation system in subsequent chapters. First, performance goals are set for the workcell. These include reduced labor costs, increased throughput, flexibility and ease of implementation.

Two cell concepts are proposed, with the first being a highly automated sequentially operating workcell. This cell concept requires a minimum of operator interaction and passes parts from one machine to the next in an automated fashion. Very little part queue is used between each machine. This method is shown to reduce work in progress time over the current production method, but not to directly increase productivity when compared to averages of the current method. Also, the highly automated cell is shown to be an inflexible design by nature, and fairly difficult to implement as well.

A second design involving a less automated manual batch transfer cell is proposed. In this concept each machine's loading and unloading process is automated, but transfer of parts between machines is manual. This method is shown not to decrease work in progress time from the current method, and to produce parts at a similar rate to the highly automated sequential cell. Parts are transferred in batches by operators between machines, which maintains flexibility in the process. Also, this method is shown to be easy to implement, with benefit realized at each stage.

The second workcell concept is chosen based on its reduction of labor, and its flexibility and ease of implementation. With this plan selected, a method to transport batches of parts through the process is evaluated. Two concepts are presented, one

requiring parts to be oriented at each machine, the other maintaining orientation during transport.

The second method is chosen, due to the large nature of parts being produced and the susceptibility of these products to contact damage with each other during orientation and transport. In order to maintain orientation throughout the manufacturing process, a tray concept currently used on a limited basis by the manufacturer is expanded upon. This decision is based on the tray and bin system's widespread use in the plant, thus making integration simple. Trays are machined with holes to transport oriented parts, and two locating features are machined on each tray to enable repeatable registration on an automation system.

CHAPTER 4

AUTOMATION SYSTEM DEVELOPMENT

In preceding chapters, the framework for an automated workcell was developed. Based on the specific goals and production needs, design criteria were established and used to evaluate two possible workcell plans. It was decided that the workcell will function by means of manual part transfer between machines, with operators moving batches of finished parts from process to process. Further analysis concluded that maintaining parts in an oriented state throughout the process was desirable, and a transport tray concept was developed to accomplish this goal.

The second and most important goal of this project was to develop an automation system for the manufacturer, using the aforementioned workcell design decisions as a basis for the system's development. One machine in the overall process was selected for automation system development and proof of concept, however it was desired that the system be adaptable to other machines in the future. The thread rolling process was specifically selected, since the particular style of machine under consideration is hand fed.

It should be noted that the scope of this project included complete mechanical design of the automation system, based on an existing automation manufacturer's pick and place robot design. Any components used without change are noted, otherwise all designs are original works of the author. System assembly and programming, as well as testing and tuning were also performed by the author as part of the scope of this project. Every component of the system developed is not discussed in this thesis in detail for

brevity; however it should be noted that this project was conducted as a complete exercise in machine design and development.

4.1 Problem Overview

The machine under consideration is a Reed cylindrical three die thread roller, shown in Figure 4.1. Threads are formed on the workpiece by three rotating and moving dies. The dies rotate continuously and move in a cyclic fashion toward and away from the centerline of the thread roller. The dies are arranged 120° from each other and are held in place by three die hangers, shown in Figure 4.2. The cyclic die movement is governed by a cam, and regulates when a part can be loaded and unloaded from the machine. When the dies are retracted fully, and furthest from the centerline of the machine, a part can be inserted or a completed part can be removed. The cam profile dwells when the dies are fully retracted, to allow time for part loading and unloading. When the cam follower begins to rise on the main cam lobe, the dies move inward toward the part, eventually contacting the part and forming the threads. It is important to note that the part will rotate numerous times during production, this will present design challenges for the part gripping system.

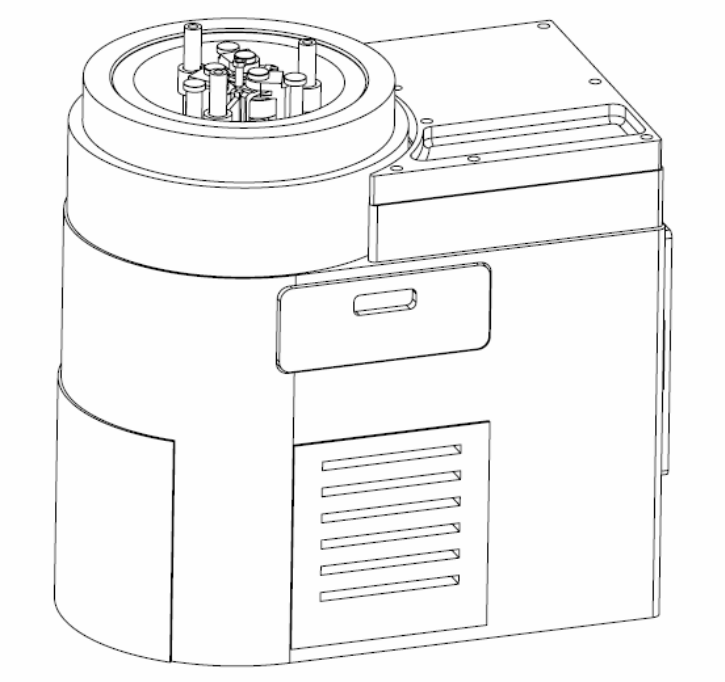

Figure 4.1 Reed cylindrical three die thread roller

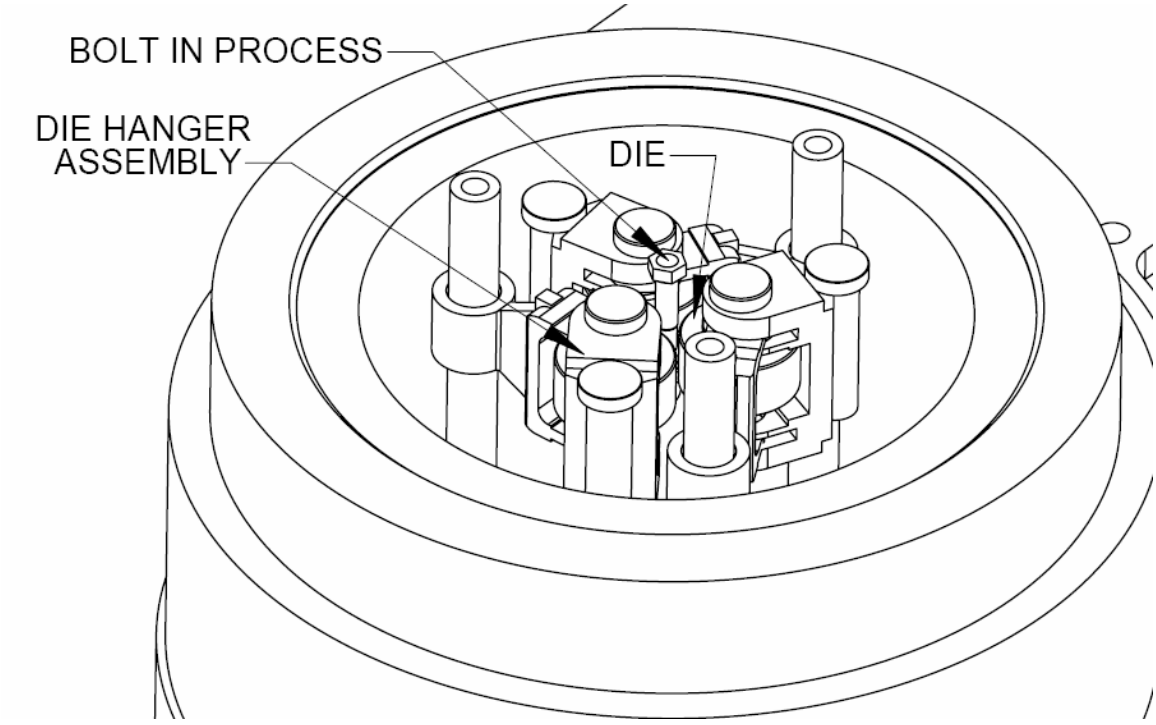

Figure 4.2 Detail of die and die hanger arrangement

The process is presently hand fed in production, and can only produce one part at a time. Associated with the process is an induction heater, as most of the parts manufactured are rolled warm, to alleviate demands placed on tooling by difficult to form materials. Only the thread area is heated, enabling operators to handle parts by their heads immediately after heating and through the rolling process. Timing for the rolling process is typically governed by this heating process, since heating takes a minimum of 10 seconds, and can take as long as 30 seconds for larger parts. The roller cycles continuously, completing a dwell and roll cycle every 3.8 seconds. These cycle times are summarized in Table 4.1.

Table 4.1 Thread rolling process cycle times

Thread Roller Timing	
Load / Unload Time	2.2s
Rolling Time	1.6s
Total Thread Rolling cycle time	3.8s
Heater Timing	
Heat Time	10s-30s (fastener size dependent)

It is clear that the heating process will govern the productivity of the thread rolling machine. In order to maximize production rates, it is desirable to ensure the heater is always heating a part. This mimics how operators hand load the machine. An operator typically removes a hot bolt from the heater while inserting the next cold part, followed by turning on the heater. With the next part heating, the hot part is inserted into the thread roller for processing. After the part is rolled, it is placed in a cooling area with other processed parts. During this time, the next part has partially completed its heating cycle. It is desired that the automation system developed will keep the heater loaded and heating at all times as well.

The induction heater normally used in production only heats one part at a time. This is the preferred method in order to ensure reliable and consistent heating. While heating multiple parts at a time in one induction heater is certainly possible, it is beyond the scope of this project; changes in the heating process would require extensive lab testing and process development to ensure the integrity of the product has been maintained.

In summary, the automation system developed must meet the following design goals:

1. Accept parts from the transport tray(s) as designed in Chapter 3.
2. Return any processed parts to the transport tray(s).
3. Keep the heater full and active at all times.
4. Allow the part to rotate during thread rolling.
5. Maintain clearance with moving dies and die hangers with any part gripping system developed. The gripping system must also be able to fit between parts nested in the transport trays.
6. Accommodate 7/16" to 1" grip diameter hex, 12 point and spline headed parts up to 10" long.
7. Allow the machine to run unattended for an average of 30 minutes.
8. Do not delay the overall cycle time beyond that of the heater, e.g. the automation system should be ready to place a cold part in the heater when the previous part is finished heating. The minimum heat time to be accommodated is 10 seconds.

4.2 Planning the Process

With design goals established, development of the system can begin. Before any physical designs are considered, the process itself should be planned. Flow of parts between the trays, heater and roller should be coordinated to ensure maximum productivity.

A post processing rack was added at this time as a safety in the design of the system. Parts are coated in oil while in the thread roller, and at the time of design it was unknown whether returning oily parts to the trays could potentially contaminate neighboring unprocessed parts. To alleviate this concern, a simple parts rack was added to the process flow, this rack will allow parts just out of the thread roller to enter a buffer area before returning to the trays. Thus the system will consist of four main areas: the trays, heater, thread roller and a post processing area, shown in Figure 4.3.

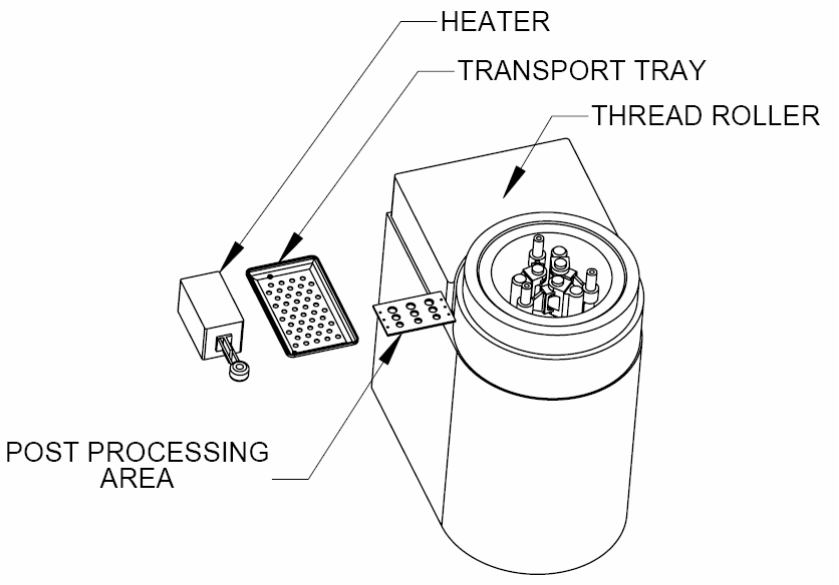

Figure 4.3 Automation system processing stations

The process will be performed as follows:

1. Remove the next part to be processed from the transport tray, move to the heater
2. Since the heater should already be heating a part, wait for the previous part to complete the heat cycle
3. Simultaneously remove the heated part from the heater while inserting the next cold part (this issue is specifically addressed in further sections)
4. Start the next heat cycle
5. Move the heated part to the thread roller, process the part
6. Place the completed part in the post-processing rack to allow excess oil to drip from the workpiece
7. Remove the part which has been in the post-processing rack the longest, return it to the tray
8. Begin again with step 1

These goals are easily achievable by a robotic motion system, with the exception of step number 3. Simultaneously inserting a part in the heater while removing the previous part is no trouble for a human operator, as two "end effectors" are available if the operator uses both hands. This subtlety however requires further thought in developing an automation system.

4.2.1 Dual Gripping System vs. Dual Heating Coil

The heater has a single station coil, meaning only one part can be placed in the heater at a time, as shown below in Figure 4.4. This presents a problem for typical automation system designs, which most often feature one end effector. A single end effector cannot simultaneously insert a part into the heater and remove the previous part, so other options are needed. Two concepts were explored to solve this problem, a dual station heating coil and a dual end effector design.

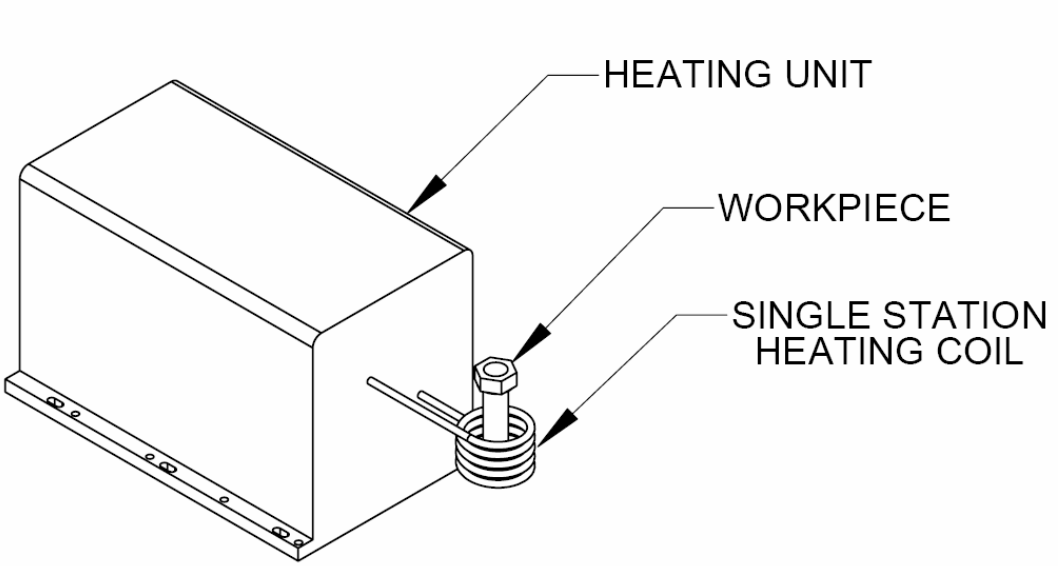

Figure 4.4 Existing single coil heating unit

The dual end effector design would function by enabling the machine to grasp more than one part at a time. Thus the previously heated fastener could be removed with gripper 1 while the next part to be processed is held in gripper 2. This concept was ruled

out quickly due to increased costs and complexity. Two gripping units would be required, twice the amount of tooling would need to be kept on hand, and logistically moving two grippers through the workspace would prove to be difficult.

The dual coil design is much simpler. It would not be used to heat multiple parts at once, for reasons discussed previously. Rather, it would provide a location to drop off the next cold part before picking up the previously heated part with a single gripping system. During heating, one side of the coil would contain a part, the other side would remain empty, as illustrated in Figure 4.5. This concept is very inexpensive; a dual coil prototype was easily constructed to test the idea.

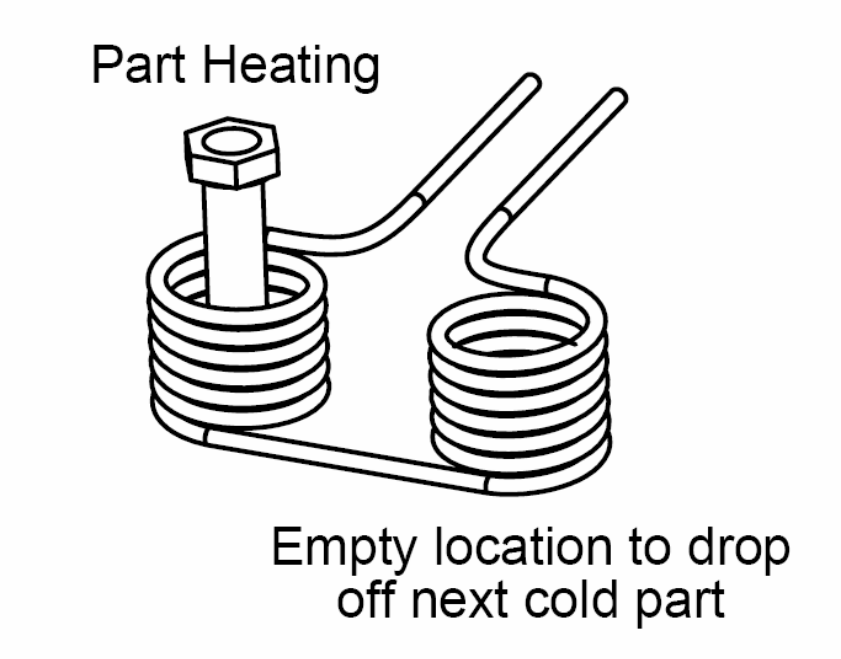

Figure 4.5 Dual induction coil design

The only concern remaining with this concept is the loss in efficiency due to adding a coil with no load in series with the coil heating a part. Two design parameters of the coil which can easily be changed are the coupling distance and the number of turns per unit height (coupling distance refers to the radial distance from the part's outer surface to the heating coil). Generally speaking, efficiency of an induction coil can be enhanced by decreasing coupling distance and increasing the number of turns per unit height (Tudbury 1960). These principles were utilized in prototyping the dual coil, with parameters shown in Table 4.2.

Table 4.2 Coil prototype design parameters

	Existing Single Coil	Prototype Dual Coil
Coil Inner Diameter	2.11"	1.5"
Coil Height	1.35"	1.66"
Number of Turns	4	6.5 (per side)
Turns per unit Height	2.96 turns / inch	3.91 turns / inch

4.2.2 Testing the Dual Coil

In order to test the efficiency of the new dual coil in comparison to the single coil previously used, a 5/8" diameter titanium part was heated to 600° F in 22 seconds. Tempilaq temperature paint was used to monitor surface temperature, and the machine's power settings were adjusted so the desired temperature was reached in the timeframe

given by the test parameters. Noting the power settings of the machine needed from one coil to another, a general approximation can be made about the efficiency of the coils, summarized in Table 4.3.

Table 4.3 Coil test results

	Existing Single Coil	Prototype Dual Coil
Part Temperature	600° F	600° F
Heating Time	22 seconds	22 seconds
Power Required	60%	52%

The dual coil required less power to heat the same part to the same temperature in the same amount of time. The efficiency lost by adding another coil was more than regained by reducing the coupling distance and increasing the number of turns per unit height.

The only remaining concern is that the parts are heated evenly from one side of the coil to another. To ensure this, five parts were heated in each side of the coil and thread rolled. For a point of experimental comparison five parts were also heated in the existing single coil. The thread rolled pieces were then subject to a tensile test, with the results shown in Table 4.4.

Table 4.4 Coil tensile test results

*All results in PSI, Ultimate Tensile Strength	Existing Single Coil	Dual Coil Side 1	Dual Coil Side 2
Test 1	41200	43780	42890
Test 2	42760	45000	43440
Test 3	45990	42480	43810
Test 4	45310	46790	45160
Test 5	45370	46750	46610
Mean	44126	44996	44382

As can be seen, the dual coil performed consistently from side to side in tensile strength values, and slightly outperformed the existing single coil. With this knowledge, the dual coil design was deemed an acceptable and inexpensive solution to the problem of keeping the heater full and active at all times.

4.2.3 Transport Tray Planning

In order to move forward in the system's design, it is desired to know how many transport trays the system will be expected to accommodate. This decision will impact the design goal that the machine function unattended for a period of approximately 30 minutes, as the machine can only operate until the supply of unprocessed parts it holds is exhausted. Too few trays will require that the system be given constant attention, while accommodating too many trays will make the system physically large.

Since the dual heat coil design enables the heater to remain active at all times, and since the heat time has been determined to pace the process, the time to process a certain number of trays of parts can be predicted. The approximate heating times based on fastener size is known from established standards, and the number of parts per tray is now known from the transport tray design already completed. The results of processing times for one, two and three trays are shown in Table 4.5.

Table 4.5 Tray processing times

Fastener Diameter (inch)	Heat Time (seconds, average)	Parts per Tray	1 Tray Processing Time (minutes)	2 Trays Processing Time (minutes)	3 Trays Processing Time (minutes)
7/16	14.0	72	16.8	33.6	50.4
1/2	16.0	55	14.7	29.3	44.0
9/16	17.0	55	15.6	31.2	46.8
5/8	20.0	45	15.0	30.0	45.0
3/4	22.0	32	11.7	23.5	35.2
7/8	24.0	26	10.4	20.8	31.2
1	26.0	21	9.1	18.2	27.3

As fastener size increases, the number of parts that can be fit on a tray decreases, while heating time increases. These factors dictate the approximate time needed to process a tray. A two tray capacity was selected as a compromise. A two tray machine will also occupy less floor space than a machine with greater capacity.

4.3 Motion Planning

Previous sections developed the problem at hand and determined that the system will contain a dual heating coil and will process two transport trays of parts at a time. The system will also contain a post processing area in which bolts will drain residual oil after rolling. The task is now to determine how these areas will be configured, and what type of device will move parts between these areas.

4.3.1 Pick and Place Point Arrangement

The system has been determined to contain four processing areas: the trays, a heating area, the thread roller and a post processing area. What spatial arrangement of these areas will yield the simplest automation solution? Two layouts are considered, a three degree of freedom end effector approach and a two degree of freedom end effector approach.

The motions needed in this system are relatively simple, the bolts hang in the transport trays in the vertical position, and each station requires the bolt to remain in this vertical position. Thus no roll, pitch or yaw motion will be needed on the end effector. With this in mind, the end effector must have a minimum of two degrees of freedom, and needs a maximum of three degrees of freedom.

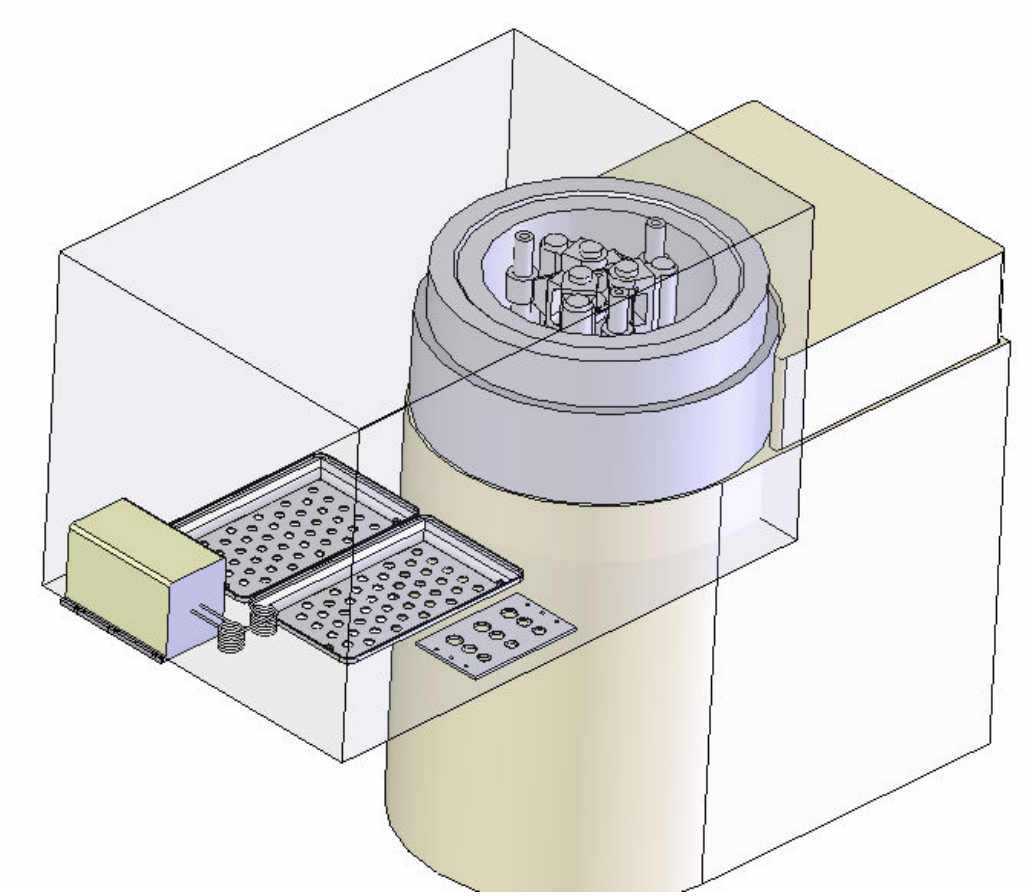

Figure 4.6 Three dimensional automation workspace

A three degree of freedom approach would form a three dimensional workspace in which the gripper could move (shown in Figure 4.6). In this layout the configuration of the transport trays, heater and post processing area is somewhat arbitrary, as long as the pick and place points fall within the robot's work envelope. A different configuration of the pick and place points can yield a yet simpler design, where the end effector only requires two degrees of freedom.

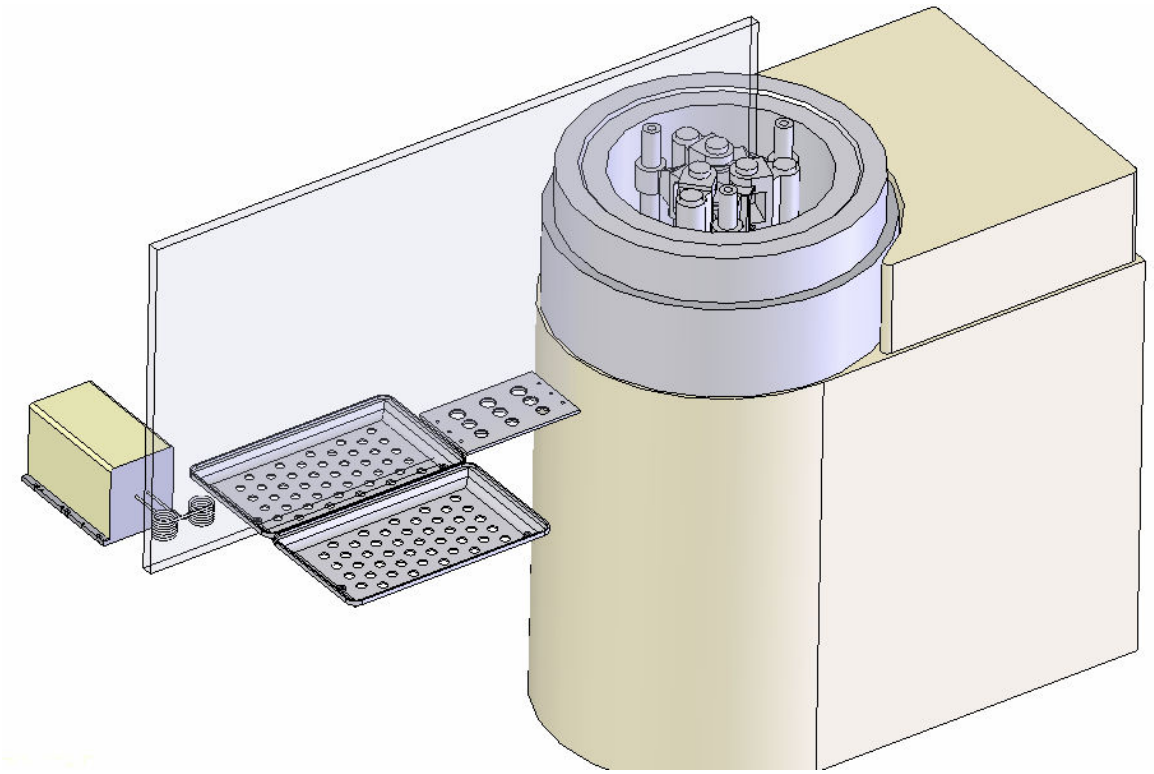

Figure 4.7 Two dimensional automation workspace

The two degree of freedom approach requires more forethought, but results in a simpler system. In this layout, all pick and place points are positioned to fall in a plane of motion, as illustrated in Figure 4.7. Both heating coils, three post processing locations, one row of tray holes and the placement point in the thread roller are coplanar. With this concept, the end effector only needs to move with two degrees of freedom, vertically and horizontally. The trays will need to index under this plane of motion, so the end effector can access all tray locations.

This method also reduces the area which needs to be guarded, since all end effector motion must be isolated from the worker. This will enable the worker to remain close to the thread roller and closely monitor the process. With its simplicity and

compact guarding envelope, the two degree of freedom with a tray indexing drive was chosen as the concept to be developed.

4.3.2 Moving in the Developed Workspace

Moving within a two dimensional workspace can be accomplished in a number of ways. Hard automation could be used if the pick and place points were few and unchanging, however this application dictates that a robotic solution will be necessary. A SCARA or articulated arm robot could be used, but to take advantage of the limited degree of freedom concept, a pick and place type robot was desired. In order to develop the robotic system, an automation integrator was selected based on the design needs encountered.

CAMotion Inc. in Atlanta, GA was chosen from a number of vendors to assist with robotic development. CAMotion was selected for its experience in building accurate, lightweight pick and place devices, and for the ability of its robot designs to be customized to suit this particular application. CAMotion's role in this thesis project was to provide the basis for the motion axis designs and control software; any components specific to this application were developed by the author. Use of existing basic motion axis designs and control algorithms allowed this project to focus on the design and analysis of components specific to this application.

4.3.3 Cycle Time Prediction

With the approximate layout of the system determined, if heights are assigned to each station the length of each motion can be calculated. From this knowledge a total cycle time can be predicted, to ensure the system can complete all required operations in under 10 seconds. This requirement will guarantee the automation system can keep pace with the fastest heat time of 10 seconds.

The optimal tray height was determined to be approximately 36" from ground level. This height was chosen purely for ergonomic reasons, as the motion to load trays to the machine will be performed repetitively. The height of the thread roller is dictated entirely by the machine. The height of the heat area and post processing area was chosen to be midway between the roller and the trays, approximately 40" from ground level.

A few other cycle times were needed for this calculation, for instance the gripper's close/open cycle time. Since a preliminary gripper design had been selected at this point, literature was available to estimate this time. Also, knowledge of the thread roller's cycle time was utilized. A best and worst case cycle time was predicted for the system, the best case being that when the gripper arrives at the thread roller, a part can immediately inserted. The worst case scenario is when the gripper "just misses" the window in the thread roller's timing when a part can be inserted. In this case the gripper will need to wait for the next cycle to insert a part.

Motion times are calculated assuming a constant acceleration until a maximum velocity is reached. A constant deceleration equal to the acceleration value brings the motion to a stop. The time to complete a motion is given by equation 4.1, which is easily derived from simple constant acceleration equations of motion.

$$t_{move} = \frac{d_{move}}{v_{\max}} + \frac{v_{\max}}{a_{move}} \tag{4.1}$$

d_{move} = move distance

v_{max} = maximum velocity

a_{move} = acceleration and deceleration magnitude

A part length of 10" is assumed, representing the longest part which will be processed. Acceleration values of 1g are used, and a maximum velocity of 2.5 m/s is assumed. These values are well within the physical capabilities of CAMotion's machines. The results for each motion are tabulated in Table 4.6.

Table 4.6 Automation cycle time prediction

Cycle Time Calculations	worst case (seconds)	best case (seconds)
Move from heater to roller		
y move from heater to roller	**0.844**	**0.844**
Thread Roll Process		
wait time for process to begin	3.8	0
z into roller (happens during wait on worst case)	0	0.133
release grasp (can also happen during wait)	0	0.09
roll	1.6	1.6
grasp	0.09	0.09
z out of roller	0.133	0.133
total	**5.623**	**2.047**
Move to Cooling Rack and Place		
y roller to cooling rack	0.428	0.428
z into cooling rack	0.308	0.308
release grasp	0.09	0.09
total	**0.826**	**0.826**
Remove from cooling rack		
no part move to next rack position	0.175	0.175
grasp	0.09	0.09
z out of rack	0.225	0.225
total	**0.490**	**0.490**
Move to Trays and place		
y over to trays	0.422	0.422
z into trays	0.328	0.328
release grasp	0.09	0.09
total	**0.840**	**0.840**
Pick From Tray		
empty move to next tray position	0.175	0.175
grasp	0.09	0.09
z out of tray	0.328	0.328
total	**0.593**	**0.593**
Move to Heater		
y tray to heater	**0.483**	**0.483**
CYCLE TOTAL (seconds)	**9.699**	**6.123**

Even the worst case satisfies the 10 second cycle time requirement, and the best case is predicted to easily perform within the specification. The proposed layout and moves are decided to be a viable process to satisfy the design goals.

4.4 Gripping System Design

With the cycle and process deemed acceptable, details of the mechanical design of the system can now be addressed. The most challenging aspect of this system's design is that of the end effector. It is required to accommodate a large range of fastener sizes as well as styles, and must be reliable and tolerant to damage. Also, numerous clearance issues will dictate the maximum size for certain features, as the gripper must fit between parts in the trays as well as between the dies and die hangers in the thread roller.

4.4.1 Design Requirements

As with the overall system, it is useful to establish design requirements for the gripping system. These guidelines can be enumerated as follows.

1. Grasp parts from 7/16" to 1" grip diameter, up to 10" long
2. Grasp hex, 12 point and spline style head shapes
3. Allow adequate clearance to grasp a workpiece from a full tray of parts
4. Allow adequate clearance to insert a short workpiece into the thread roller's moving dies

5. Allow the workpiece to rotate during processing
6. Perform the above tasks with a minimum of tooling changeover between varying styles and size

4.4.2 Concept Selection

So as not to rule out any "outside the box" solutions, any method of moving a part was initially considered. Vacuum was ruled out as a viable option due to the limited surface area available on the part heads. A magnetic gripper would be very versatile, but very few of the parts to be grasped are ferrous. Considering these limitations, mechanical grasping was chosen.

Many gripper base units are available commercially in a variety of sizes and styles. A three jaw design was selected, as the three finger design is most conducive to inserting a part between the roller's three dies. Also, since the transport tray pattern was designed with a nested rather than square hole layout, a three jaw gripper will fit between adjacent parts with proper planning.

Before selecting a base gripping unit, the issue of allowing the workpiece to rotate while inserted in the thread roller was addressed. As stated earlier, the thread roller is constantly cycling, with the dies moving toward and away from the roller's centerline. With the dies retracted, a part can be inserted, and the bolt's tip is allowed to contact a workrest along the machine's centerline. If the part is released at this point, it will begin to tip and possibly fall between the dies. This can severely damage the machine and must be avoided. Once the dies move in and contact the workpiece, the part can be released

and the machine will completely support it. However, as soon as the dies contact the workpiece it will begin to rotate, so the grasp must be released by this point.

This problem presents a very difficult timing issue, since the gripper must release the part precisely at the moment the dies contact the part, then must grasp the part again at the exact moment the dies release it. This would be almost impossible to predict with simple sensing systems and could result in machine damage if the timing was not properly tuned.

To find a solution, the operator's hand loading method was carefully analyzed. It was observed that when an operator loads a part, he/she inserts the part into the machine with a full grasp, then lightly supports the head of the part with an index finger until the dies make contact. This allows the part to spin on the operator's finger, and the light support is all that is necessary to prevent the part from falling before die contact is made.

To simulate this, it was decided to include a pneumatic cylinder on the gripper's centerline. This cylinder will be actuated when the part is inserted into the gripper, and will allow the gripper fingers to be released before the part is stabilized by the thread roller's dies. Since the cylinder is supporting the part along its centerline, it can remain actuated during the thread rolling process when the part rotates. This will also prevent the part from falling once the dies release the part, and provides a timing window for the gripper to resume its grasp and remove the part from the thread roller. The pneumatic cylinder concept is illustrated in Figure 4.8.

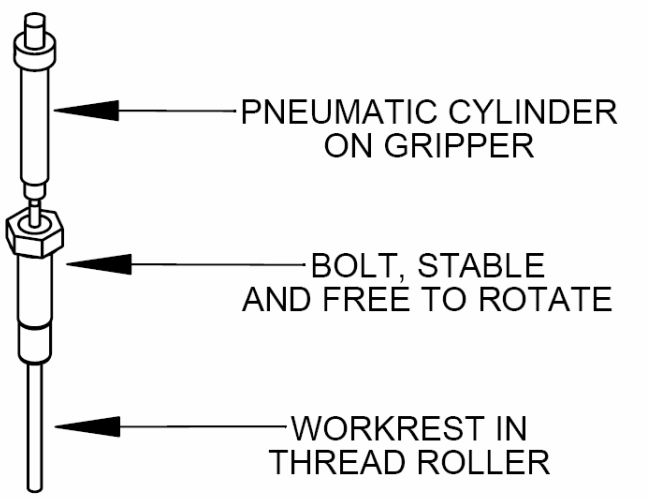

Figure 4.8 Gripper pneumatic cylinder concept

With this design in mind, a three jaw gripper with center clearance for the cylinder was selected. The Schunk PZB-100 was found to be an ideal candidate. It has 6mm of stroke per finger, and its through bore along its centerline facilitates incorporation of the cylinder concept. The gripper is shown in Figure 4.9 with a standard set of fingers, which need to be customized to suit the present application.

Figure 4.9 Schunk PZB-100 with generic finger blanks

4.4.3 Shaping the Gripper Fingers

With the base gripping unit selected, the finger design must be made to satisfy the design requirements enumerated in section 4.4.1. The first design decision is how to accommodate the various fastener head styles produced. Hex shaped parts present the greatest challenge, since no effort is being made to orient the parts rotationally in the parts trays. It is not known exactly where the tips of the hex shape will contact the gripping face, so a design is desired which will perform equally well regardless of part orientation. A gripper with a semicircular face was proposed to overcome this issue, shown in Figure 4.10.

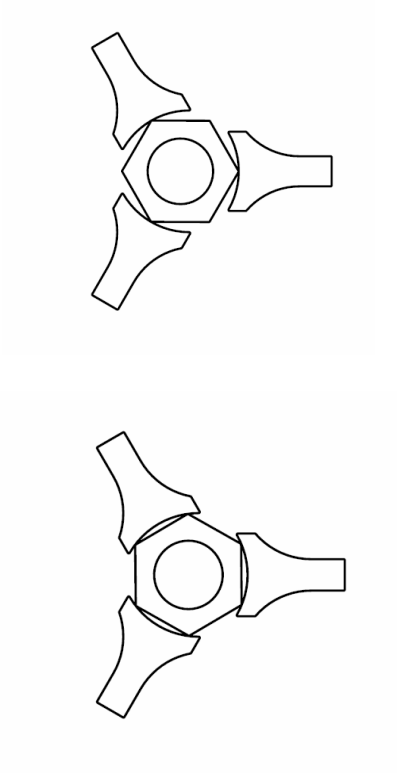

Figure 4.10 Modes of hex headed grasping

This design will at worst make contact with three points on the part, and at best will contact all six points of the hex head. Clearly this design will easily grasp more symmetric part shapes such as a spine and 12 point head design. The radius of the semicircular arc is determined by the average part size to be grasped by a particular set of tooling. The radius is set equal to that of an arc traced by sweeping the tip of a hex headed part about its central axis, so as to promote symmetric gripping regardless of axial part orientation.

A few other aspects of the gripper finger profile are dictated by the design requirements. The remaining features are limited on their shape by clearance restrictions imposed by where the gripper must move, shown in Figure 4.11.

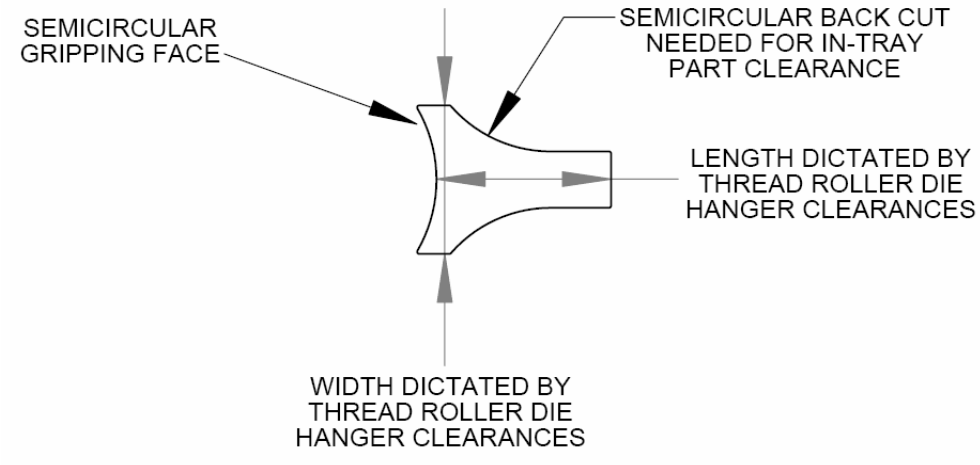

Figure 4.11 Finger profile shape restrictions

The semicircular back cut on each gripper profile is needed to fit the fingers between adjacent parts when retrieving and placing bolts in the transport trays. This feature was determined by moving the gripping finger to its furthest open position, and assumes the largest headed part encountered for a certain tray type is present. Also, since the tray holes are oversized, the neighboring parts may not be centered at all times. In the worst case they will be shifted in the oversized hole directly toward the gripper finger.

The back cut was sized so that even in this worst case scenario, the gripper can still fit between neighboring parts. The illustration in Figure 4.12 shows a tray layout, with the dark black circles representing the nominal location and size of a large headed part, and the outer black circle representing the outer limits of where the part can move due to hole oversize.

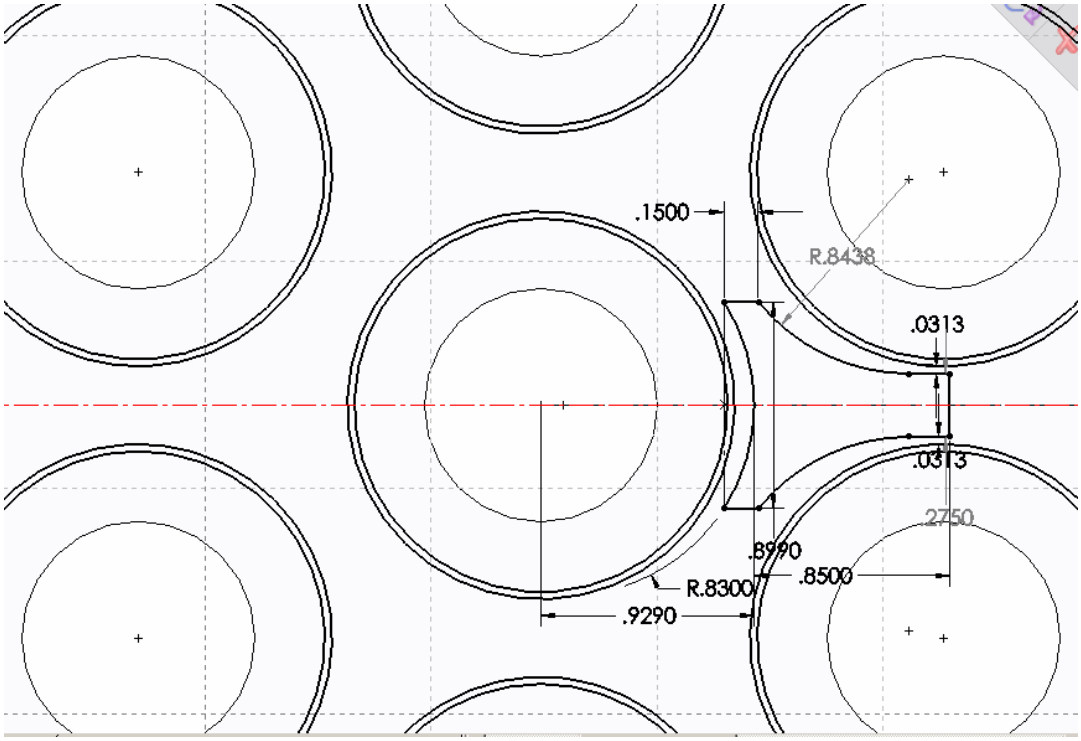

Figure 4.12 Gripper finger clearance in transport tray

The height and width of each finger type is dictated by the thread roller die hangers. The gripper must be able to fully open when inserted into the die hangers, to allow the part to rotate during processing. The illustration in Figure 4.13 shows the fingers in the fully open position, nested between the corresponding die hangers it is designed to work with. It can be noted that an increase in width of the finger would cause interference with the circular part of the die hanger body, while increase in the length would cause interference with the die hanger fork.

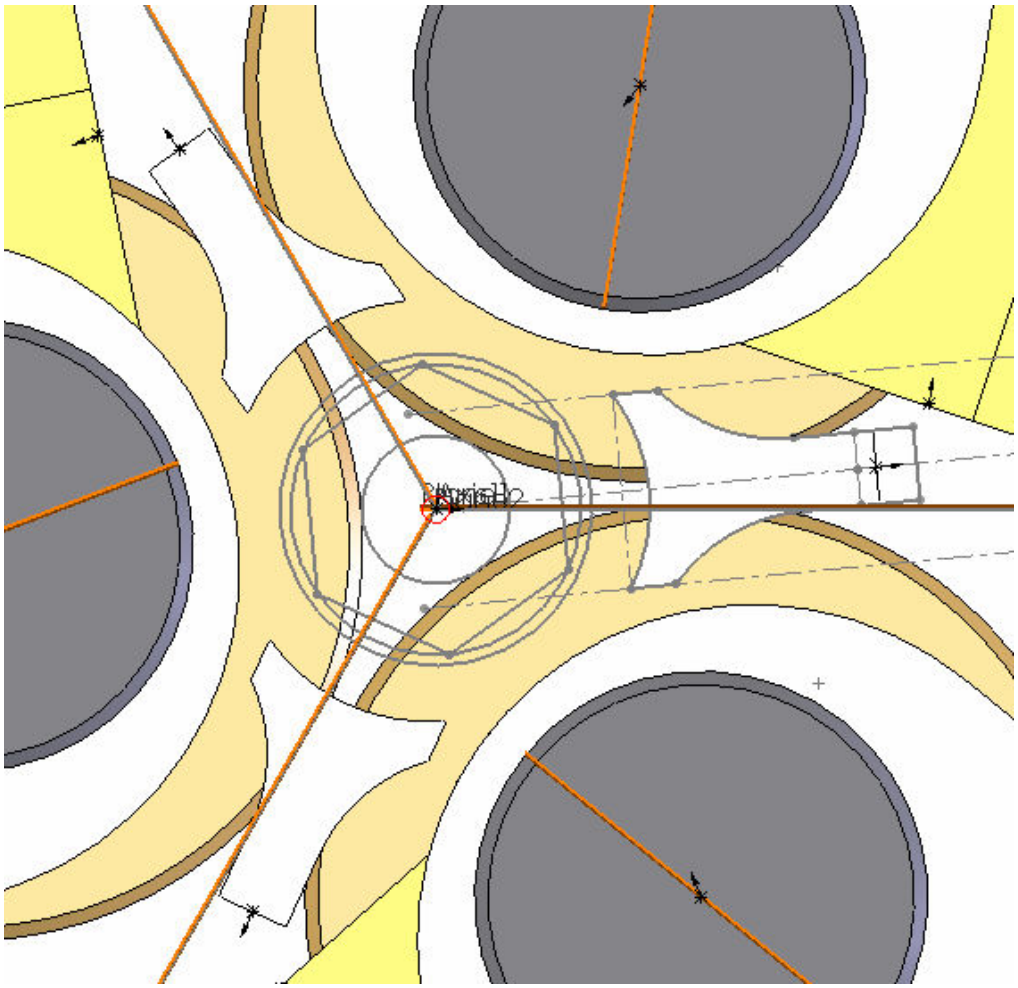

Figure 4.13 Gripper finger clearance in thread rolling die

Since each fastener size uses its own die sizes and tray sizes, sets of fingers were customized to suit each size. This was also made necessary by the fact that the gripper has 0.315” of stroke per finger, and the head sizes to be grasped span a much larger range. Crossover between tools was possible, and a total of four sets of tooling accommodates the entire range of parts specified. The sizes corresponding to each tooling set are listed in Table 4.7.

Table 4.7 Gripper tooling sizes

Tooling Set	Fastener Sizes Accommodated
1	7/16”-1/2”
2	9/16”
3	5/8”-3/4”
4	7/8”-1”

Finally the finger profile is extruded atop a base flange, which has two dowel holes for reliable location and two bolt holes to secure the finger to the gripper. The overall height of the finger was dictated by the depth of the die hangers, so that even the shortest part can be inserted fully to the proper thread depth. The back relief on each finger is for tray clearance, since the side of each tray curves upwards with a certain radius. This will permit the gripper to grasp parts close to the edges of the tray. These features are illustrated in Figure 4.14.

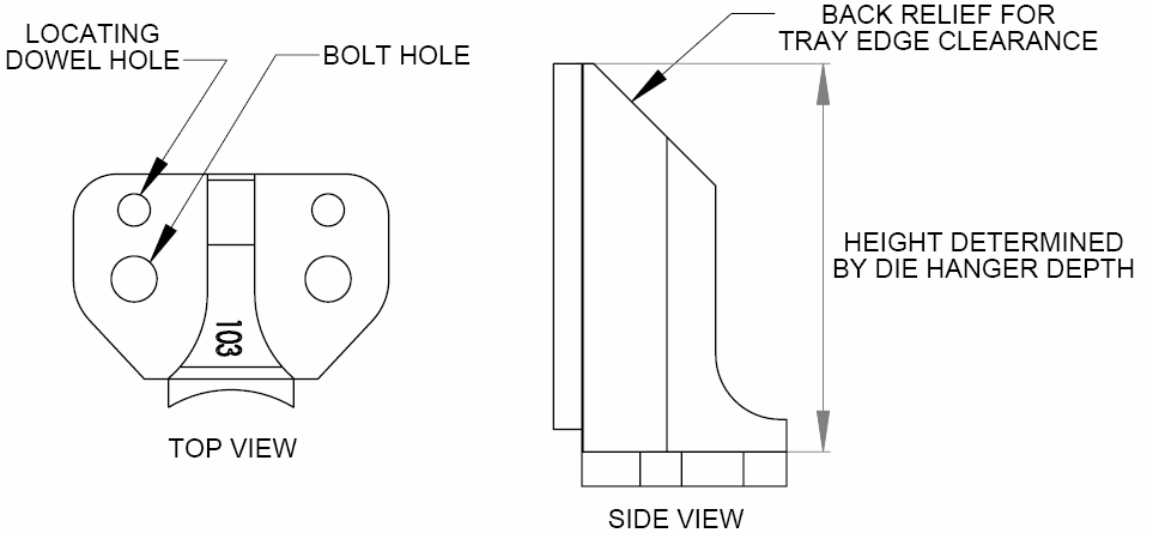

Figure 4.14 Gripper finger features

4.4.4 Gripper Finger Material Selection

For the body of the gripping finger, 6061 aluminum alloy was proposed due to its ease of availability, strength, and good machining qualities. A finite element analysis was conducted in ANSYS to ensure the finger body could withstand the grasping force applied. A 45 pound (200 N) grasping force was used, as this is an average value the Schunk PZB-100 gripper can produce and will mimic or exceed the forces seen during actual use.

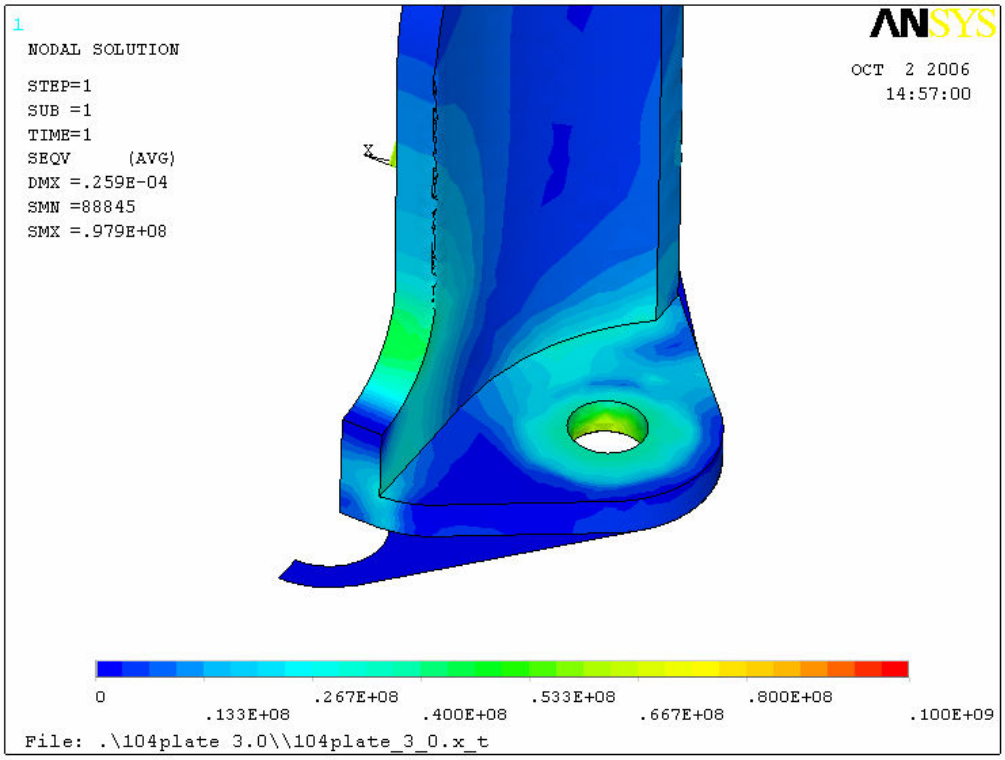

Figure 4.15 Gripper finger finite element analysis

The finite element analysis in Figure 4.15 showed the area of highest stress concentrations to be around the bolt holes, and along the rear spine's radius where the finger joins to the base. The perpendicular cut where the finger joins to the base was not noted to be a problematic area, as it was a concern during design. Even the areas of highest stress were far below the yield stress of 6061 aluminum (40,000 psi), with a factor of safety of approximately 3 observed in this test.

The faces of the fingers required more design attention, as they will likely be subject to much abuse. The sharp corners of a hex headed part pose a threat to any soft material over time, and the prospect of a machine crash dragging a grasped part along the finger face prompted the development of replaceable finger faces. A-2 tool steel was chosen for the finger face material, since it is easily handled by most machine shops and can then be heat treated to increase the hardness of the part. The face profile is shown in Figure 4.16.

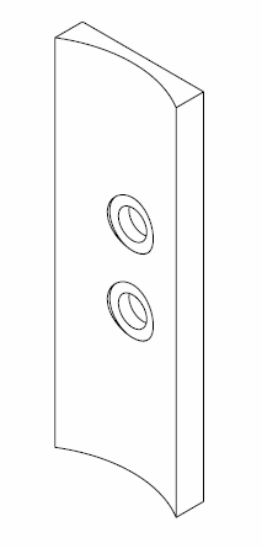

Figure 4.16 Replaceable gripper finger face

The finger face was designed to be symmetric about its center, such that should one gripping surface become damaged, the finger can be rotated 180° and reused. The A-2 tool steel was hardened to a hardness of 50HRC. The assembled finger and finger faces can be seen for one set of tooling in Figure 4.17.

Figure 4.17 Prototyped gripper fingers with replaceable faces installed

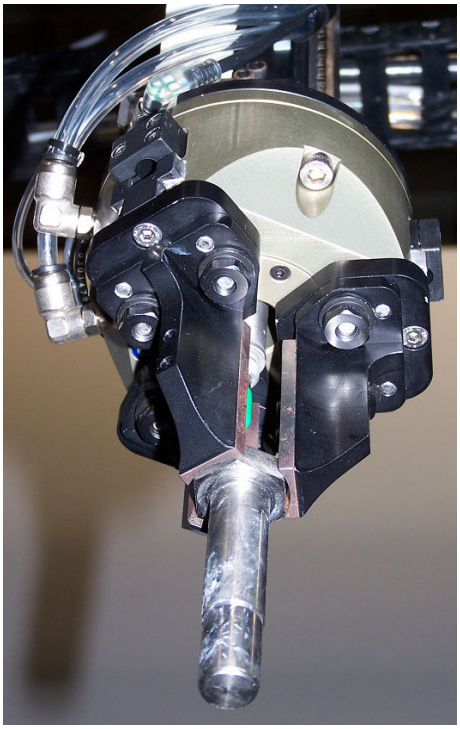

Figure 4.18 Prototyped gripping system

The prototyped gripping system shows all of the developed design concepts together. The pneumatic cylinder can be seen protruding from the center bore of the gripper. The A-2 steel tooling faces can be seen on each finger, as well as the dowel holes and bolt holes which locate and anchor each finger to the base. The gripper is shown in Figure 4.18 with tooling set #3 grasping a 5/8" diameter hex headed bolt. By removing the two bolts fastening each finger to the base, the gripper can be set up to handle any size part in under two minutes.

4.5 Overview of Remaining Design Details

Much planning was required in designing the rest of the machine. Each detail is not of concern to the topics of this thesis, however an overview of the rest of the machine will be given to illuminate various problems solved.

The layout of the system can be seen below in Figure 4.19. The end effector can move in two dimensions, designated by Y and Z. The plane formed by the Y/Z motion contains pick and place points. The tray drive system indexes two transport trays under this plane, designated by X. It can be seen in Figure 4.19 how the two axis design allowed the long Y axis to be cantilevered over the thread roller, while keeping the frame for the machine completely contained to the left of the thread roller. This design permitted the system to be installed with no modification or attachment to the roller.

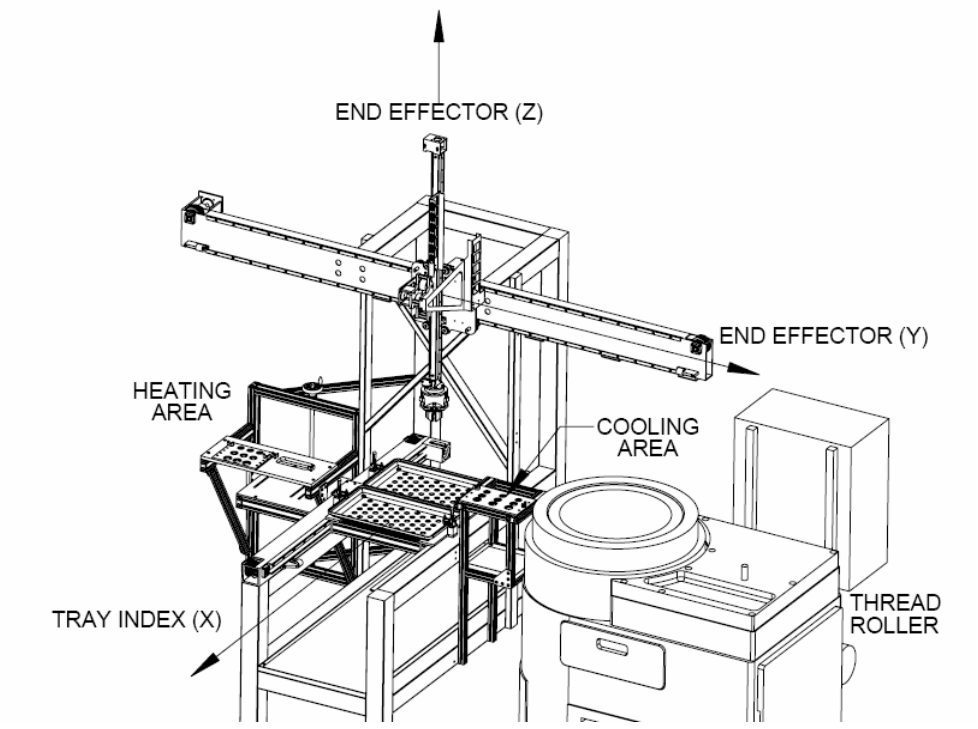

Figure 4.19 Automation system axes of motion

4.5.1 Main Frame

The main frame is a welded structure constructed primarily of 3/16" wall 3"x 3" mild steel tubing, shown in Figure 4.20. Two mounting flanges provide a mounting area for the long Y axis aluminum extrusion. These steel flanges are threaded instead of placing threads in the thin walled aluminum axis, as these mounting points support all forces produced by end effector motion. A large aluminum drip pan under the tray area catches any residual oil dripping from the parts when returned to the trays. An X brace stiffens the Y axis mounting area, as finite element analysis showed end of axis deflection to be unacceptable without this feature.

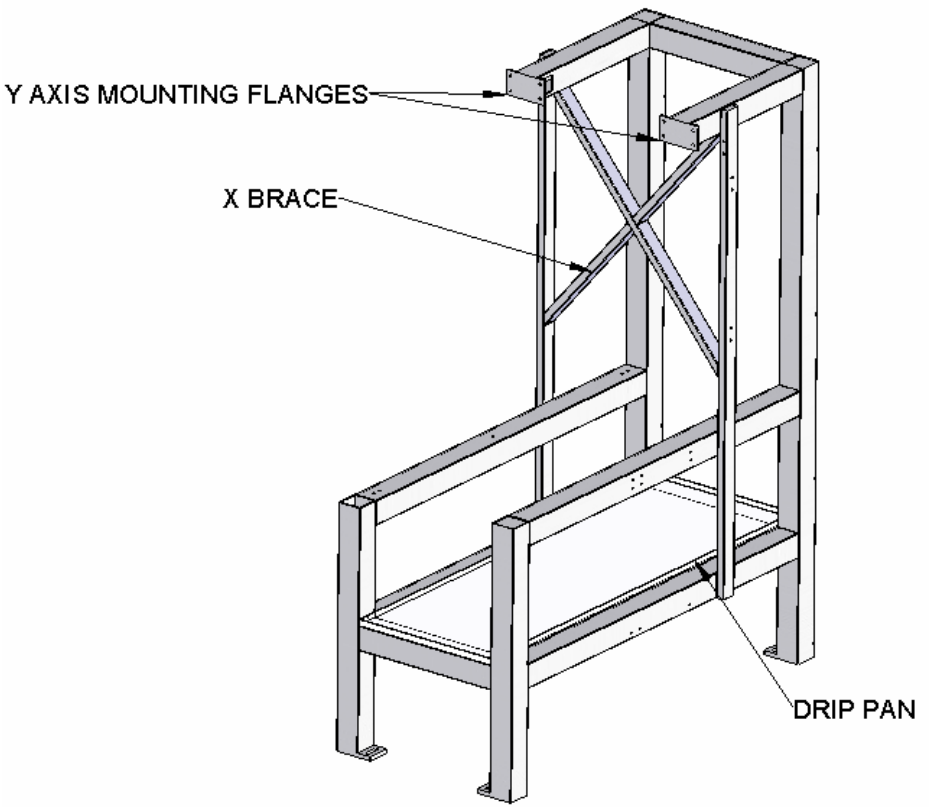

Figure 4.20 Welded steel main frame

4.5.2 Y and Z Axes

The Y and Z axes accomplish all end effector motion, and are shown below in Figure 4.21 with the gripping system attached to the bottom of the Z axis. This design was adapted from CAMotion's CRP-1000 pick and place robot, which is typically a 3 axis design. Motion is driven by Kollmorgen servomotors, and Parker Bayside gearboxes provide gear reduction for each axis. The motion of each axis is guided by Bishop-Wisecarver linear bearings, and Gates timing belts and pulleys provide power transmission to each axis. Typically this design features a theta drive enabling a wrist motion on the end effector. This feature was removed for the current application.

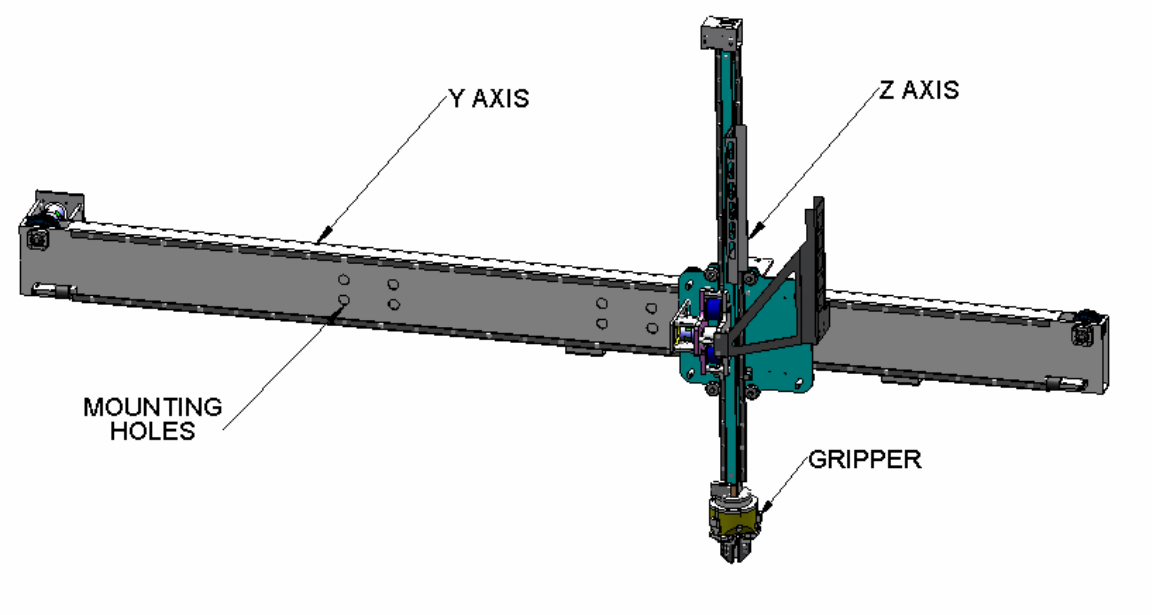

Figure 4.21 Y/Z axis assembly

4.5.3 Tray Drive

The tray indexing system for this application was adapted from CAMotion's CRP-1000 X axis assembly. It is shown below in Figure 4.22 with one tray mounted on the machine. Two dowel pins are present to locate each tray, utilizing the tray's steel locating feature developed in Chapter 3. To secure the trays to the machine, toggle clamps are used. This allows fast replacement by an operator during runtime. The left hand side of the drive is supported by the axis itself and a Rollon sliding bearing mounted on the axis, while the right hand side is supported by the steel welded frame and a Rollon sliding bearing mounted directly to the frame. The trays are driven by the same motor/gearbox/timing belt arrangement which drives the Y and Z axes.

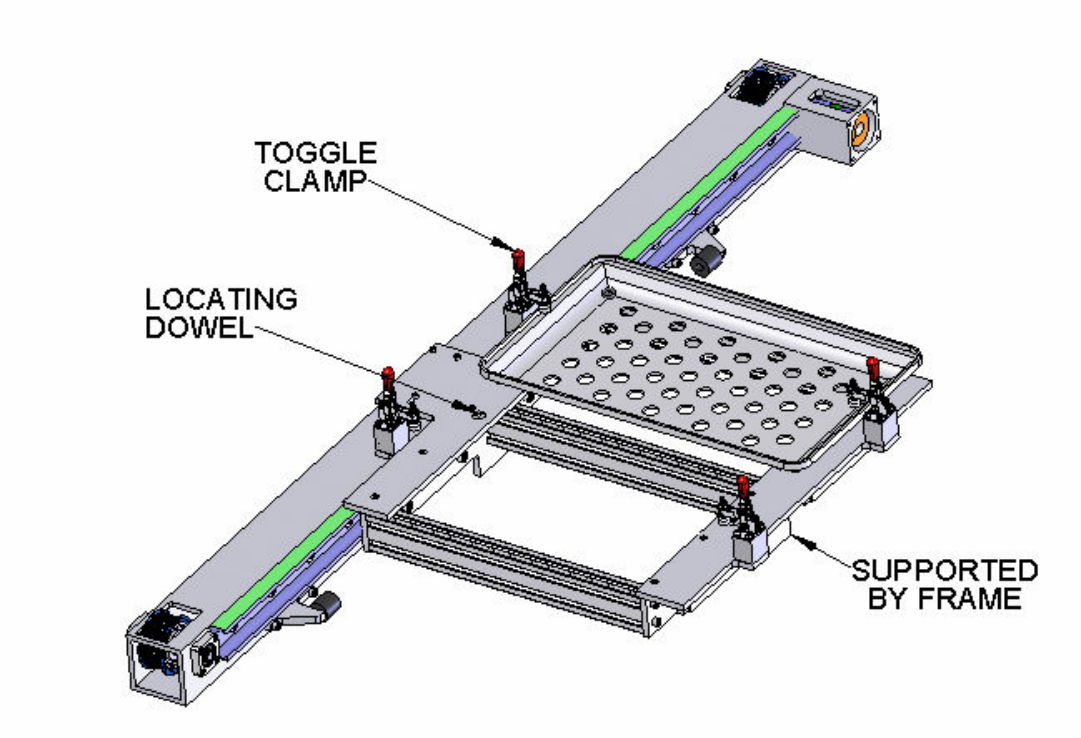

Figure 4.22 Tray drive assembly

4.5.4 Heating Frame

The heating frame was designed to bolt to the side of the main frame, and is constructed of modular 80/20 aluminum extrusion. This will allow easy redesign should an update to the heating process become necessary in the future. The frame is shown in Figure 4.23 with one heating unit in place, but has the capacity to hold two heating units, should one wish to use two heaters to aid long heat times in the future.

Parts near the induction coil were made from electrically nonconductive materials. The base plate is machined from Delrin, while the plates which will hold the heating parts were manufactured from machineable glass-mica ceramic. The machineable glass mica ceramic did not require firing and was machined using standard practices. It was chosen for its temperature resilience, since parts can be heated to over 600°F in this area. Nonconductive nylon bolts and wing nuts affix the ceramic plates to the Delrin base.

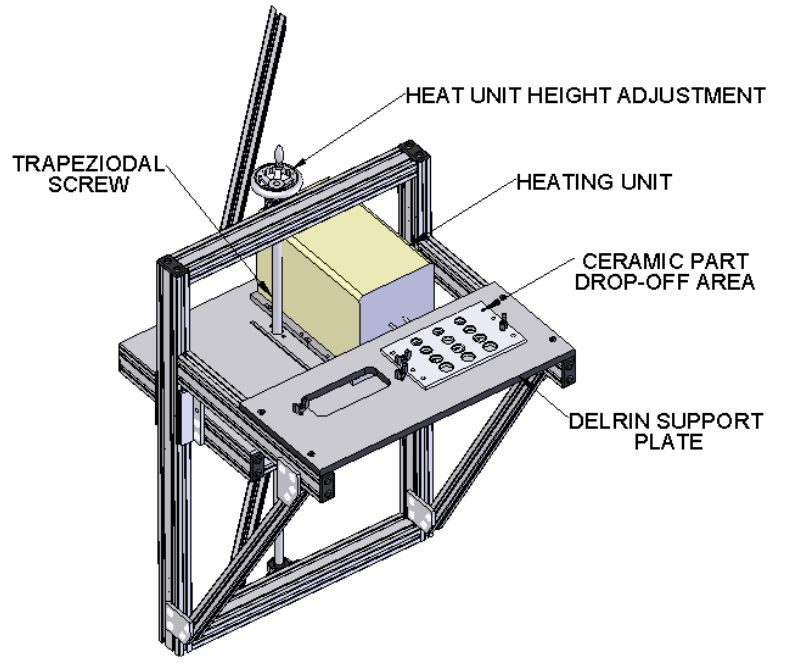

Figure 4.23 Heating subframe

The table which supports the heating unit can be adjusted vertically to compensate for different length fasteners hanging from the ceramic plate. The height adjustment handle rotates a trapezoidal screw which drives against a trapezoidal nut fixed to the table, also shown in Figure 4.23. Both ends of the trapezoidal screw are attached to the 80/20 frame and are supported by ball bearings.

The glass mica bolt plate shown in Figure 4.24 features a row of holes for each fastener size. The plate is indexed to the correct row during machine setup, and a second plate (not pictured) is used for sizes 3/4”-1”. The outer holes are used when the dual coil design is implemented, but the plate can be used with the heater’s existing single coil as well. This makes the functionality of the automation system independent of the dual coil. Should a situation arise where the dual coil is not usable, the automation can still function.

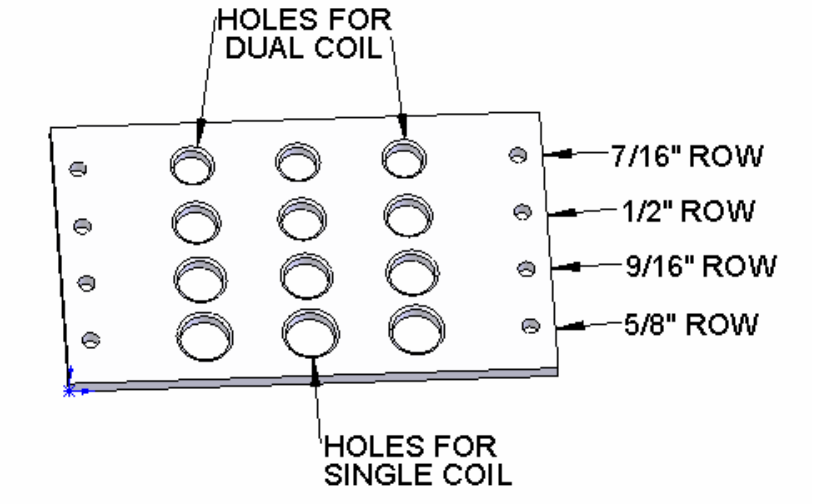

Figure 4.24 Ceramic bolt heating plate

4.5.5 Post Processing Area

The post processing area is similar in concept to that of the heating area, and is shown in Figure 4.25. It is modular in design and constructed from 80/20 aluminum extrusion. A plate similar to the ceramic plate on the heater contains holes for different part sizes, however this plate is made from aluminum. A drip pan beneath the placement points catches oil dripping from the parts after rolling. The drip pan's height is above that of the oil resevior in the thread roller, so should oil accumulate quickly in the pan, a drain can be run to the thread rolling machine to allow automatic drainback.

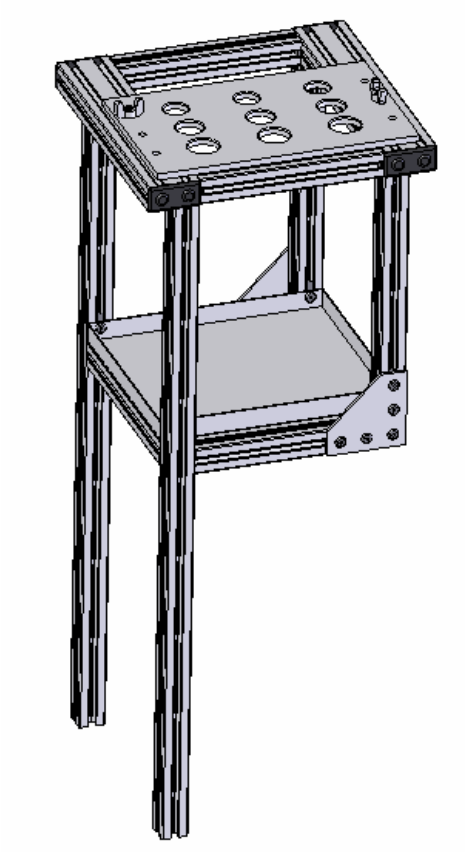

Figure 4.25 Post processing area

4.5.6 Alignment Issues

One drawback to the two degree of freedom approach is that the pick and place points must be precisely aligned under the plane of motion. A design for assembly methodology was employed to allow each station to be adjusted mechanically, to enable each pick and place point to be "zeroed" under the motion plane, as illustrated in Figure 4.26. The position of the trays under the plane of motion can be zeroed via the control software. Both the mechanical and software zeroing are part of the initial machine setup, and need only to be performed once. The system does not contain any type of vision system or closed loop method of dynamically adjusting placement points for simplicity.

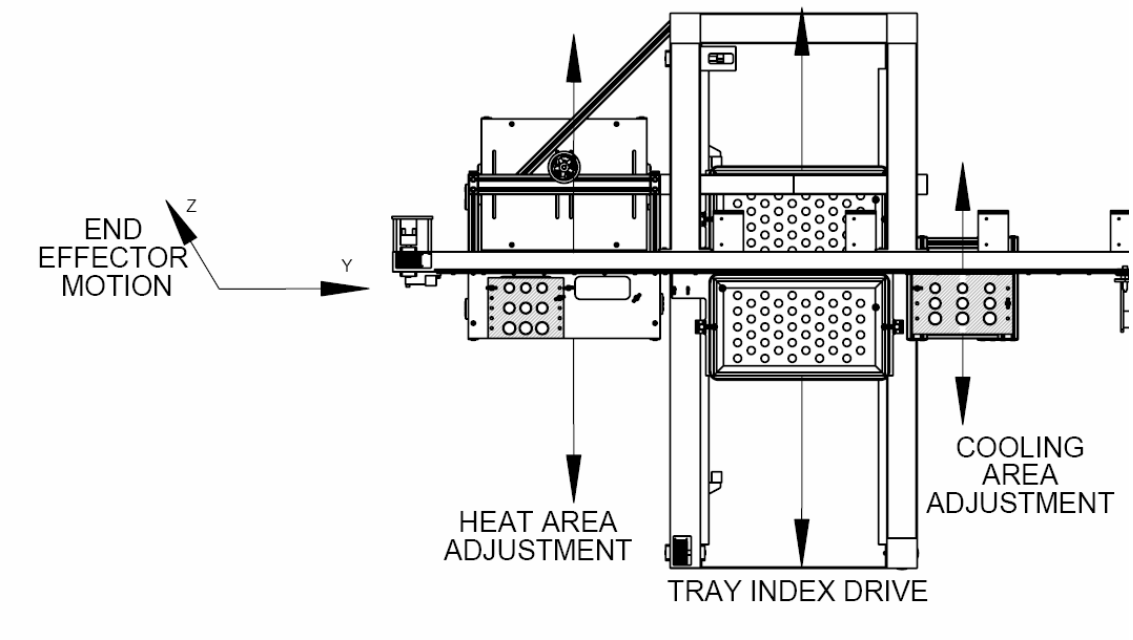

Figure 4.26 Adjustable design for assembly concept

4.5.7 Guarding Scheme

The guarding is also constructed out of 80/20 aluminum extrusion, shown below in Figure 4.27. The guarding is affixed to the main steel welded frame, and has doors which open to allow for machine setup and tray replacement. The doors over the thread roller are a clamshell design which folds back from the machine to allow complete access to the roller during setup. The operator interfaces with the machine through a touch screen, which can store automation setups by fastener part number.

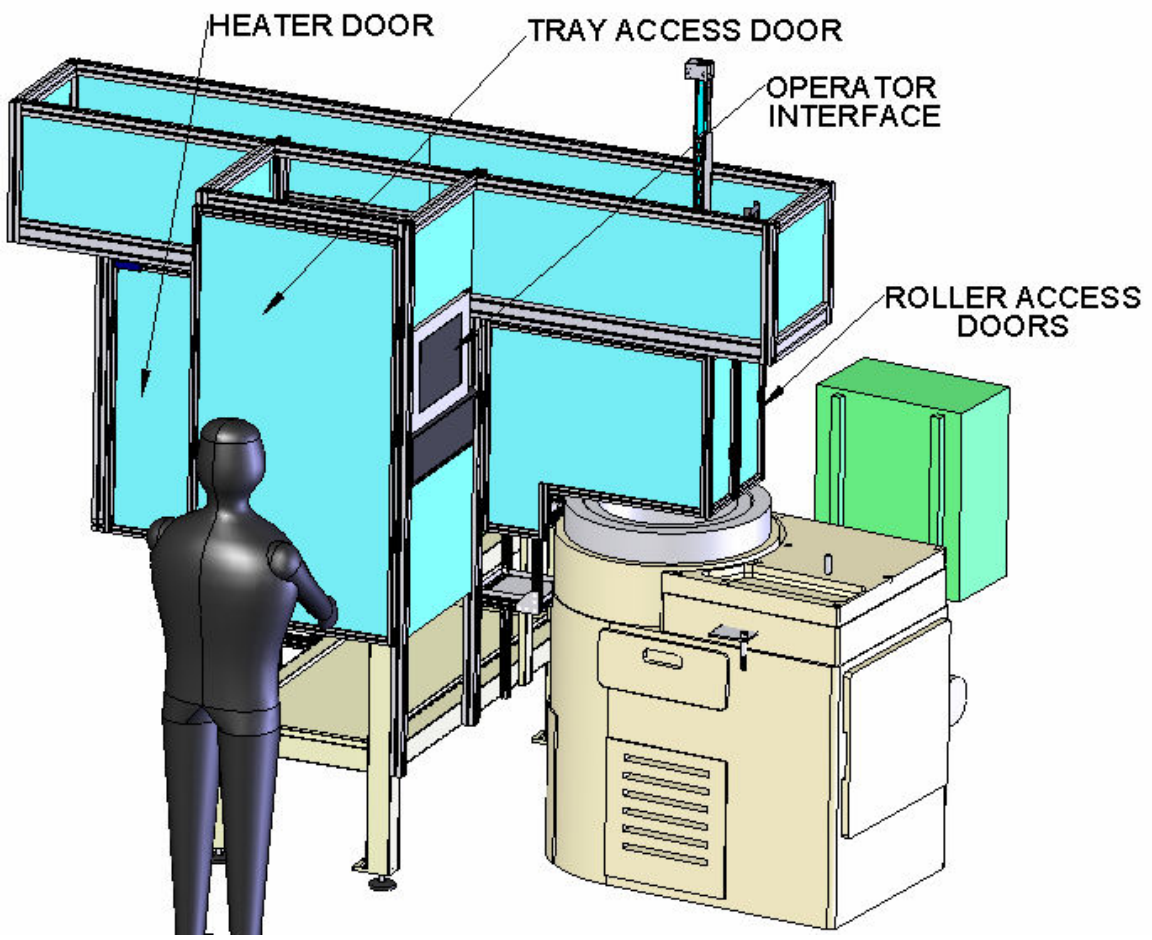

Figure 4.27 Machine guarding scheme

4.5.8 Sensing The Thread Roller's Position

In order for the automation system to function properly, knowledge of the roller's position in its cycle is required. Since the motion of the thread rolling dies is governed by the cam, a proximity sensor near the cam follower provides feedback. When the follower is beyond a certain threshold from the sensor, the dies have begun to open, and the automation senses it is safe to load a part. When this threshold is crossed again and the sensor returns a high logic signal, the automation senses that it is not safe to insert a part, and if a part is in the machine it is allowed to process.

4.6 Summary

This chapter followed the design process to develop an automation system with respect to the overall workcell plan developed in Chapter 2. A three cylindrical die thread roller was chosen for proof of concept of the automation system. Preliminary design work included establishing timing within the rolling process, which led to development and testing of a dual station induction heating coil.

Secondary timing studies dictated that the system should be capable of accommodating two transport trays as designed in Chapter 3. This capacity enables the machine to run for approximately 30 minutes unattended. Finally, the layout of the system was designed to utilize a two axis end effector motion. With this layout, the cycle time was predicted and found to be acceptable per the design requirements.

The gripper was designed around a Schunk PZB-100 base unit, with a central pneumatic cylinder to steady the workpiece when placed in the thread roller. The

gripping fingers were designed using a semicircular face to accommodate a variety of fastener styles. The remaining profiles of the gripping fingers were determined by various clearances throughout the system. 6061 Aluminum was chosen for the finger body, and the gripping faces were constructed of A-2 tool steel.

CAMotion, Inc. of Atlanta, GA was chosen as the robotic integrator, and the system was designed based on CAMotion's CRP-1000 pick and place machine. Other design decisions encountered included the development of a tray drive system, heating area, post processing area, and guarding scheme.

CHAPTER 5
GRASPING MODEL DEVELOPMENT

Thus far, gripper geometry has been established purely qualitatively. Development has stemmed from intuitive decisions based on the variety of part styles which will be grasped.

How well can the proposed gripper geometry be expected to perform? This question needs to be answered quantitatively, and is of concern in a variety of grasping applications. Many measures of performance can be predicted for a particular design. Clearly, the application dictates which criteria are of value to the designer.

5.1 Motivation for the Grasping Model

Since this application is essentially a peg-in-hole problem at each pick and place point, the issue of part alignment in the gripper merits further analysis. This particular gripping system must not only firmly grasp the part, but deliver it within a certain placement tolerance at each point. A grasp in which the part tip is unable to enter its destination hole can be considered a failed grasp.

5.1.1 Modes of Part Grasping

In this case it will be assumed that the placement tolerance of the automation system itself is adequate, thus leaving part alignment in the gripper as the only variable

which can adversely affect a grasp and move operation. In a general sense, close placement tolerances in a gripping system can be accomplished in two ways.
The first method of achieving close placement tolerances is to present the part in its fully oriented state to the gripper. This method assumes that during and after the grasp, there is no relative motion of the part in the gripper. Any errors in orientation will remain, and still be present when the part reaches its destination. This method in many cases requires the method of presenting parts to the gripper to be more complex.

A second methodology involves presenting parts to the gripper in a loosely oriented state, and using the grasping process to bring the part to its final state of orientation. Herein this will be defined as "self-alignment", when the part being grasped experiences relative motion during the grasping process, and the relative motion experienced moves the part in a manner such that the errors in part orientation are minimized to an acceptable level.

This method requires the part to be grasped to contain at least one reference feature, by which the part will be oriented relative to the gripper. Since motion relative to the gripper is present during this process, the coefficient of friction will clearly play an important role. Part geometry will also have a pronounced effect, since some parts may tend to "jam" rather than move when forces are applied.

5.1.2 Current Application

In the current application, it is desired to predict which regime of gripping will be present. This is useful analysis for the designer; if a self-aligning effect is anticipated, a

fairly tight placement tolerance can be enforced on the peg-in-hole problem at each pick and place point. If the gripper will not serve to self-align the part in a useful manner, the design of the system should present the part to the gripper with as little error as possible, or the peg-in-hole tolerance at each pick and place point should be relaxed.

As stated earlier, if the self-alignment principle is to be used, the part being oriented must have a reference feature by which the gripper will align the part. In the case of grasping fasteners using the proposed gripper design, the sides of the fastener head can be used, as shown in Figure 5.1. The underlying assumption in this case is that the side of the part head is parallel with the centerline of the part. If the part head seats correctly on the gripper face, the centerline of the part will be parallel to the gripper by default.

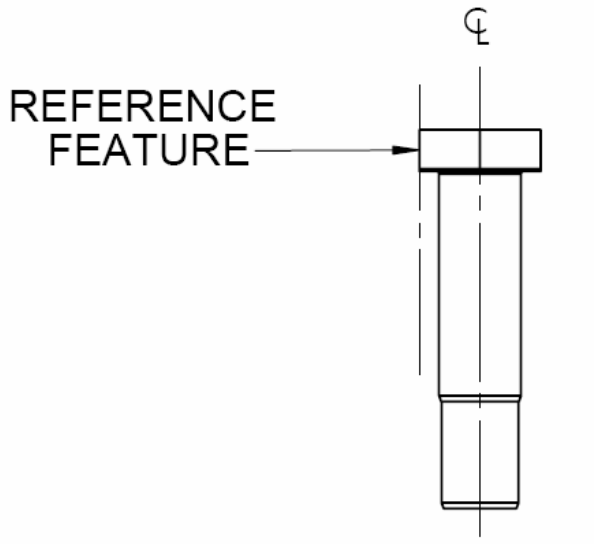

Figure 5.1 Example of part reference feature

The goal of the following analysis is to determine if a given part and gripper geometry will exhibit a beneficial self-aligning effect. If they will, under what conditions will this occur? Since there is a maximum error the gripper can correct during grasping, what is this maximum? Also, the effect of different coefficients of friction, as well as varying geometries of the part to be grasped, will be examined.

5.2 The Two Dimensional Case

A simple two dimensional case will first be examined to illustrate the approach to analyzing the self-alignment principle. This analysis assumes two parallel gripper jaws, which move in the direction of the arrows shown in Figure 5.2. The angle α in the figure represents the angular error in fastener orientation as it is being grasped. As is typical in much grasping analysis, quasi-static conditions will be assumed, neglecting any inertial effects.

Also, gravity is neglected in this case since the gravitational force is small compared with the grasping forces applied (the parts being grasped weigh approximately 1 pound, while the grasping force is approximately 40 pounds). The zero gravity assumption is not always valid; grasping heavy workpieces with a light grasp force will necessitate the inclusion of gravity in the model. In the case of a heavy workpiece / light grasp force, gravity's contribution to the force and moment sum becomes much more significant. Also, grasping workpieces in the horizontal position may necessitate inclusion of gravity, as the gravitational force acting on the workpiece's center of mass may provide a significant moment contribution in this configuration.

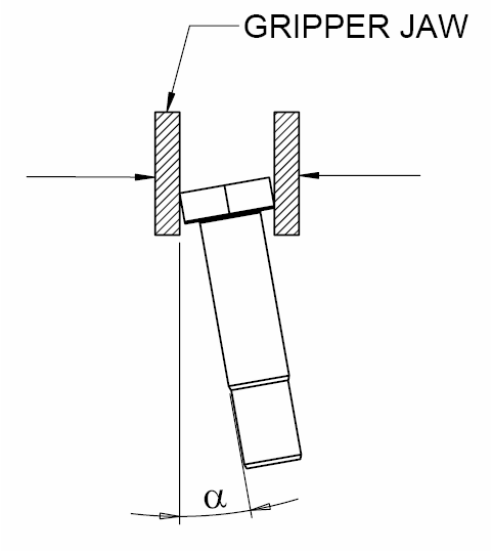

Figure 5.2 Part error in two dimensions

5.2.1 Two Dimensional Error Formulation

In this case, the part alignment error can only occur in one dimension. Note that α denotes the angular error in part alignment, with α=0 representing the desired orientation of the part. The α=0 case occurs when the reference feature on the part, namely the side of the bolt head, is aligned with the gripper jaw.

Knowing the dimensions of the bolt and μ_s, the coefficient of static friction, the conditions under which relative motion on the gripper surface is expected can be computed. This will involve a simple equilibrium analysis. Dimensions of the part and dimensions needed for the force balance are shown in Figure 5.3 and Figure 5.4.

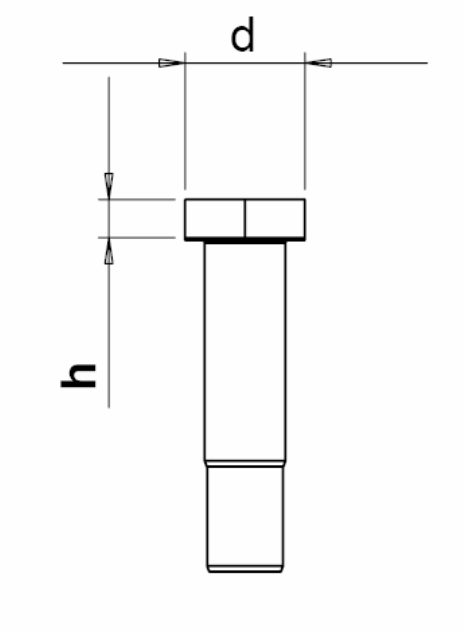

Figure 5.3 Part dimensions for 2D analysis

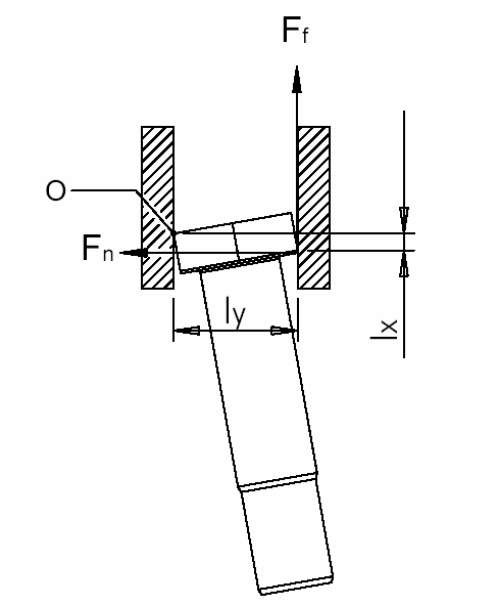

Figure 5.4 Dimensions for 2D force and moment balance

$$\begin{aligned} \sum M_o &= F_f l_y - F_n l_x \\ Ff &= \mu F_n \\ \therefore l_x &= \mu l_y \end{aligned} \tag{5.1}$$

Summing moments about point O in Figure 5.4 yields the equations listed above. Relationships between α and l_x and l_y are developed from simple geometry. Combining these relationships yields the desired result:

$$\alpha_{\max} = \tan^{-1}\left[\frac{\frac{h}{d} - \mu}{\frac{\mu h}{d} + 1}\right] \tag{5.2}$$

α_{max} denotes the maximum angular error from which the part will experience relative motion and self-align in the gripper. Note that the applied gripping force does not appear in this equation. This is due to the fact that the result deals with a ratio of the normal and frictional forces. As the applied gripping force is increased, the reaction frictional force increases linearly as well. The only factors affecting the alignment error tolerance are the coefficient of static friction, and the height to diameter ratio of the part.

5.2.2 Two Dimensional Results

This simple analysis yields intuitive results shown in Figure 5.5. Even in the absence of friction, there is a maximum error from which self-alignment will occur. This is due to the geometry of the part. Note that in the case where h/d=1, where the bolt head

is a square shape, 45 degrees is the maximum allowable angle in the absence of friction. This is logical, since a square part turned 45 degrees in the gripper would yield both vertices of contact horizontally aligned with each other, with no resultant moment to induce part motion. As friction increases, the maximum allowable error further decreases from this value of α.

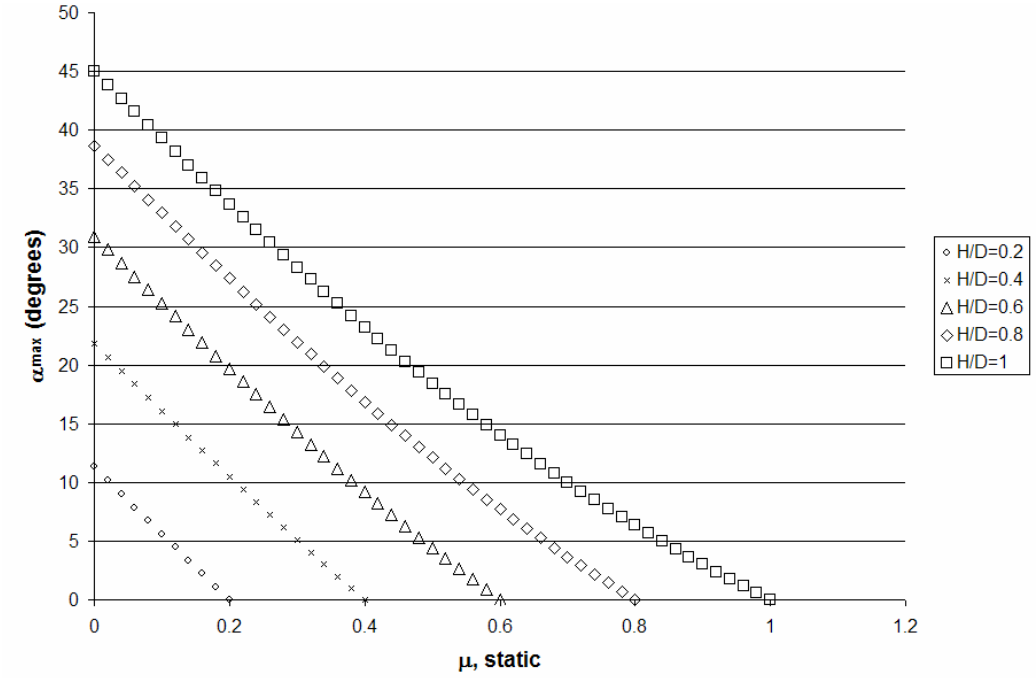

Figure 5.5 Results for 2D error analysis

This first pass analysis leads to the conclusions that for part alignment to occur, the coefficient of friction and part geometry must be within specified bounds. Long, slender parts with a high *h/d* ratio are more likely to self align, as are parts which have a low value of μ at the gripper to part interface. It will be shown in Chapter 7 that these

underlying design guidelines remain true in the more complex three-dimensional case as well.

5.3 The Three Dimensional Case

The three dimensional case is much more interesting to analyze, and presents a new set of challenges. First, part error is no loner restricted to one dimension. The part can now be rotated about any of its three axes, as shown below. Therefore the solution will not be a maximum angle from which the part can be corrected, but rather a solution space or combination of angular errors from which the part can be aligned. In the three dimensional case, the gripper faces must also be modeled to represent their actual profile, rather than the simplified flat case used in two dimensions.

5.3.1 Three Dimensional Approach

The approach for three dimensions will proceed as follows. Given the part and gripper dimensions and a combination of angular errors, the point of contact on each gripper face will be determined. With knowledge of these points of contact, the unit vectors for the forces in question will be calculated. An equilibrium analysis in three dimensions will yield the unknown values of these forces for the particular combination of errors under consideration. Once all forces are known on each gripper face, the *minimum* value of μ that would prevent part motion on each interface can be computed. If the actual value of μ_s at the interface in question is less than the minimum value

required to prevent motion, it will be assumed that there will be relative motion at that point. The direction of relative motion can be determined by the direction of the frictional force at each interface. Criteria will then be established to determine which combinations of relative motion yield desirable part alignment. This process will be repeated for the next combination of angular errors, and a solution space will be assembled in a point by point manner. A summary of the algorithm is given in Figure 5.6.

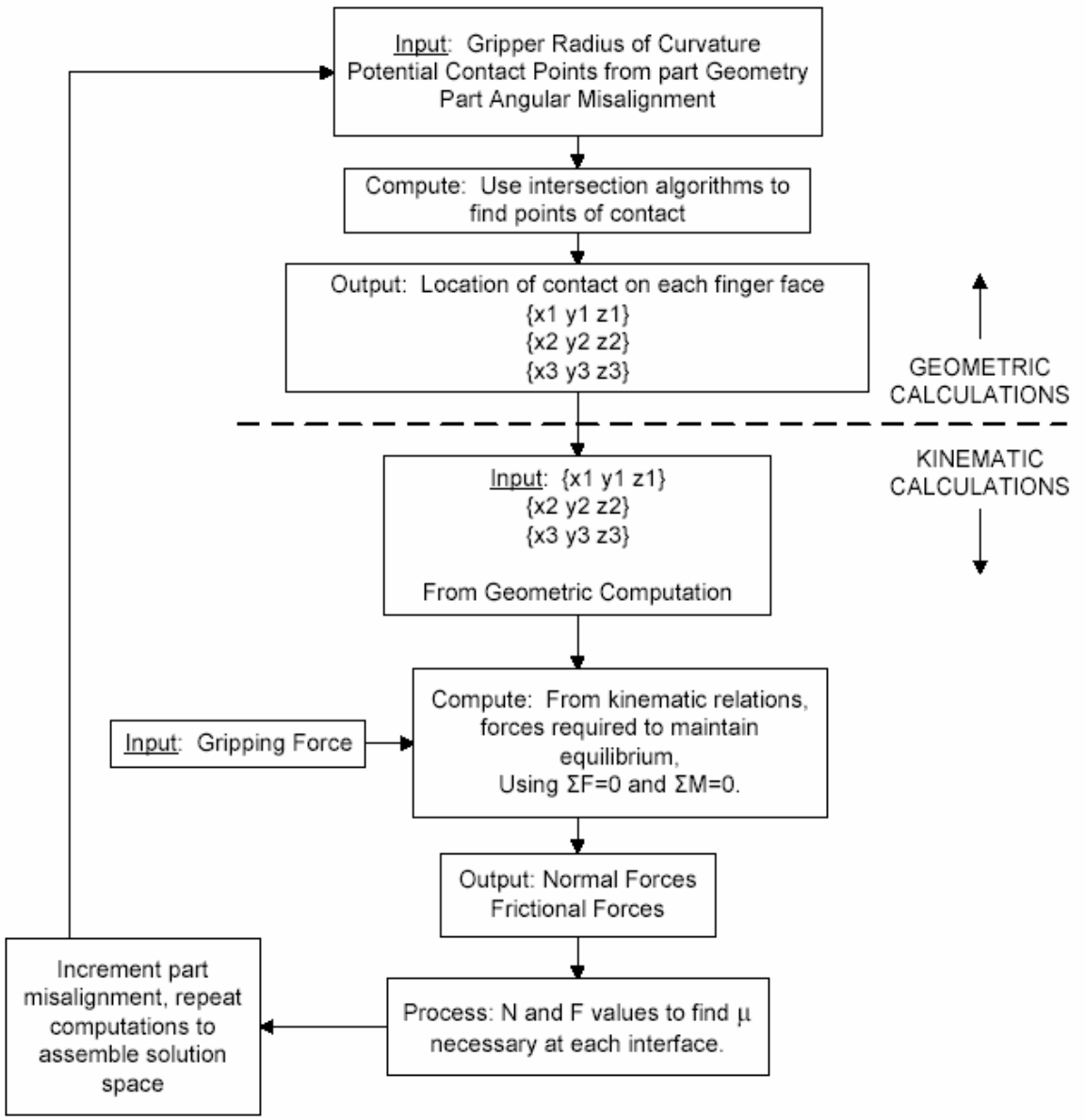

Figure 5.6 Three dimensional analysis flow chart

5.3.2 Three Dimensional Error Description

It is possible to induce angular errors about three axes in the part's coordinate system (with axes X_p, Y_p, and Z_p), as shown below in Figure 5.7. In this particular case, a rotation about the Z_p axis cannot be considered an error, since no effort has been made to orient the parts about this axis. It is also inconsequential to the pick and place process whether or not the part is rotated about the Z_p axis. The solution space in which the part will self-align however will likely be a function of this rotation about the Z_p axis, so it must be considered. A rotation about the Z_p axis will be treated as an initial condition rather than an error itself. The analysis will be concerned with combinations of angular errors about the X_p and Y_p axes.

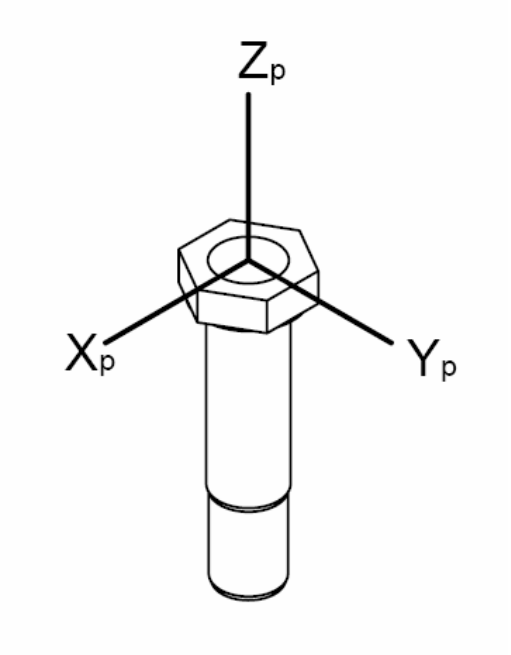

Figure 5.7 Part axes in 3D

5.3.3 Representing the Gripper Faces

Since the gripper faces are of a semicircular design, it is natural to model them as a continuous surface. Figure 5.8 shows a *bottom* view of the gripper. Note that the three gripper fingers are each separated by 120 degrees, and the internal design of the gripper dictates that each finger is opened an equal amount from the origin at all times. The gripper is represented with respect to a global coordinate system, with axes X, Y and Z.

Each finger can be represented by a cylinder in three dimensions, even though the face is only a portion of the cylinder. Note that each cylinder will have one degree of freedom, to move along the axis of motion of the finger it represents. As each finger closes, the center of each cylinder will move further from the origin. Finger 1's cylinder moves directly on the X axis, while fingers 2 and 3's representative cylinders move on axes that are 120 degrees from the X axis.

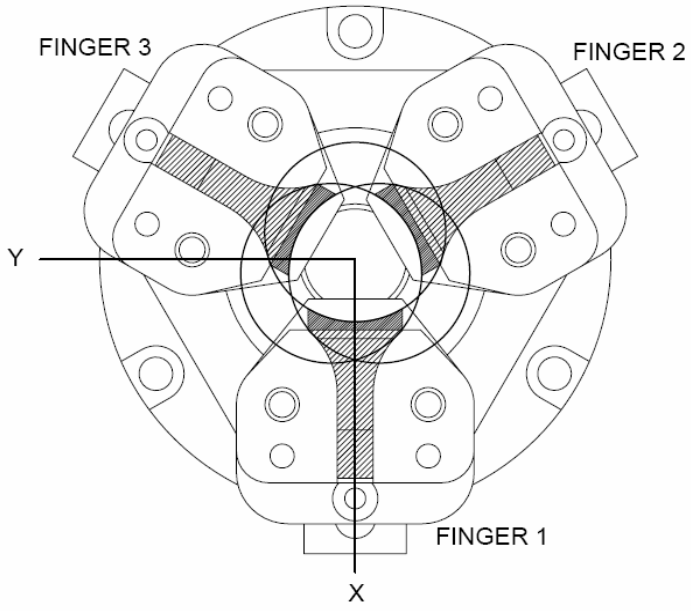

Figure 5.8 Gripper and representative geometry

Figure 5.9 shows the representation of the gripper which will be used for all further analysis. This is a view from the *top* of the gripper looking down. Note that each cylindrical surface has a radius R_g, which is equal to the radius of curvature of each gripper face. Dimension d_g represents the distance each gripper finger is open along its axis of motion.

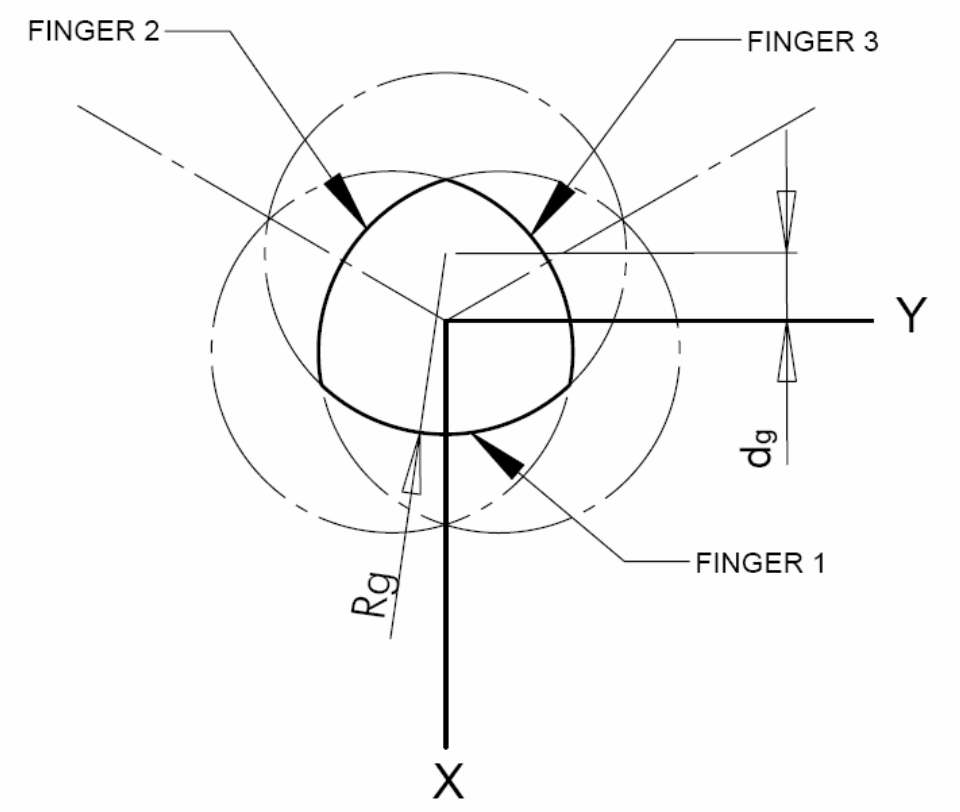

Figure 5.9 Analysis geometry with relevant dimensions

The following equations will be used to represent the gripper faces. Note that no restriction is placed on Z, since it is assumed that each finger has adequate depth to contact the part in all error configurations.

$$\text{Finger 1: } \left(x + d_g\right)^2 + y^2 = {R_g}^2 \tag{5.3}$$

$$\text{Finger 2: } \left(x - d_g \sin(30)\right)^2 + \left(y - d_g \cos(30)\right)^2 = {R_g}^2 \tag{5.4}$$

$$\text{Finger 3: } \left(x - d_g \sin(30)\right)^2 + \left(y + d_g \cos(30)\right)^2 = {R_g}^2 \tag{5.5}$$

5.3.4 Representing the Parts to be Grasped

Mathematically representing the part to be grasped presents a different set of challenges. A robust method is desired, since a variety of parts will ideally be grasped with one set of gripper jaws. In the example of a hexagonal (hex) shaped part, it would be quite difficult to represent the surface to be gripped with continuous equations. For spline shaped or twelve point parts, this method would also prove to be difficult.

Since the interest of this analysis lies in finding the points of contact, it is not necessary to represent the entire surface. In the example of the hex shaped part, the only possible points of contact are on the tips of each hex feature. This argument holds since the gripper surface is concave, therefore it can never contact the part along the flat surfaces between the hex points. In this case, the contact surface of the hex bolt can be modeled as 12 discrete possible points of contact, 6 for the upper surface of the bolt and 6 for the lower surface. This method is very flexible, since a part of any configuration can

easily be represented by a number of discrete possible points of contact. If a continuous surface such as a cylinder is to be represented as the part to be grasped, the number of points can be increased to approximate this continuous surface. The input to this portion of the analysis will be the coordinates of each of *n* possible points of contact, when the part is in its initial state with no error induced. These coordinates are with respect to the part axes, X_p, Y_p and Z_p.

$$points = \begin{bmatrix} x_1 & x_2 & \dots & x_n \\ y_1 & y_2 & \dots & y_n \\ z_1 & z_2 & \dots & z_n \end{bmatrix} \tag{5.6}$$

5.4 Geometric Calculations

The task of representing both the part and gripping faces is now complete. It is now desired to determine which contact points will touch each gripper face, and where exactly on each face this contact occurs. These calculations will be purely geometric in nature. No kinematic analysis or knowledge of coefficients of friction is needed at this point in the analysis.

5.4.1 Inducing Error

Since the possible points of contact are modeled in a discrete manner, it is easy to apply a rotation about any number of axes with a series of rotation transformations. The

points of contact will be specified in the part coordinate system described above, with Z_p=0 representing the center of the part area to be grasped. The part coordinate system is initially coincident with the global coordinate system before any error is applied. Rotation transformations are applied to move the part coordinate system with respect to the global coordinate system. Rotation transformations must be applied carefully, in order to produce symmetric error results at each gripping face. Simply applying two rotations about the X_p then Y_p axes will not produce the results expected, since applying a series of rotation transformations can produce subtle differences in final point position when rotation angles become large.

The rotation transformations are applied in a manner consistent with a rotation about an arbitrary axis (Ginsberg 1998). First, the part coordinate system is temporarily rotated about its Z_p axis, to make the X_p axis coincident with the arbitrary axis about which the error rotation is desired. The error rotation about X_p rotation is then applied, followed by the inverse of the Z_p rotation to "undo" the initial temporary rotation. In this way, error can be induced in two dimensions, but only one rotation transformation actually induces the error. This ensures that the error is consistently applied regardless of the direction the part is moved with respect to the coordinate axes. The coordinates of the possible points of contact are now known with respect to the global coordinate system.

$$[R_x] = \begin{bmatrix} 1 & 0 & 0 \\ 0 & \cos\theta_x & \sin\theta_x \\ 0 & -\sin\theta_x & \cos\theta_x \end{bmatrix} \tag{5.7}$$

$$[R_z] = \begin{bmatrix} \cos\theta_z & \sin\theta_z & 0 \\ -\sin\theta_z & \cos\theta_z & 0 \\ 0 & 0 & 1 \end{bmatrix}$$

$$R_t = [R_z]^T R_x R_z \tag{5.8}$$

$$Points_{witherror} = [R_t]^T \, Points \tag{5.9}$$

5.4.2 Determining Points of Contact

The discrete representation of the part is now in its desired state of error. The next task is to determine which points will make contact with the gripper, and where exactly on each gripper face this will occur.

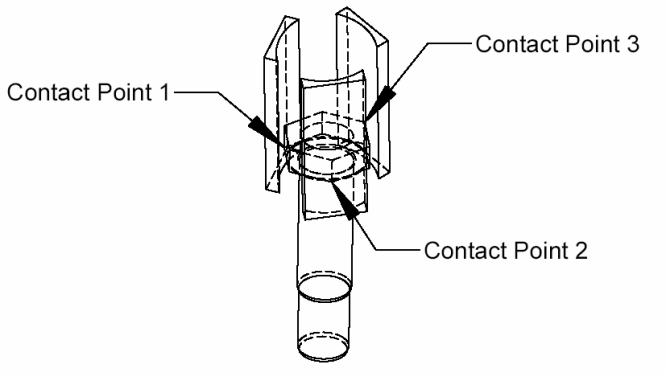

Figure 5.10 Contact points in 3D

An assumption this analysis will make is that only one point of contact will be made on each gripper face. This will greatly simplify the kinematic analysis, as shown in later sections. Also, the scenario where two points of contact are present on each gripper face can be considered a distinct line in the overall solution space, a very specific set of scenarios encountered infrequently compared to the single point of contact case. While using the present approach it is not possible to obtain the solution under multiple point contact, it can be shown where in the solution space these conditions exist.

The algorithm for determining which discrete point will contact each gripper face is as follows. It is known that each gripper face can only move parallel to its axis of motion. This fact can be used to readily determine which point will make contact first. In Figure 5.11, Finger 2 is shown with three possible points of contact, A, B and C. The gripper finger is represented by the dark black surface, and moves along the motion axis in the direction of the arrows shown. Clearly, point B will be the first to make contact. The distance the gripper must move to make contact with any point is given by the distance from the point, along a line parallel to the axis of motion, to the gripper face. This distance is labeled as "distance to contact" in the case of point B. The point which has the least distance to contact will make contact first, and is the desired result. Care must be taken to choose the correct solution for the intersection of the parallel line and the circle, since the system of equations will yield two solutions for each case.

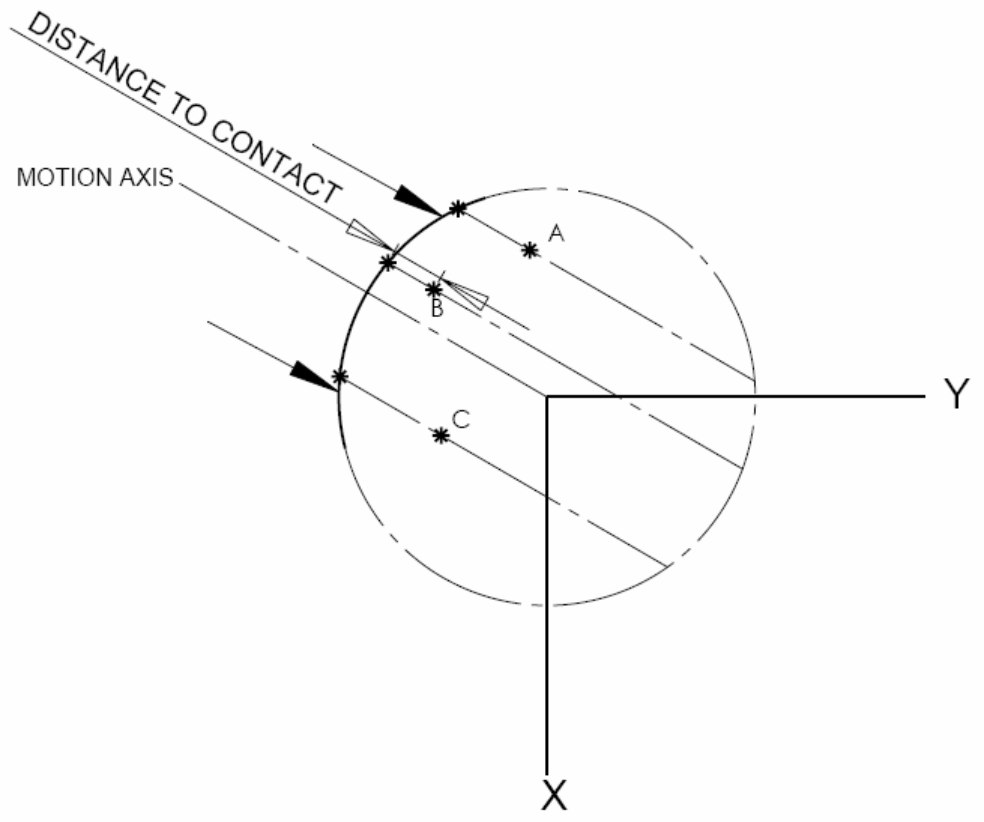

Figure 5.11 Determining points of contact

Lines parallel to each axis of motion are given by the following. The value of *b*, the *y* intercept, will be dictated by the *x* and *y* values of the point being considered.

$$\text{Finger 1:} \quad y = b \tag{5.10}$$

$$\text{Finger 2:} \quad y = \cot(30)x + b \tag{5.11}$$

$$\text{Finger 3:} \quad y = -\cot(30)x + b \tag{5.12}$$

The intersection of each gripping face and each of these lines is given by equating the formula representing each gripping surface with Equations (5.10)-(5.12). For these calculations, the gripper opening is taken to be d_g=0 for simplicity. This has no effect on the final result, since the radius of each gripper face is larger than the part to be grasped by design. x_c and y_c denote the points on the circle intersected by the line parallel to the axis of motion through the point under consideration, and x_p and y_p denote the discrete points under consideration. Values of the y intersect, b are computed from Equations (5.10)-(5.12). The results are the following, for fingers 1, 2 and 3 respectively.

$$\begin{aligned} x_{1c} &= \sqrt{R_g{}^2 - y_p{}^2} \\ y_{1c} &= y_p \end{aligned} \tag{5.13}$$

$$\begin{aligned} x_{2c} &= \frac{-2\cot(30)b - \sqrt{4\cot^2(30)b^2 - 4(1+\cot^2(30))(b^2 - R_g{}^2)}}{2(1+\cot^2(30))} \\ y_{2c} &= -\sqrt{R_g{}^2 - x_{2c}{}^2} \end{aligned} \tag{5.14}$$

$$\begin{aligned} x_{3c} &= \frac{2\cot(30)b - \sqrt{4\cot^2(30)b^2 - 4(1+\cot^2(30))(b^2 - R_g{}^2)}}{2(1+\cot^2(30))} \\ y_{3c} &= \sqrt{R_g{}^2 - x_{3c}{}^2} \end{aligned} \tag{5.15}$$

Once the values of x_{nc} and y_{nc} are calculated, a simple application of the distance formula will show the travel distance needed by each gripper finger to make contact with the point being considered. This calculation is repeated for all combinations of gripper faces and points, and the point with the smallest travel distance for each gripper face recorded.

5.4.3 Final Geometric Calculations

Two final issues must be resolved before kinematic analysis can begin. It has been determined for each gripping face which discrete point on the part will contact the face in question. However, the value of d_g, the amount each gripper finger is open, is still not known. Also, a possibility exists that upon grasping, that the center of the part may not remain exactly at the origin after the grasp. This possible part offset in the XY plane can be designated by two variables, o_x and o_y, as shown in Figure 5.12. The origin of the part coordinate system will be coincident with this shifted origin location.

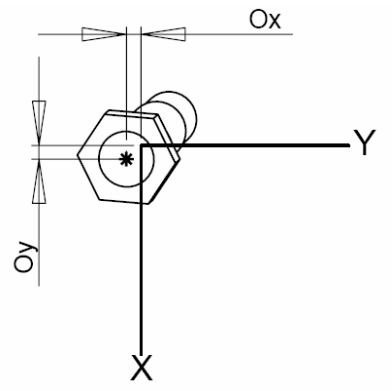

Figure 5.12 Determining part offset

Using the equations for each gripper face developed previously, and allowing for an offset of each discrete point in the X and Y directions yields the following results. x_{pn} and y_{pn} represent the discrete point found to contact finger n in the previous step.

$$\text{Finger 1: } \left(x_{p1} + o_x + d_g\right)^2 + \left(y_{p1} + o_y\right)^2 = {R_g}^2 \tag{5.16}$$

$$\text{Finger 2: } \left(x_{p2} + o_x - d_g \sin(30)\right)^2 + \left(y_{p2} + o_y - d_g \cos(30)\right)^2 = {R_g}^2 \tag{5.17}$$

$$\text{Finger 3: } \left(x_{p3} + o_x - d_g \sin(30)\right)^2 + \left(y_{p3} + o_y + d_g \cos(30)\right)^2 = {R_g}^2 \tag{5.18}$$

These three equations are solved for three unknowns, o_x o_y and d_g. With this knowledge, a full three dimensional description of the contact problem is known.

5.5 Kinematic Calculations

The problem now moves from a purely geometric realm to one involving the kinematic descriptions desired. The approach will proceed as follows. Three forces will be defined at each contact point. Using knowledge of the contact location and geometry of each gripper finger, the unit vector for each unknown force can be computed. This will result in 9 unknown force magnitudes. Summing forces and moments in each of three dimensions will produce 6 equations, leaving the solution underdetermined. Knowledge of the applied gripping force will be used to add a constraint at each finger,

thus leading the system to a unique solution. As in the two dimensional case, quasi-static conditions will be assumed and gravity neglected, for reasons discussed in section 5.2.

5.5.1 Determining Unit Vectors

Each point of contact (x_{pn}, y_{pn}, z_{pn}) can have three forces acting upon it. These are a normal force normal to the gripping surface, a tangential frictional force tangential to the gripping surface, and a frictional force in the z direction. The unit vectors acting in these directions are illustrated for the example case of finger 1 in Figure 5.13. These vectors are defined with respect to the global coordinate system.

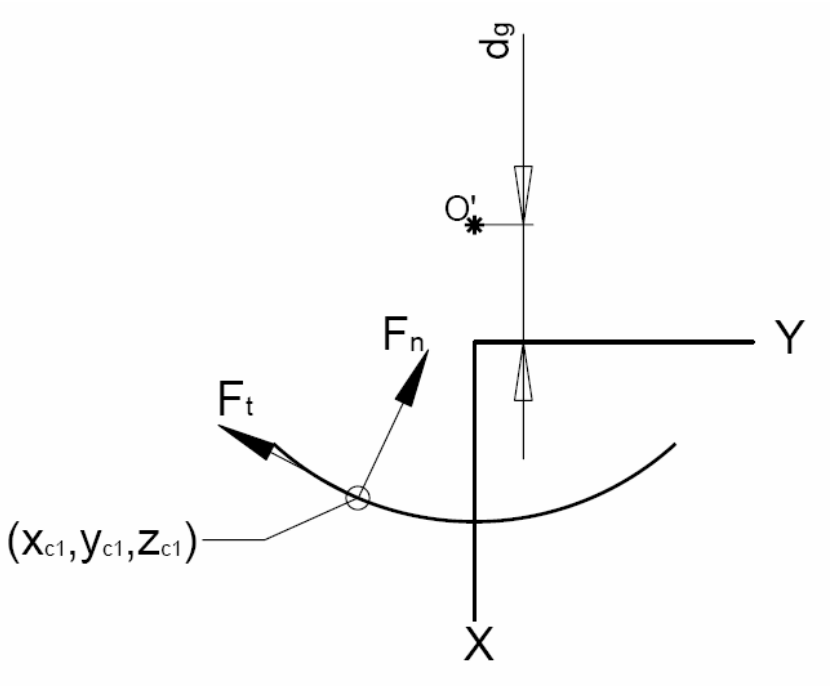

Figure 5.13 Normal and tangential unit vectors

5.5.2 Unit Normal Vectors

The direction of each normal vector is intuitive to derive. Since each gripping surface is circular, the normal force must act toward the center of each finger's radius of curvature. The amount of opening of each finger's representative cylinder, $d_{g,}$ is known, so the vector connecting the contact point and the center of curvature can be calculated. To obtain each unit normal vector, this result is divided by the length from contact point to center of curvature, which is always the gripper radius R_g. The results, for each finger, are as follows.

$$\text{Finger 1:}\quad \hat{e}_{n1} = \frac{-\left(d_g + x_{p1}\right)}{R_g}\hat{i} - \frac{y_{p1}}{R_g}\hat{j} \tag{5.19}$$

$$\text{Finger 2:}\quad \hat{e}_{n2} = \frac{\left(d_g \sin(30) - x_{p2}\right)}{R_g}\hat{i} + \frac{\left(d_g \cos(30) - y_{p2}\right)}{R_g}\hat{j} \tag{5.20}$$

$$\text{Finger 3:}\quad \hat{e}_{n3} = \frac{\left(d_g \sin(30) - x_{p3}\right)}{R_g}\hat{i} - \frac{\left(d_g \cos(30) + y_{p3}\right)}{R_g}\hat{j} \tag{5.21}$$

5.5.3 Unit Tangent Vectors

The direction of each tangent vector is not as easily computed from the known geometry. Knowledge of the normal vector however is all that is needed to compute the unit tangent vector, using the properties represented in the equations of (5.22).

$$\hat{e}_t \cdot \hat{e}_n = 0$$

$$\sqrt{e_{tx}{}^2 + e_{ty}{}^2} = 1 \tag{5.22}$$

Two properties of unit vectors will be employed, namely that the dot product of the normal and tangential vectors is zero, and the magnitude of the tangential vector must by definition be 1. Derivation as described leads to:

$$e_{ty1} = \sqrt{\frac{1}{1 + \frac{y_{p1}{}^2}{\left(d_g + x_{p1}\right)^2}}}$$

Finger 1:

$$e_{tx1} = \frac{-y_1}{\left(d_g + x_1\right)} e_{ty1} \tag{5.23}$$

$$\hat{e}_{t1} = e_{tx1}\hat{i} + e_{ty1}\hat{j}$$

$$e_{ty2} = \sqrt{\frac{1}{1+\frac{\left(d_g \cos(30) - y_{p2}\right)^2}{\left(d_g \sin(30) - x_{p2}\right)^2}}}$$

Finger 2:

$$e_{tx2} = \frac{-\left(d_g \cos(30) - y_2\right)}{\left(d_g \sin(30) - x_2\right)} e_{ty2} \tag{5.24}$$

$$\hat{e}_{t2} = e_{tx2}\hat{i} + e_{ty2}\hat{j}$$

$$e_{ty3} = \sqrt{\frac{1}{1+\frac{\left(d_g \cos(30) + y_{p3}\right)^2}{\left(d_g \sin(30) - x_{p3}\right)^2}}}$$

Finger 3:

$$e_{tx3} = \frac{\left(d_g \cos(30) + y_3\right)}{\left(d_g \sin(30) - x_3\right)} e_{ty3} \tag{5.25}$$

$$\hat{e}_{t3} = e_{tx3}\hat{i} + e_{ty3}\hat{j}$$

5.5.4 Determining Forces

It is now known in which direction all forces at each interface act. The unknown quantities are the magnitudes of each force. Once these magnitudes are known, the analysis will be complete, with the only remaining task being to interpret the results.

This system in its current state has 9 unknowns, three force magnitudes at each of three contact points. Simply summing moments and summing forces will only lead to six

equations, which results in an underdetermined system. Also, no provision has been made for an input of the gripping force applied. It was shown in the two dimensional analysis that the applied gripping force did not impact the final result, and it will be shown the same is true for the three dimensional case. However, since the magnitudes of the computed forces may be of interest in later analysis, it is desired to include force applied by the gripper itself. This inclusion, when done correctly, will also overcome the problem of the underdetermined system. The following notation will be used:

N_1, N_2, N_3 - Normal forces
F_{t1}, F_{t2}, F_{t3} - Tangential frictional forces
F_{z1}, F_{z2}, F_{z3} - Z direction frictional forces

5.5.5 Gripping Force Input

The system of equations in its current state contains nine unknowns, however summing forces and moments in three dimensions will only yield six equations. Fortunately, the applied gripping force can be computed from the pneumatic pressure applied to the gripper, and the direction in which the gripping force is applied is known. This knowledge can be used to find six of the nine forces desired.

The gripping force is given as a function of line pressure and finger length by the gripper manufacturer in Figure 5.14. As finger length increases, the applied force per finger decreases due to an increased moment on the sliding surfaces of each finger's guidance track. The finger length in this application is approximately 70 mm, so a gripping force of 800 N is expected for a line pressure of 87 psi.

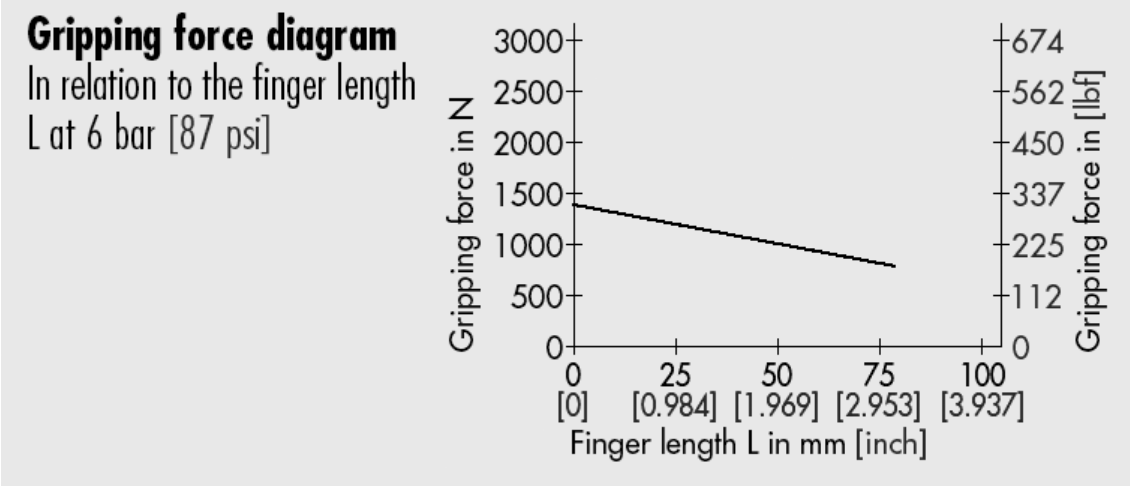

Figure 5.14 Gripping force relationships (provided by Schunk, Inc. for Schunk PZB-100)

Since this application must take care not to damage any part features, the gripper will typically be operated at pressures less than the maximum recommended. Also, it will be assumed that since the gripper is powered by a pneumatic cylinder drive, the applied force will decrease linearly with line pressure. Testing was conducted at a pressure of 40 psi, yielding a force per finger of 367N per finger with the linear force assumption.

With knowledge of the force magnitude, a free body diagram is used to find the unknown forces in question. Two of the gripping fingers and the part being grasped are treated as a rigid body, and the third gripping finger is replaced by its reaction forces (Figure 5.15). The unit vectors are known from calculations in previous sections.

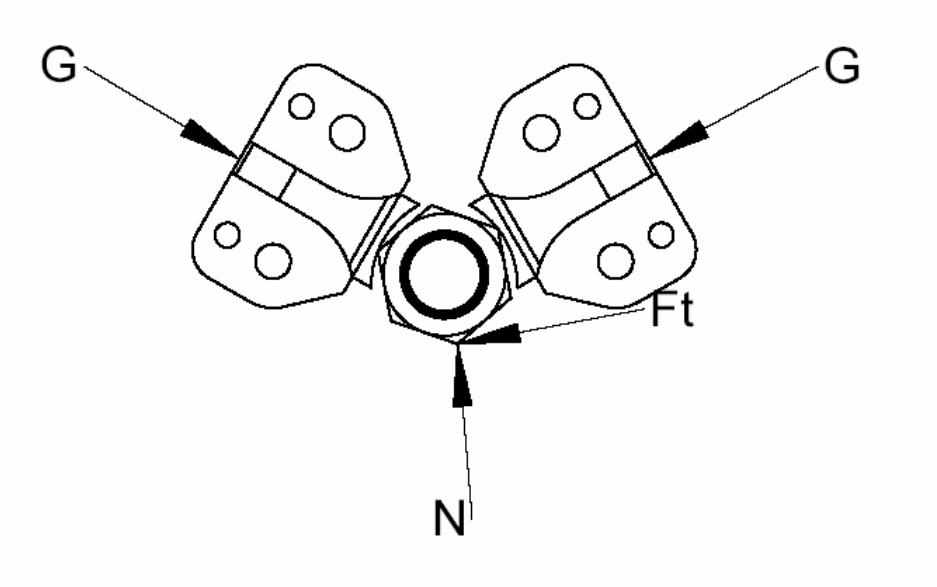

Figure 5.15 Free body diagram for relating gripping forces

The force sum yields equations (5.26)-(5.28). The free body diagram procedure is repeated to find the forces at each finger. Note the equations are the same except for the direction in which the gripping force acts, as expected.

Finger 1:
$$\begin{bmatrix} e_{nx1} & e_{tx1} \\ e_{ny1} & e_{ty1} \end{bmatrix} \begin{bmatrix} N_1 \\ F_{t1} \end{bmatrix} = \begin{bmatrix} -G \\ 0 \end{bmatrix} \tag{5.26}$$

Finger 2:
$$\begin{bmatrix} e_{nx2} & e_{tx2} \\ e_{ny2} & e_{ty2} \end{bmatrix} \begin{bmatrix} N_2 \\ F_{t2} \end{bmatrix} = \begin{bmatrix} G\cos(60) \\ G\cos(30) \end{bmatrix} \tag{5.27}$$

Finger 3:
$$\begin{bmatrix} e_{nx3} & e_{tx3} \\ e_{ny3} & e_{ty3} \end{bmatrix} \begin{bmatrix} N_3 \\ F_{t3} \end{bmatrix} = \begin{bmatrix} G\cos(60) \\ -G\cos(30) \end{bmatrix} \tag{5.28}$$

5.5.6 Assembling the Matrix of Equations

Using the preceding equations, the only unknowns which remain are the forces acting in the z direction. Three more equations are needed to complete this formulation, shown in (5.29). Summing forces in the XY plane would be redundant to the formulas already developed, so a force balance in the Z direction is all that is necessary. Summing moments about the origin will yield three more equations, one in each dimension, but only two will be needed. The sum of the moments about the Z axis will yield a redundant equation, since the Z forces do not contribute and all forces in the XY plane are already known. Vectors to each contact point taken from the global origin will be used in summing moments.

$$r_n = x_n\vec{i} + y_n\vec{j} + z_n\vec{k}$$

$$\begin{aligned}\sum M_o = {} & \vec{r}_1 \times (N_1\vec{e}_{n1}) + \vec{r}_2 \times (N_2\vec{e}_{n2}) + \vec{r}_3 \times (N_3\vec{e}_{n3}) + \\ & \vec{r}_1 \times (F_{t1}\vec{e}_{t1}) + \vec{r}_2 \times (F_{t2}\vec{e}_{t2}) + \vec{r}_3 \times (F_{t3}\vec{e}_{t3}) + \\ & \vec{r}_1 \times (F_{z1}\vec{k}) + \vec{r}_2 \times (F_{z2}\vec{k}) + \vec{r}_3 \times (F_{z3}\vec{k}) = 0\end{aligned} \tag{5.29}$$

$$\begin{aligned}\sum F = {} & N_1\vec{e}_{n1} + N_2\vec{e}_{n2} + N_3\vec{e}_{n3} + \\ & F_{t1}\vec{e}_{t1} + F_{t2}\vec{e}_{t2} + F_{t3}\vec{e}_{t3} + \\ & F_{z1}\vec{k} + F_{z2}\vec{k} + F_{z3}\vec{k} = 0\end{aligned}$$

A complete force and moment sum is given above. As stated, not all terms will be necessary. Expanding all cross products, eliminating unnecessary terms, and adding the equations developed previously, yields the final matrix of equations.

$$\begin{bmatrix} z_1e_{ny1} & z_2e_{ny2} & z_3e_{ny3} & z_1e_{ty1} & z_2e_{ty2} & z_3e_{ty3} & -y_1 & -y_2 & -y_3 \\ z_1e_{nx1} & z_2e_{nx2} & z_3e_{nx3} & z_1e_{tx1} & z_2e_{tx2} & z_3e_{tx3} & -x_1 & -x_2 & -x_3 \\ 0 & 0 & 0 & 0 & 0 & 0 & 1 & 1 & 1 \\ e_{nx1} & 0 & 0 & e_{tx1} & 0 & 0 & 0 & 0 & 0 \\ e_{ny1} & 0 & 0 & e_{ty1} & 0 & 0 & 0 & 0 & 0 \\ 0 & e_{nx2} & 0 & 0 & e_{tx2} & 0 & 0 & 0 & 0 \\ 0 & e_{ny2} & 0 & 0 & e_{ty2} & 0 & 0 & 0 & 0 \\ 0 & 0 & e_{nx3} & 0 & 0 & e_{tx3} & 0 & 0 & 0 \\ 0 & 0 & e_{ny3} & 0 & 0 & e_{ty3} & 0 & 0 & 0 \end{bmatrix} \begin{bmatrix} N_1 \\ N_2 \\ N_3 \\ F_{t1} \\ F_{t2} \\ F_{t3} \\ F_{z1} \\ F_{z2} \\ F_{z3} \end{bmatrix} = \begin{bmatrix} 0 \\ 0 \\ 0 \\ -G \\ 0 \\ G\cos(60) \\ G\cos(30) \\ G\cos(60) \\ -G\cos(30) \end{bmatrix} \quad (5.30)$$

5.6 Interpreting the Results

The matrix of equations developed in the previous section will determine, for a specific combination of angular errors, the normal, tangential and Z directional forces at each contact point. The tangential and Z directional forces are frictional, while the normal component is purely a normal reaction force to the gripping force applied. This information can be used to predict if motion will occur at a contact point, and if the resulting motion is in a desirable direction.

5.6.1 Predicting Motion

In order to determine if motion will occur on a given face, the minimum coefficient of friction necessary to prevent motion can be tabulated from the matrix calculations by Equation (5.31). The equilibrium solution's normal and frictional forces will yield the limiting value of the friction coefficient. If the value obtained in reality is

lower than the tabulated value for the material pair in contact, the frictional forces experienced will be unable to hold the part in equilibrium.

$$\mu = \frac{\sqrt{F_t^2 + F_z^2}}{N^2} \tag{5.31}$$

If motion is expected to occur, it is only of benefit if it moves the part in a desirable direction. Many cases exist where motion can be expected on all gripping faces, yet the part moves farther from equilibrium. This occurs mainly in cases of large applied errors, where the grasping serves to only accentuate the part error rather than correct it.

In order to ensure that the motion predicted is desirable, the simple assumption that the resultant frictional force will directly oppose the direction of motion will be employed. Since each contact point's original and error induced position is known, it can easily be determined in which direction the contact point needs to move in order to achieve part orientation. Since this case deals largely with movement of the contact points in the z direction only, the assumption will be made that the Z component of the frictional force will be adequate to determine whether or not the motion experienced is in the correct direction. Simply put, the sign of the frictional force must be opposite to the direction in which the point must move to orient the part. A summary of the decision process can be seen below in Figure 5.16.

It should be noted that other gripper designs may be concerned with orienting contact points in more than the z plane. For example, if the gripper was desired to spin the part about its axis, a check of the sign of the tangential force would instead be performed.

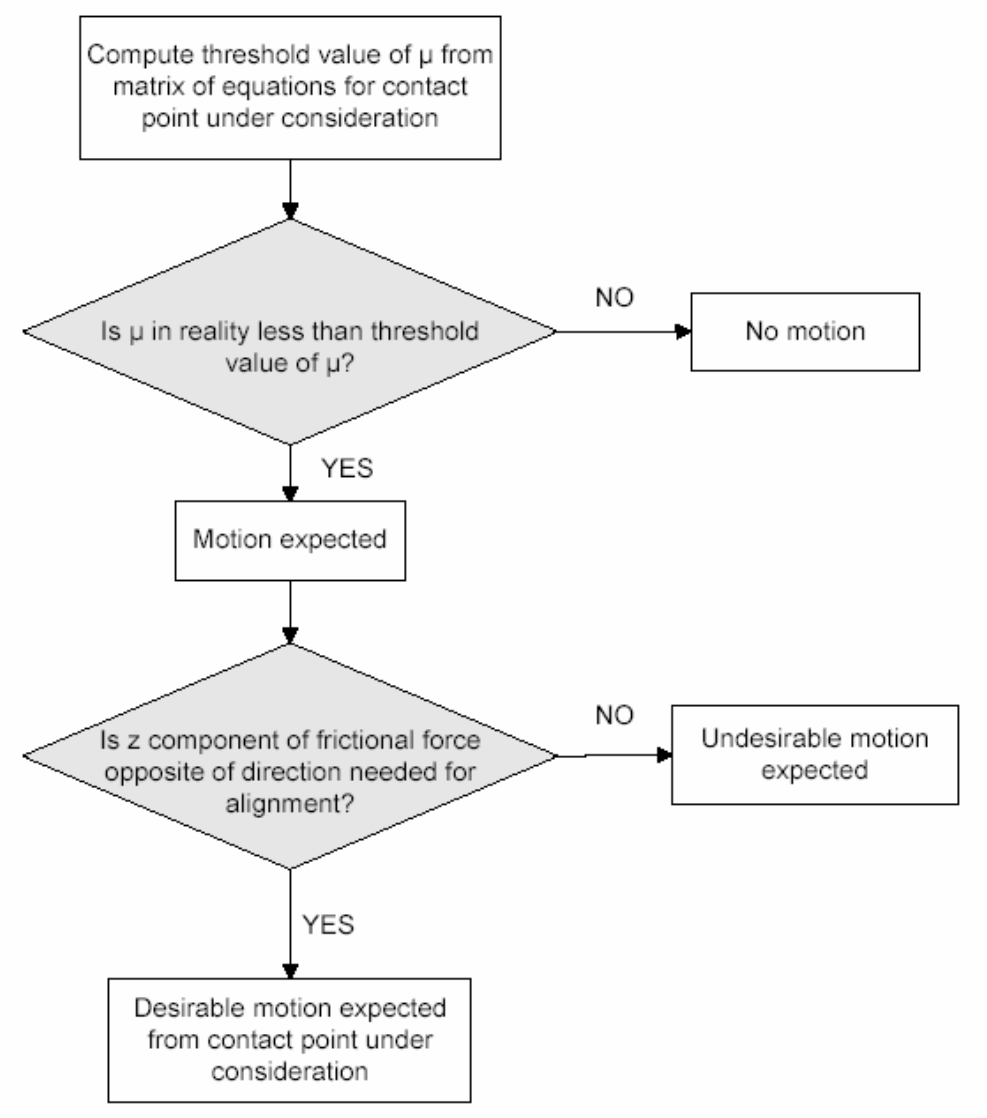

Figure 5.16 Decision process to determine desirable motion

5.6.2 Criteria for Part Alignment

Lastly, criteria must be developed to determine how many desirable points of motion are needed to properly orient the part. The case of only one point of motion will yield alignment only if the remaining two points of contact already have equal Z values. For example, if contact points 2 and 3 in Figure 5.17 have equal Z values (are aligned vertically), the part can align by movement at point 1. The part will "pivot" about the axis shown and still allow the correct orientation to be achieved.

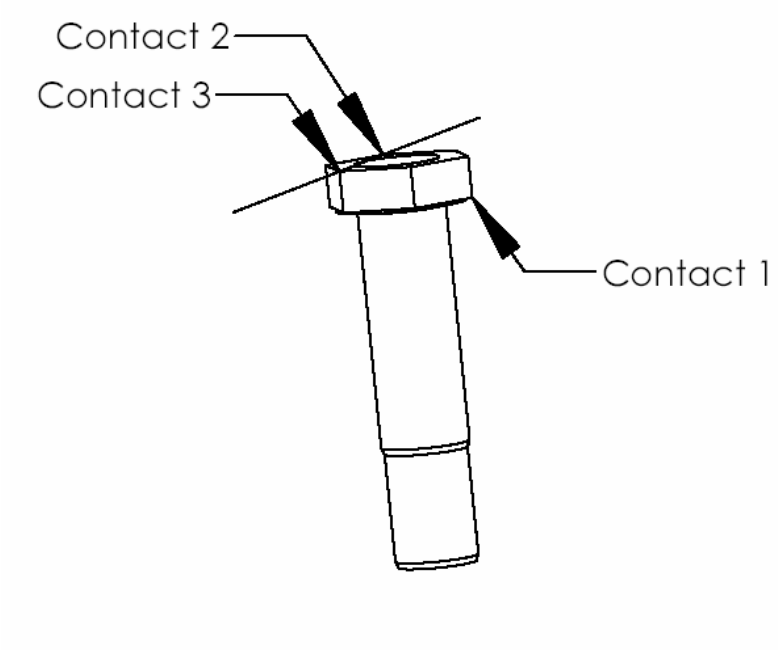

Figure 5.17 Example of alignment with one point of motion

In any other case, at least two points must experience motion in directions which promote self-alignment. Obviously, a condition where all three points can experience

relative motion in the correct direction will lead to part alignment. The case where two points of motion have equal Z values and can be used as a pivot occurs very infrequently in the solution space. The case requiring two or more vertices of motion is much more common and is the dominant mode of part alignment in this case.

It should be noted as before that the criteria developed are specific to this case. However, for other grasping applications, simple criteria such as these can be developed to decide whether the predicted motion will be adequate to align the part as desired.

5.7 Summary

This chapter developed a measure of gripper performance which deals with the concept of self-alignment, defined as a grasp which serves to bring a loosely oriented part into its final state of alignment. This is accomplished by relative motion of the part on the gripping faces and a reference feature on the part aligning with the gripper faces. A simple two dimensional model shows that the part geometry and coefficient of friction determine what error tolerance, if any, the gripping system will possess.

A more complex three dimensional model is developed to model the gripping system prototyped in this project. In this case, the part error can occur in two dimensions, represented as rotational error about two axes. The part is modeled as a number of discrete possible points of contact, while the gripping faces are modeled as continuous surfaces.

Geometric algorithms are used to compute which points will contact each gripper face, and exactly where on the gripping surface contact will take place. This location is

used to compute the unit vectors at each point of contact; a normal, tangential and Z directional force. Knowledge of the applied gripping force is utilized to reduce the number of unknown forces from nine to three, and the remaining forces are solved for by means of a three dimensional force and moment balance.

Upon solving for all unknown forces, the minimum coefficient of friction necessary at each interface to prevent motion can be tabulated. This value is compared to that experienced in reality, if the actual value is less than the threshold value predicted, motion can be expected to occur. The direction of the resultant frictional force is used to determine if the motion predicted moves the part in a desirable direction. Criteria are then developed to establish how many points of desirable motion are necessary for part alignment to occur. This process is repeated for each possible combination of errors to assemble a solution space for which self-alignment will occur.

CHAPTER 6
GRASPING ALIGNMENT MODEL RESULTS AND VERIFICATION

The previous chapter developed a gripping model which predicts, for a given part and gripper geometry, if a self-aligning effect will be experienced during the grasping process. The model predicts whether this effect will be experienced for a specific combination of angular part errors. By iteratively running the model, a solution space of angular errors can be assembled, and all combinations of errors which yield the desired results can be found. This chapter will show the results for a number of parts under consideration, and will show the effect of varying part shape, coefficient of friction and grasping force. Finally, the model results will be verified with the prototyped gripper and an experimental part grasping setup.

6.1 Model Implementation

The equations and techniques developed in the previous chapter were input into a Matlab script for iteration and analysis. This technique proved to be fairly efficient in using computation time; the program analyzed 57,600 error combinations in under 20 minutes on a 3GHz processor. A main processing program analyzes each combination of errors, and logs the error transformation angles as well as the coefficient of friction required to prevent motion at each interface for each error combination. This results file is then analyzed by a post processing script which utilizes the criteria for self-alignment developed in section 5.2.2. to determine if the combination of errors will yield favorable

part motion. In this way, the results are tabulated only once, while a variety of post processing techniques can be performed quickly on the raw data at any time.

6.1.1 Visualizing the Results

Transforming the results into a visually intuitive form of output will add greatly to the model's usability. As described in section 5.4.1, a series of rotation transformations about two axes is used to induce the desired error to the discrete points of part contact. Unfortunately, visualizing a series of rotation transformations about two axes in space is not immediately intuitive, and the user may not have a physical feel of what a part error of a few degrees looks like.

In order to move the error from the domain of angular errors to that of physical space, a reference plane at a fixed distance from the part head is utilized. The combination of angular errors applied by the rotation transformations can be represented by visualizing where an axis through the centerline of the part will intersect the reference plane, shown in Figure 6.1 For small values of angular errors, it can be visualized as moving the tip of the part in two dimensions in the reference plane. Clearly the location of the intersection point on the plane will be a function of the distance of the plane from the head of the part. In all further analysis, this distance will be taken as 1", in order to facilitate easily scaling of the results to any length of part.

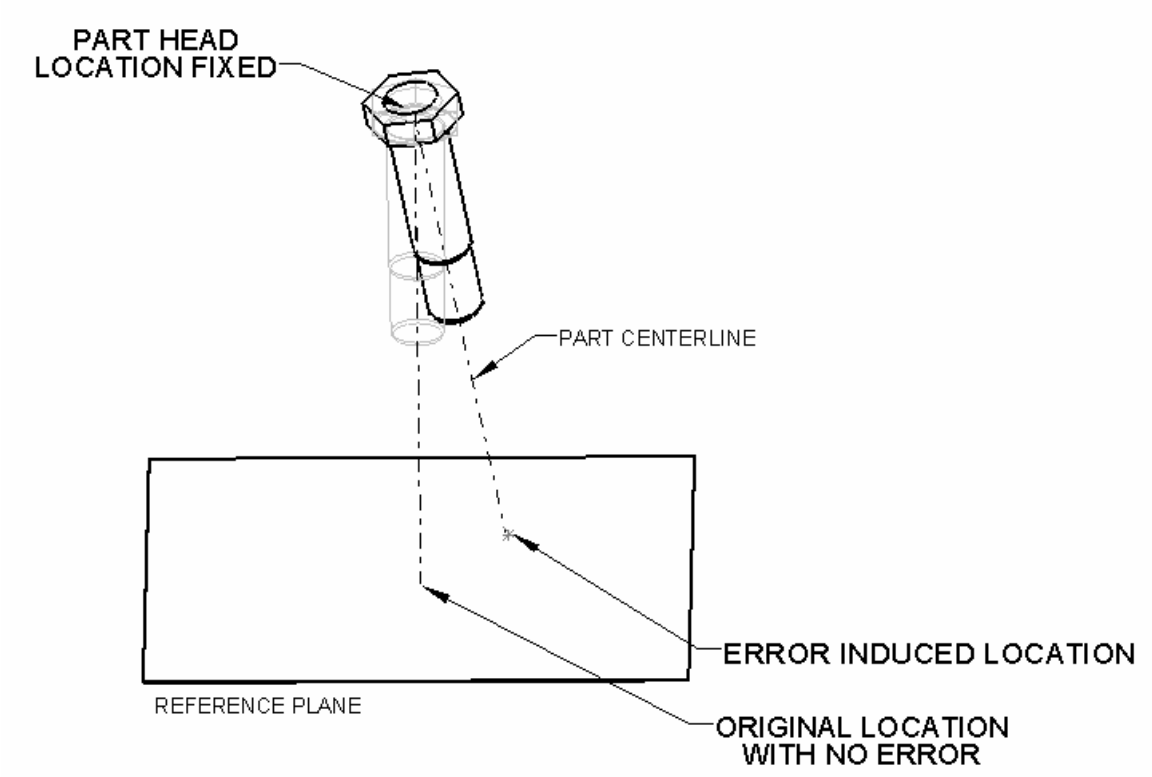

Figure 6.1 Describing part error using a planar projection

Each combination of angular errors can be represented by a point of intersection on the reference plane. The further the point deviates from the origin, which is the original location with no error, the more misaligned the part will be. Using this concept, a solution space of points which will yield self-alignment can be assembled.

6.1.2 Formatting the Results

Now that each combination of angular errors can easily be visualized, the form the output will take must be determined. The model aims to predict what points on the reference plane, if any, will result in the part self-aligning in the gripper after the part

centerline has been moved to the point under consideration. It is expected that if this effect will occur, there will be a limit on how far the part can deviate from its original aligned position and still self-align. This would yield a set of points, likely centered around the origin, which will create a space of satisfactory errors the gripper can tolerate.

For simplicity of output, only the boundary where points transition from self-alignment to no self-alignment will be plotted, shown below in Figure 6.2. The boundary pictured is circular, but this will likely be a more complex shape in reality. If the centerline of the part is contained within this boundary, self-alignment will occur. The model aims to predict if the boundary exists at all, or if the part will not self-align for any error induced. If the boundary does exist, the model will predict its shape as well as its size. The shape of the boundary will predict in which directions part alignment will be most favorable, and the size will predict the magnitude of errors that can be corrected by the gripper.

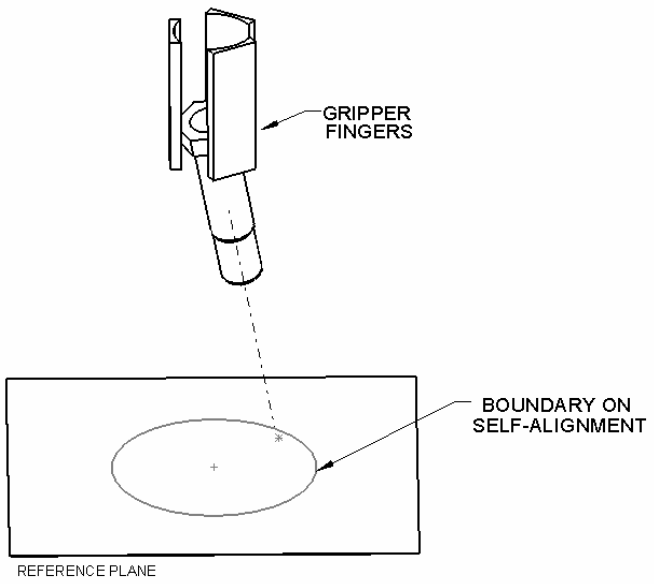

Figure 6.2 Illustration of self-alignment boundary concept

6.1.3 Initial Model Results

The model was first run for a hex shaped part, with a head height of .400" and a width across the hex flats of 1", shown in Figure 6.3. A gripping force of 50 pounds was used as an input to the gripping portion of the model. Part geometry and grasp force were selected to match the experimental validation setup, discussed further in later sections.

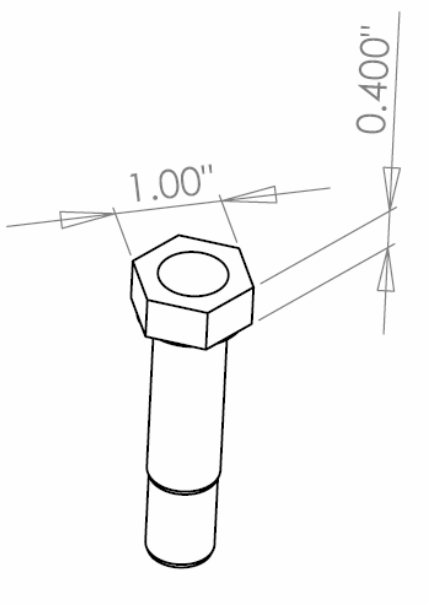

Figure 6.3 0.400" tall 1" wide hex part as tested in grasping model

The contour shown in Figure 6.4 plots the predicted boundary for μ_s (coefficient of static friction) values of 0.05, 0.1, 0.15 and 0.2. Values of $\mu_s > 0.25$ did not yield any predicted self-alignment region. For a given value of μ_s, the boundary shown represents the "Boundary on Self-Alignment" illustrated in Figure 6.3. The actual values of X and Y error are normalized, that is the plane is assumed to be a distance of 1 unit of length (inches in this case) from the part head.

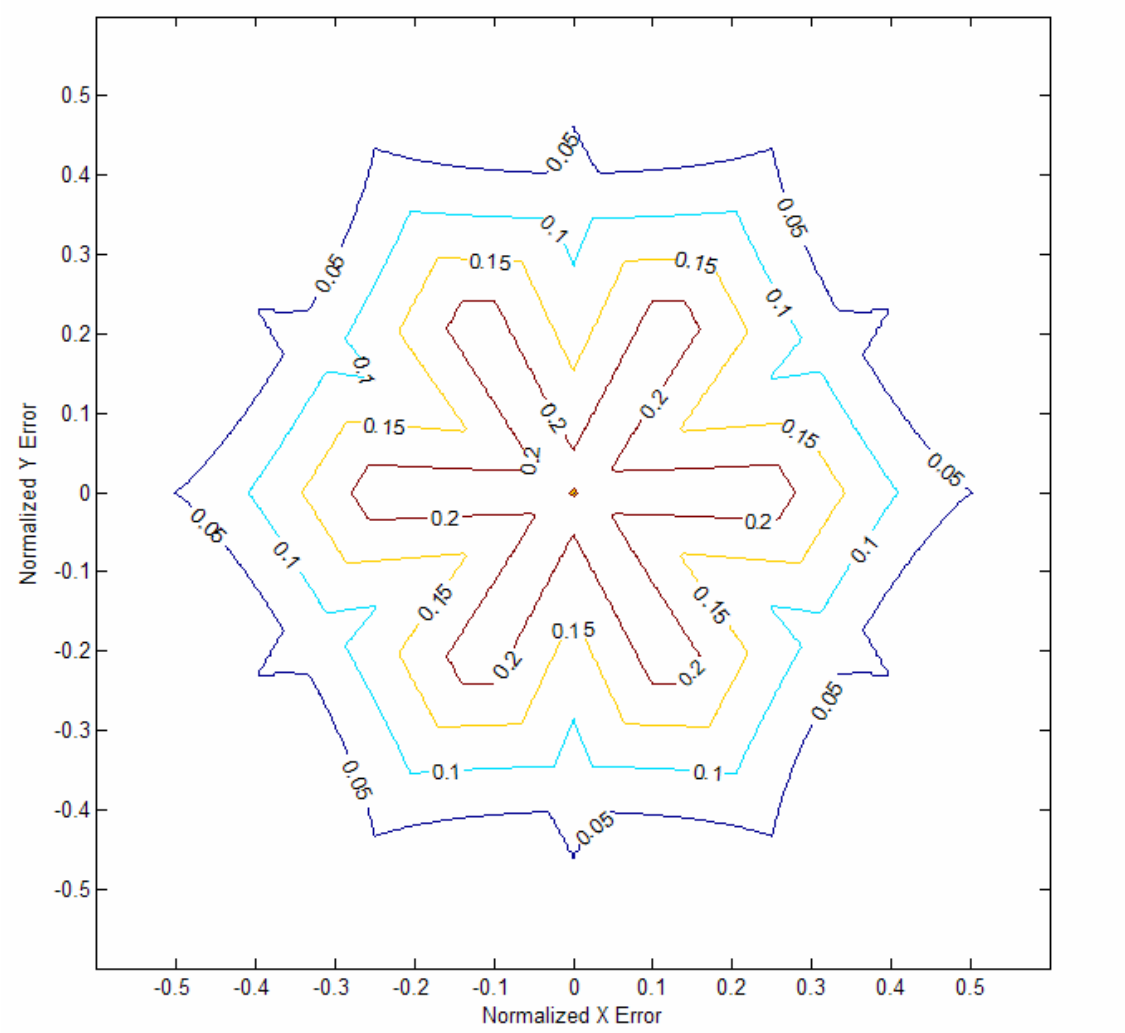

Figure 6.4 Model results with contours for varying values of μ_s, calculated for .400" tall 1" wide hex headed part.

Since the part is hex shaped and not axially symmetric, the rotation of the part about its central axis will likely have an impact on the results of the model analysis. This analysis assumes the hex points of the part align with the center of the gripping faces before error is induced. The model can be run for other rotations of the part, by specifying it as an initial condition before analysis begins.

Figure 6.5 shows the calculated self-alignment region on a reference plane below the gripper fingers. The gripping unit itself is not pictured for clarity. If a part were grasped in the fingers, a line could be projected onto the reference plane through the part's centerline. If the projection intersected within the boundary given by the value of μ_s experienced between the part and gripper, part self-alignment would be expected for the particular combination of angular errors considered.

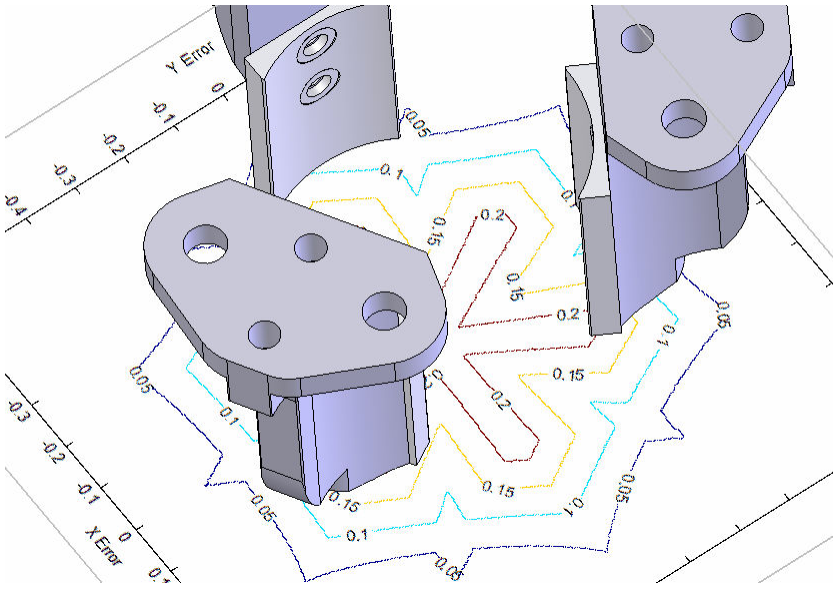

Figure 6.5 Self-alignment boundaries pictured relative to gripper finger position

Figure 6.6 shows the predicted boundaries relative to the gripper finger locations from a top view. The results are symmetric about each gripping finger, as expected. From this view, conclusions can be drawn about what types of errors the gripper will be most tolerant to.

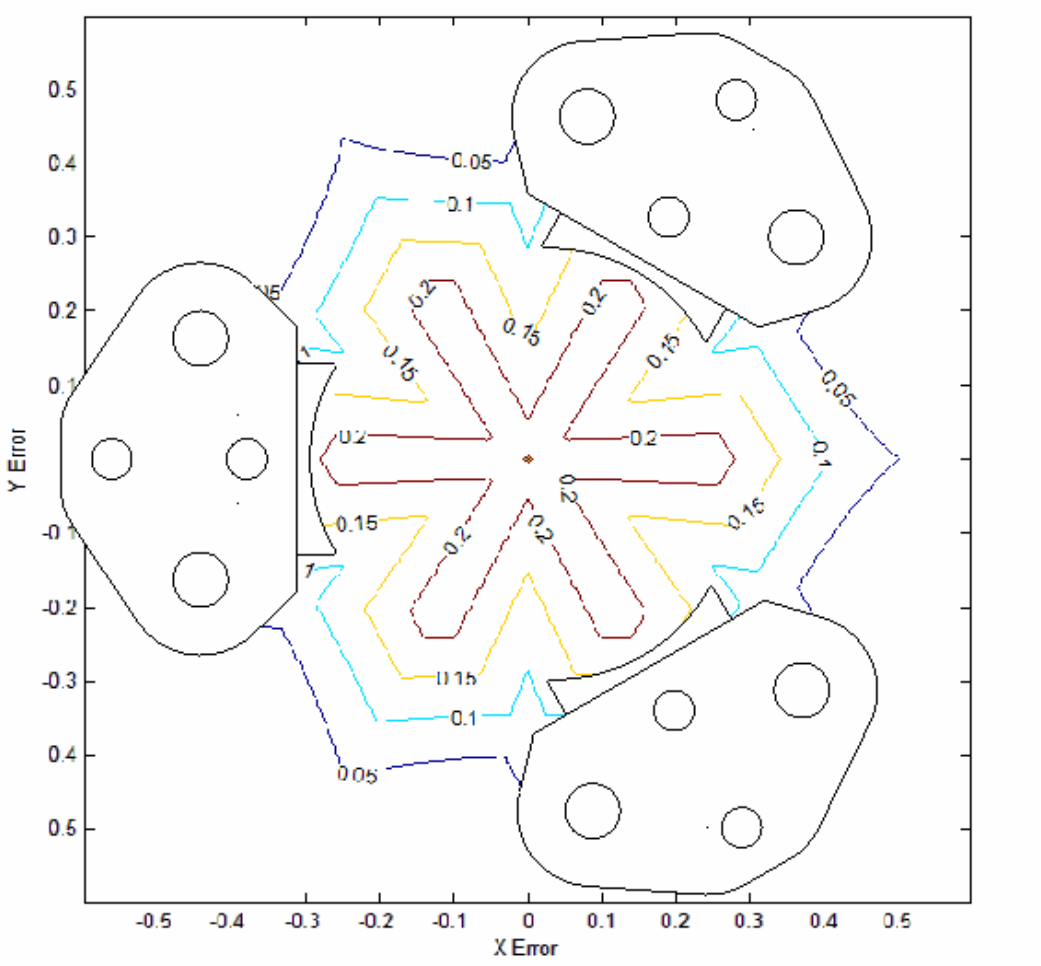

Figure 6.6 Top view of model results and gripper finger locations

6.1.4 Conclusions about Model Results

Figure 6.4 yields interesting conclusions about the predicted performance of the gripper. First, the error tolerance of the gripper will be greatly influenced by the value of μ_s experienced between the part and the gripping faces. A value of $\mu_s = 0.05$ will yield a very fault tolerant design, while a value of $\mu_s = 0.25$ will experience no part motion in the gripper while grasping. This is very useful information for the designer, since if a high value of μ_s is expected, additional design efforts will be needed to ensure the part is presented to the gripper in a fully oriented fashion. Likewise, if μ_s is very low, the part can be very loosely presented to the gripper. For example, if $\mu_s = 0.05$, and the part is 3" long, the gripper will tolerate an error in tip position of almost 1.5" in each direction. This is obtained by viewing the boundary for $\mu_s = 0.05$, and multiplying the X and Y normalized error axes by the part length.

A second observation is best seen in Figure 6.6. The boundary for self-alignment is largest when the part axis moves directly toward or directly away from one of the gripping faces. This is especially true for higher values of μ_s. Between each of these favorable regions exists a less favorable region, which becomes more prominent for higher μ_s values.

6.2 Variation of Model Parameters

The benefit of any engineering model is the ability to vary parameters and examine their effect on the results. This section will examine what parameters influence the magnitude and size of the self-alignment boundary, including gripping force, part shape and part height.

6.2.1 Varying Gripping Force

In the two dimensional model developed in section 5.2, gripping force was not a determining factor in the maximum error which could be tolerated by the gripper. This is the case for the three dimensional model as well. Since the model uses calculated values of μ_s to decide if acceptable motion will occur on a given gripping face, forces are not being considered directly. It is the ratio of the tangential and normal forces at each face which leads to the desired value of μ_s, as a consequence an increase in gripping force will cancel out in this ratio of forces. This is a result of the system in consideration being linear. A system where forces increased in a nonlinear fashion would not exhibit this independence to gripping force.

For example, suppose μ_s is calculated for a gripping force G_1, as shown below in Equation 7.1. Now suppose the gripping force is changed by a constant c and called G_2 as in Equation 7.2. Normal force N increases linearly with gripping force G, as given by equations 6.27-6.29. Equation 7.3 shows that this constant c will cancel out upon calculation of μ_s, thus proving the independence of the model results from the gripping force applied.

$$\mu_1 = \frac{F_f}{N} \qquad (7.1)$$

$$G_2 = cG_1 \qquad (7.2)$$

$$\mu_2 = \frac{cF_f}{cN} = \frac{F_f}{N} = \mu_1 \qquad (7.3)$$

6.2.2 Varying Part Shape

Previously it was noted that the alignment boundary calculated exhibited a six-sided pattern. Since a hex shaped part was under consideration, intuition might suggest that this leads to the six-sided boundary. To examine this effect, a 1" diameter 0.400" tall round headed part is modeled and input to the grasping model. An illustration of the part shape is shown in Figure 6.7.

Representing a round headed part is a simple extension of a hex headed part, since the input to the model only requires possible points of contact. These points were the tips of the hex part's feature in the first case. In the case of a round headed part, any point along the upper and lower head surface can make contact with the gripper. If the number of possible contact points is increased to an acceptable level, the discrete model can approximate the continuous surface well. A total of 300 points each for the upper and lower surfaces were used, with little degradation in model computation time.

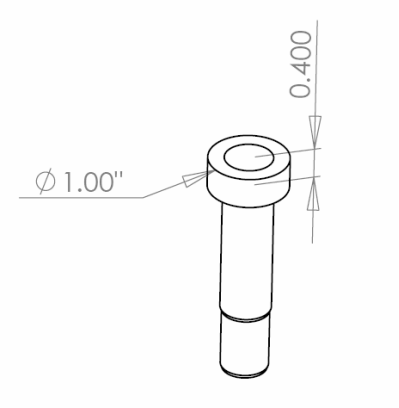

Figure 6.7 1.00” diameter 0.400” tall round headed part

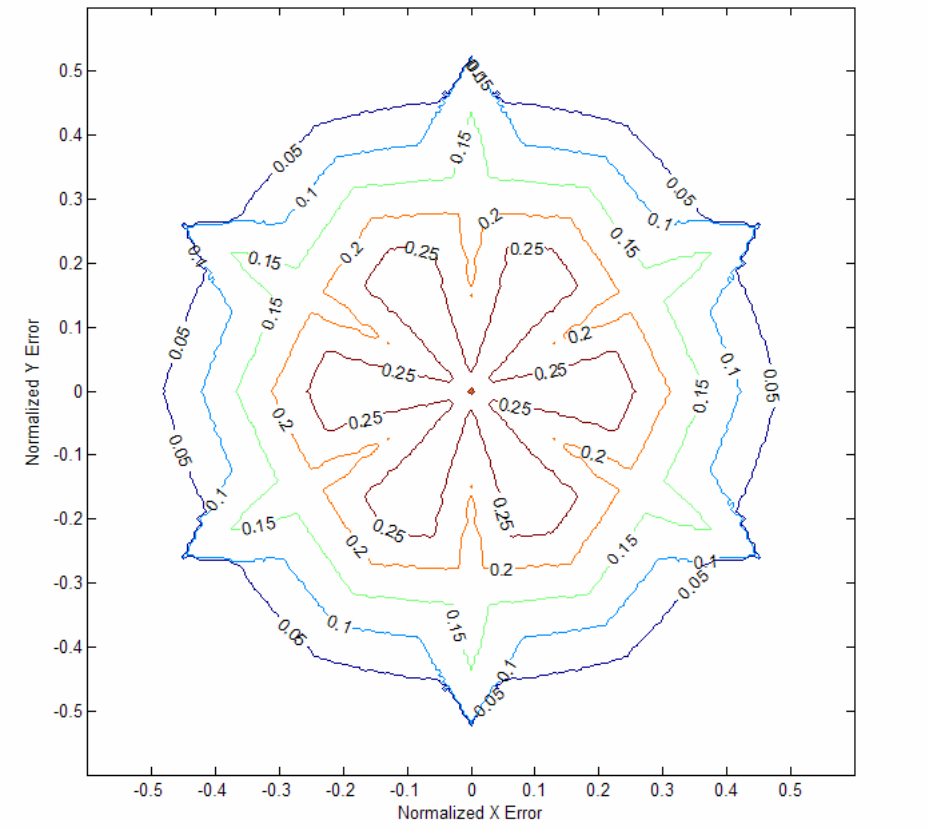

Figure 6.8 Model results with contours for varying values of μ_s, calculated for .400” tall 1” diameter round part.

The model results for the round part can be seen in Figure 6.8. As seen with the hex shaped part, a boundary with six nodes is still present. The shape of the boundary changes slightly, however the overall trends remain the same when compared to the results for the hex shaped part in Figure 6.4. It is deduced from these results that the six sided shape is a product of the three fingered gripper.

This shape arises from the fact that moving directly toward and directly away from each gripping face produces the same results, since gravity in this case is assumed to be negligible. Each finger then produces a symmetric boundary toward and away from it, and these symmetric boundaries are separated by 120 degrees. These three axes of symmetry cross at the origin, and produce the six sided result observed. This concept can be readily visualized by referring to Figure 6.6. If the gripper fingers were not evenly spaced from each other, this six sided symmetry would not result; rather a six sided asymmetric boundary would result.

6.2.3 Varying Part Dimensions

It has already been shown that the model output is independent of gripping force, and that the six sided boundary is a product of the three fingered gripper design. Each map of the alignment boundaries easily shows the effect of changing coefficient of friction. It is now desired to examine what effect the dimensions of the part have on the model output and the gripper's fault tolerance.

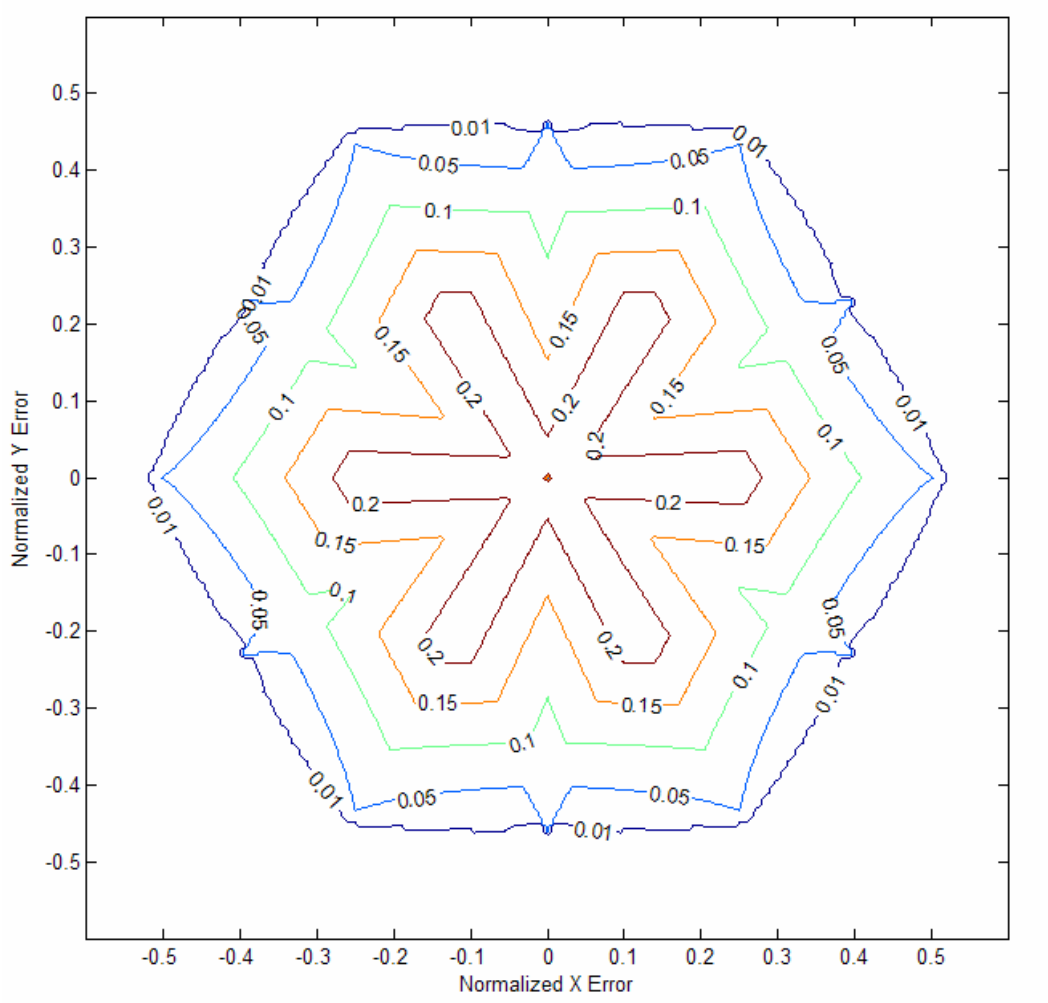

Figure 6.9 Model results with contours for varying values of μ_s, calculated for .400" tall 1" wide hex headed part.

Figure 6.9 again shows the results for a .400" tall 1" wide hex headed part. The gripper can tolerate a fairly large amount of misalignment in this case, especially at low values of μ_s. Also, the maximum value for μ_s which will result in any self-alignment is approximately 0.2. This part would be a good candidate for self-alignment if a value of μ_s below 0.2 was expected.

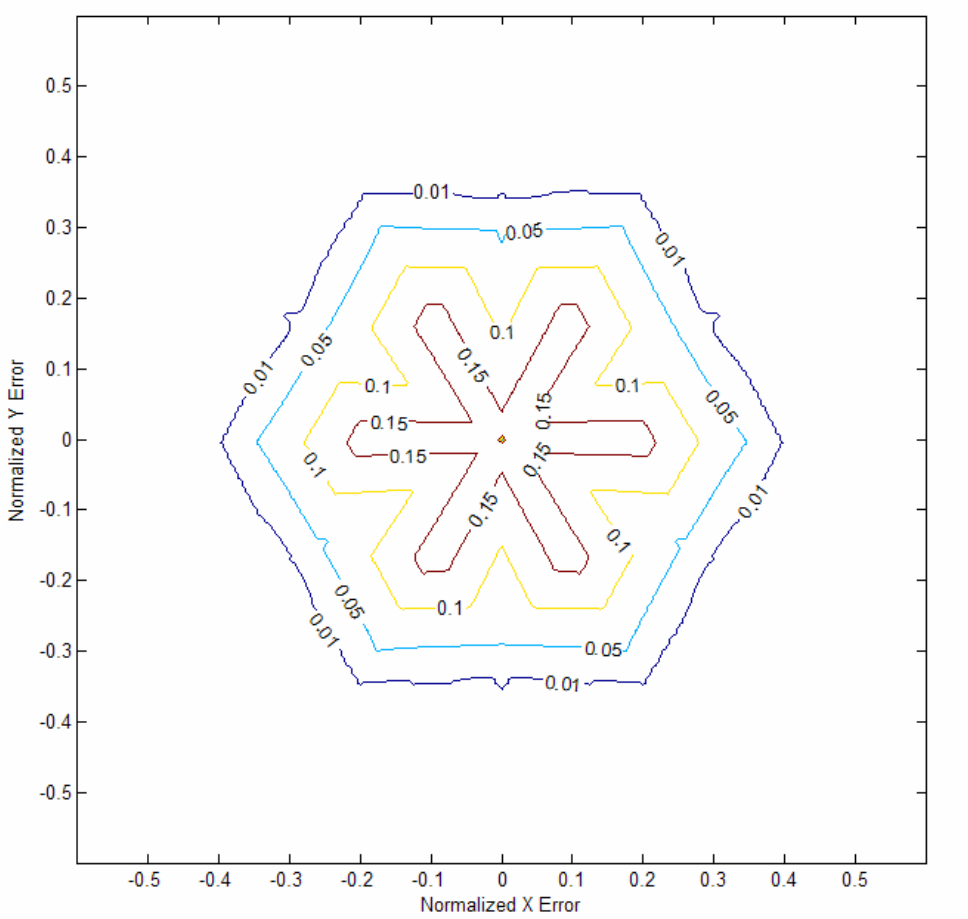

Figure 6.10 Model results with contours for varying values of μ_s, calculated for .300" tall 1" wide hex headed part.

Figure 6.10 plots on the same axes a 0.300" tall part with the same hex dimensions used in Figure 6.9. Two phenomena can be observed here, first the size of the boundaries are beginning to decrease. Thus, for a given coefficient of friction, this part will be less tolerant to errors, as expected. Also the maximum value of μ_s which will tolerate any error at all has decreased to 0.15. The decrease in the part's height-to-diameter ratio is hindering the self-aligning qualities with respect to both error magnitude tolerance and friction coefficient uncertainty.

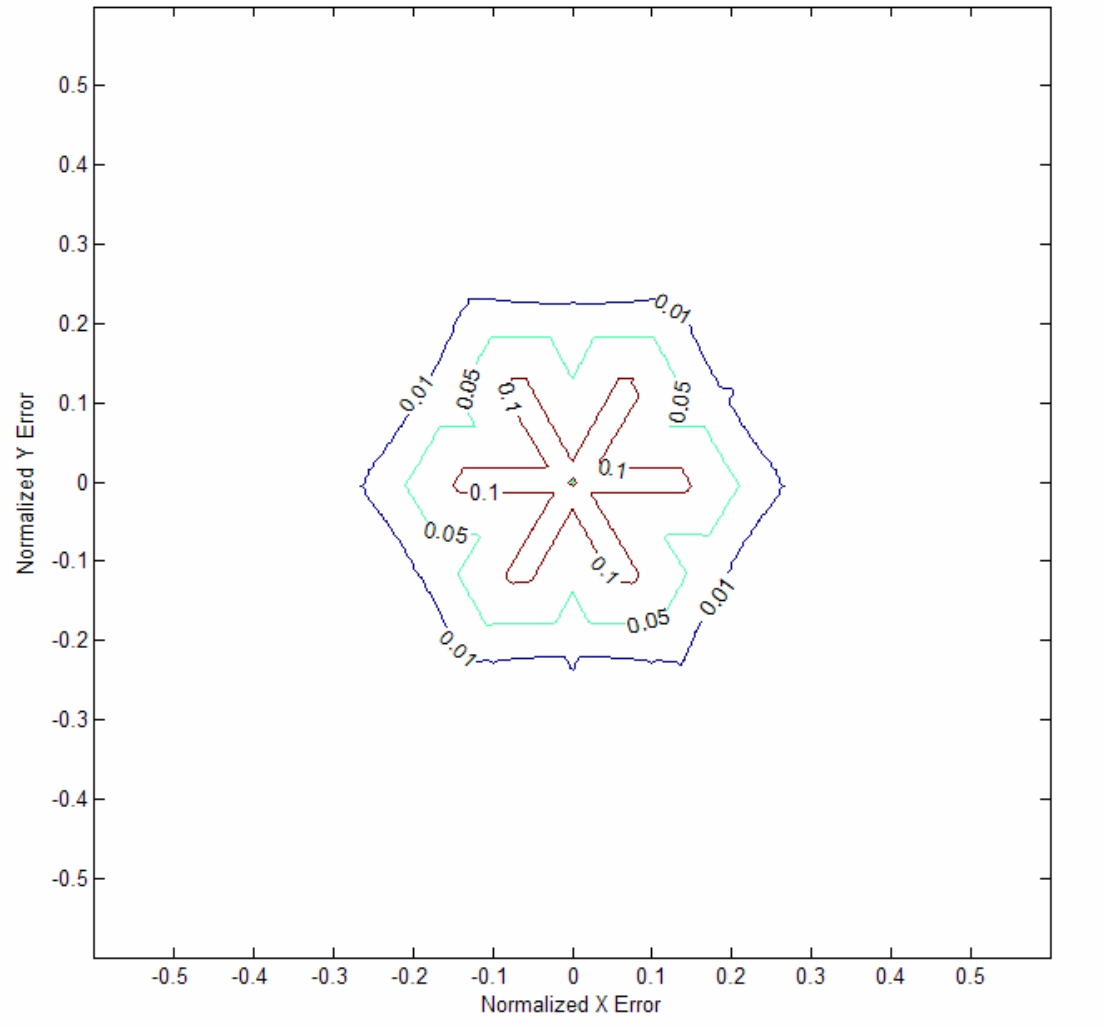

Figure 6.11 Model results with contours for varying values of μ_s, calculated for .200" tall 1" wide hex headed part.

Figure 6.11 shows a 0.200" tall hex part, with axes and hex dimensions identical to those previously considered. Again, the size of the boundaries decrease further from previous plots. Likewise, the maximum value of μ_s which can be tolerated is 0.1, a further decrease from previous cases. Unless this part exhibited an extremely low coefficient of friction on the gripper faces, it would likely not be a good candidate to rely solely on self-aligning principles for orientation.

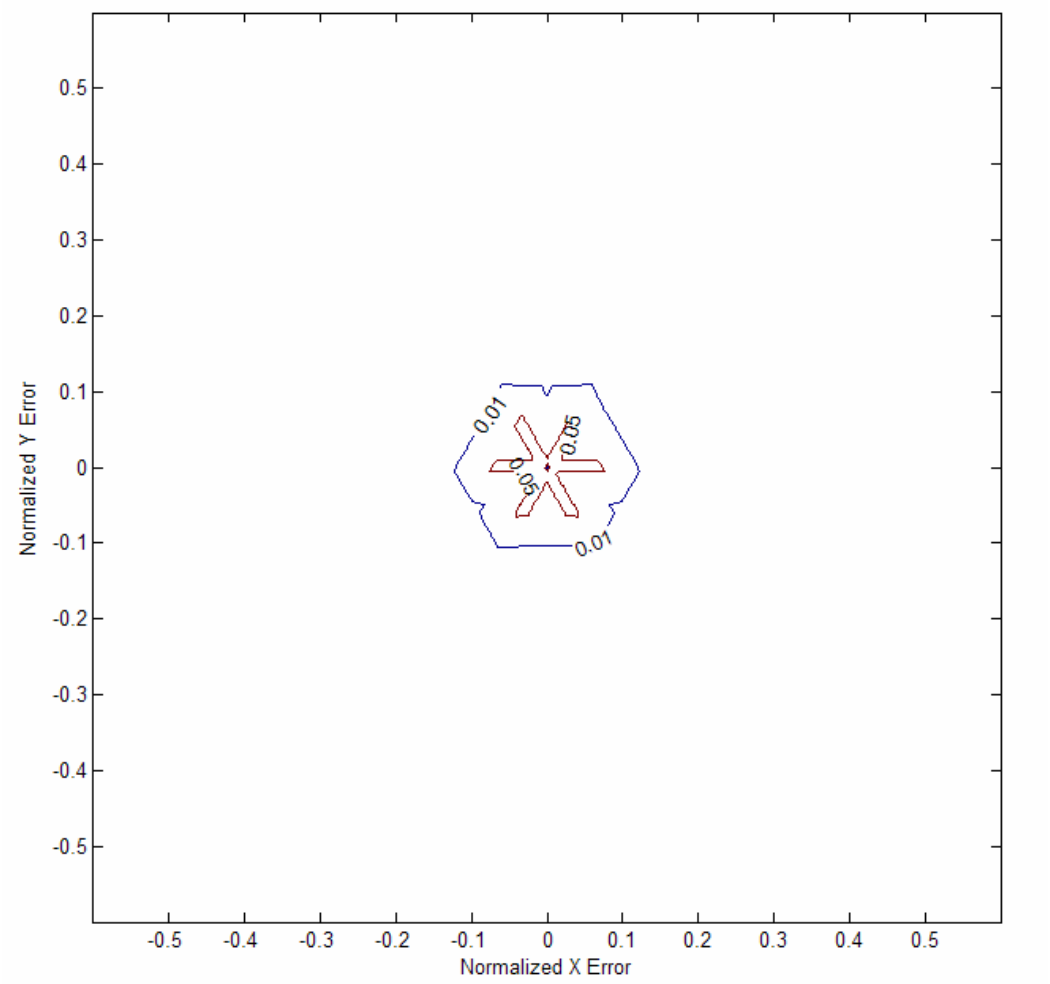

Figure 6.12 Model results with contours for varying values of μ_s, calculated for .100" tall 1" wide hex headed part.

Finally, Figure 6.12 shows a plot for a 0.100" tall hex part with other relevant dimensions again unchanged from previous cases. The size of the boundaries have decreased even further, and the magnitude of μ_s which can be tolerated is now extremely low, approximately 0.05. This part would be very sensitive to an increase in friction, and even under optimal sliding conditions would not be very tolerant to errors. The designer should plan to fully orient this part by other means than the grasping process.

It is clear upon review of these results that part geometry, namely height-to-diameter ratio of the head, will have a pronounced effect on how the part will behave during grasping. Certain parts may not prove to be good candidates for self-alignment, even under conditions of very low friction. A part requiring an extremely low coefficient of friction would likely work initially under controlled conditions, but realities such as debris on gripper surfaces and gripper surface degradation must be accounted for.

6.3 Validating the Model Results

In order to validate the model results, two sets of data are needed. First, an experimental setup must reliably determine the error tolerance of the gripper. For a given test part, the boundaries of the self-alignment region must be determined. Second, the model must know the exact value of μ_s between the part and the gripping faces, in order to select the appropriate error tolerance boundary.

6.3.1 Experimentally Determining the Error Boundaries

Since the results are visualized using a projection through the part's centerline to a horizontal reference plane, the experimental setup will utilize this concept to validate the model. It was desired to be able to test parts while varying parameters such as μ_s and head height, so it was decided to machine test parts from hex stock of AISI 1018 steel rather than use existing available configurations.

In order to project a line along the part's centerline to a horizontal reference plane, a small laser was mounted in the tip of the test part, as shown in Figure 6.13. This enables testing in a manner identical to the scenario illustrated in Figure 6.2.

Figure 6.13 Test part for experimental validation

The results are logged by placing a paper surface on the floor, which serves as the reference plane, at a known distance from the gripper. The coordinates of the recorded points will be divided by this distance, to normalize the results for comparison with the model data. An origin is established by grasping an aligned part and marking the resultant coordinate on the paper surface. Figure 6.14 shows the reference plane below the grasped part. The laser spot can be seen projecting onto the test surface.

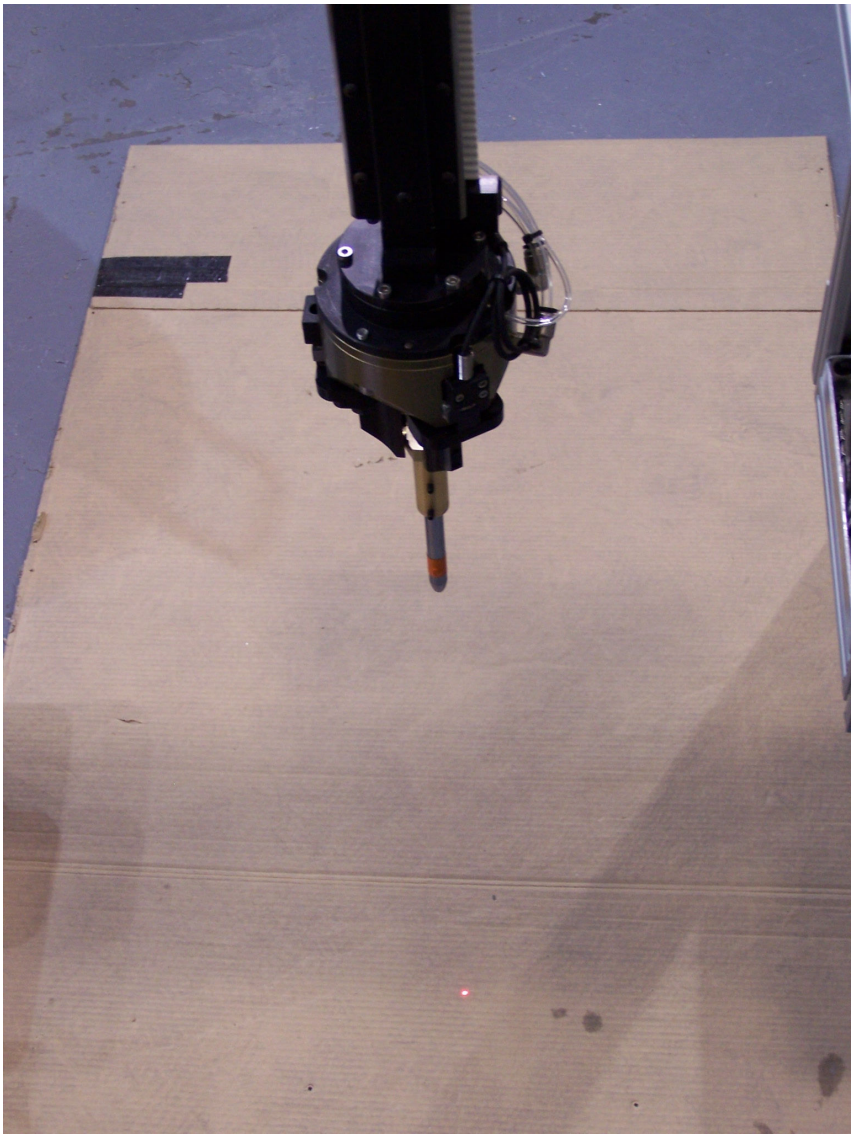

Figure 6.14 Grasped test part projecting alignment onto reference plane

The gripper is opened, and the part projection moved away from the origin in a specific direction to induce an angular error. The gripper is then closed, and the part motion observed to monitor the self-alignment process. If the part self-aligns, the process is repeated only with more induced error. The first location in a certain direction at which the part does not self-align is recorded on the reference plane as the threshold

where the gripper can no longer self-align the part. This is repeated in all directions to assemble a two dimensional boundary of error tolerance. Care must be taken when testing hex shaped parts to match the axial rotation about the part's centerline to that which was input to the model. The part can be axially aligned before any error is induced, then the projection moved to the desired error location.

6.3.2 Determining Coefficient of Friction

Since the coefficient of friction values are known to be difficult to predict for different material pairs and varying surface conditions, the values for the materials considered were determined experimentally. The sensitivity of the model to varying friction coefficients provided further argument to experimentally determine the values.

In order to obtain results that were more accurate than a simple inclined plane type friction test, a 3-axis piezoelectric transducer based force dynamometer was used to determine normal and resultant frictional forces under controlled conditions. The A-2 tool steel gripping face was mounted to the dynamometer and a material sample from the test part was mounted via a collet in a milling machine spindle.

The dynamometer was then zeroed, and a preload applied to force the material pair together. A preload of approximately 120 N was used to simulate the gripping forces experienced during testing. After the force was applied, the milling table was moved horizontally to induce a resultant frictional force on the part-gripper interface. The normal and frictional forces were logged using data acquisition software.

A typical profile of μ over time can be seen in Figure 6.15. Initially values are somewhat random, until a preload is applied. Values then stabilize as the normal load is applied, however their value is not of interest until relative motion occurs between the material pair. As expected, μ rises to an initial maximum value, during which time the materials are not sliding relative to each other. Since the analysis at hand is concerned with μ_s, the coefficient of static friction, this maximum value is the desired measurement. The maximum value of μ occurs just before gross sliding begins between the materials, at which point μ decreases to a slightly lower value, representing μ_d, the coefficient of dynamic friction.

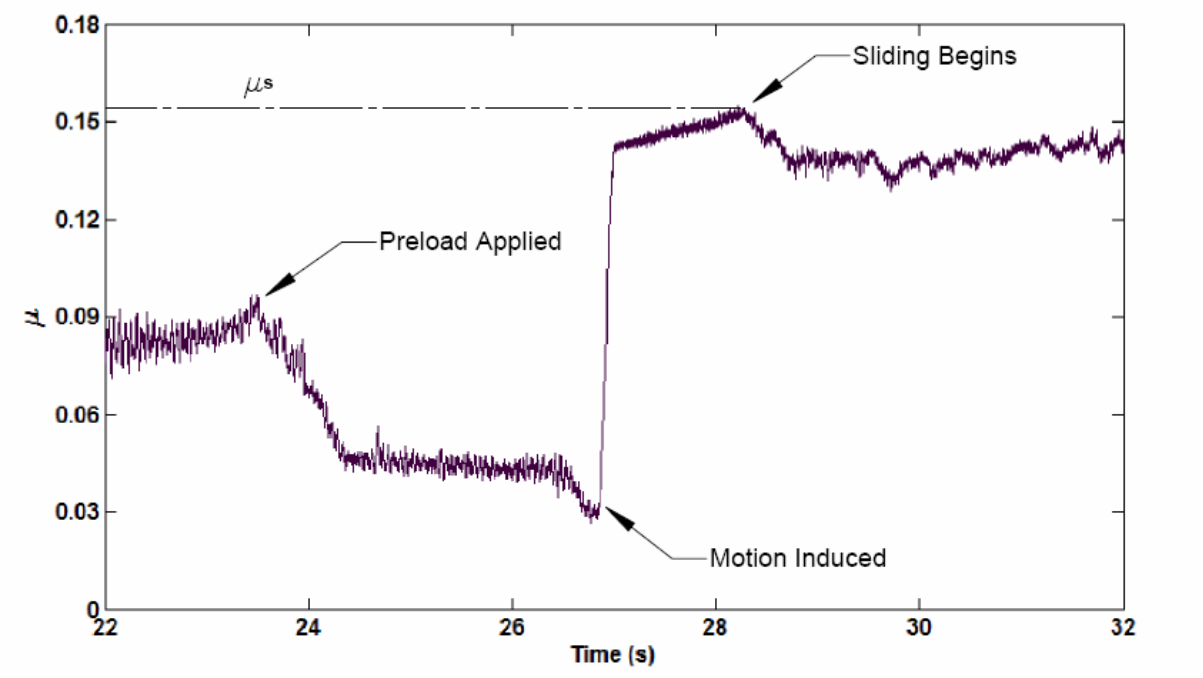

Figure 6.15 Typical profile of μ during friction experiment

Since each experiment only yields one value of μ_s, it is desirable to perform the experiment numerous times to account for experimental error and variability in material conditions across different locations of the workpieces. The material under consideration for testing was 1018 carbon steel, the same material used to construct the test piece illustrated in the previous section. A series of 20 experiments was performed, yielding the set of data shown in Table 6.1. Each result represents the value of μ just before relative motion between the workpieces was experienced.

These 20 experiments produced a range of data for the value of μ_s. For purposes of analysis, the standard deviation of this set of data is computed, as well as the mean. A 95% confidence interval can be calculated, and the results are shown in Table 6.2.

Table 6.1 Coefficient of static friction, μ_s on A-2 tool steel (50 HRC)

1018 Carbon Steel on A-2 Tool Steel	
Experiment	μ_s
1	0.1583
2	0.1337
3	0.1247
4	0.1145
5	0.1304
6	0.1193
7	0.1249
8	0.1563
9	0.1242
10	0.1293
11	0.1291
12	0.1340
13	0.1415
14	0.1258
15	0.1412
16	0.1336
17	0.1402
18	0.1558
19	0.1212
20	0.1545

Table 6.2 Statistics of experimental results

μ_s for 1018 Carbon Steel on A-2 Tool Steel	
Mean	0.134
Standard Deviation	0.0131
Upper limit (with 95% confidence)	0.160
Lower limit (with 95% confidence)	0.109

6.3.3 Model Verification

With test data from the experimental gripping setup and knowledge of the measured value of coefficient of friction, the model predictions can be compared to the results observed. The first test was performed on a 1018 carbon steel test bolt, with a .400" tall hex head. The test piece was machined from 1" hex stock, thus the width across the hex flats was 1". Discrete points where the transition to self-alignment occurred were recorded and normalized by dividing by the distance to the reference plane. The results are shown in Figure 6.16.

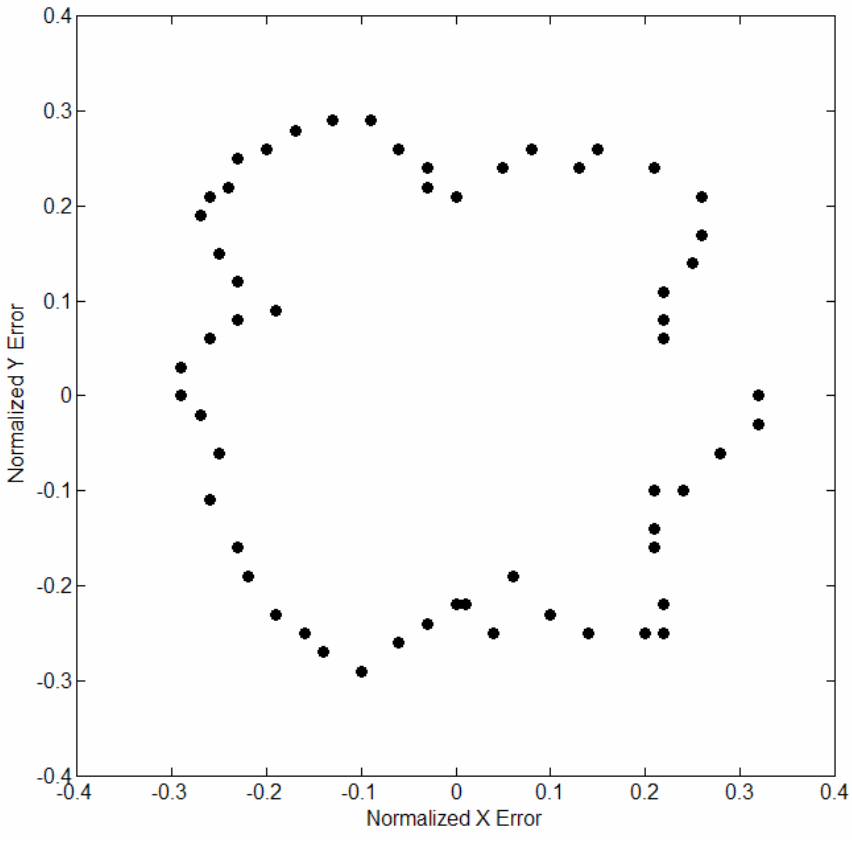

Figure 6.16 Experimentally determined boundary for 1018 steel hex part with .400" tall head

Next, the model is used to predict the boundary for self-alignment, shown in Figure 6.17. Since the value of μ_s has been experimentally determined to lie within a 95% confidence interval, the bounds for the lower and upper limit of this interval are plotted.

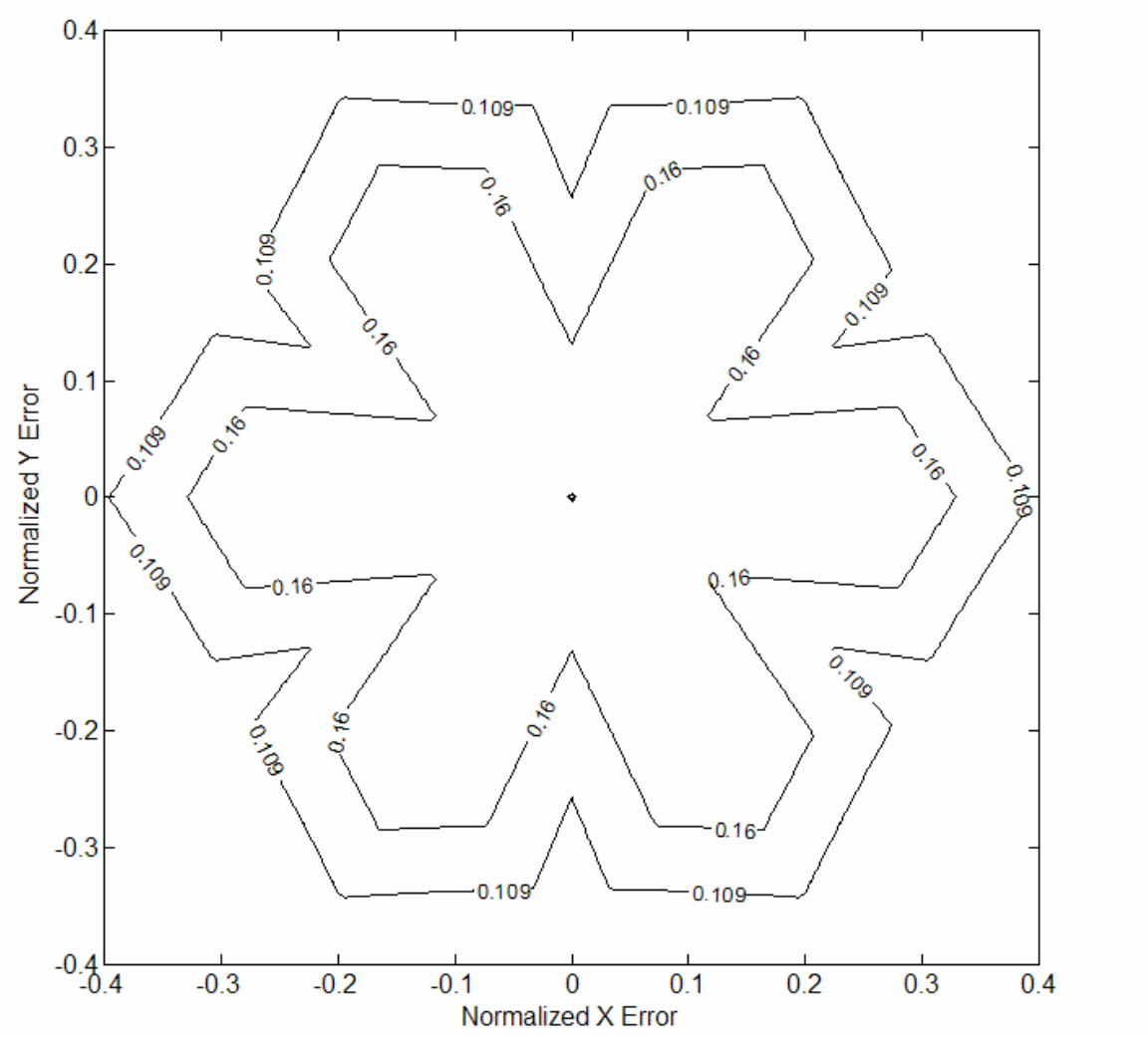

Figure 6.17 Predicted boundary limits for 1018 steel hex part with .400" tall head, using $0.109 < \mu_s < 0.160$

Finally, the recorded data is superimposed onto the predicted boundary limits, shown in Figure 6.18. From the model results and friction analysis, it is expected that the experimentally determined transition points will lie within the boundaries plotted, as μ_s should lie within this interval with 95% certainty. The results show the recorded data matches the boundary limits predicted quite well.

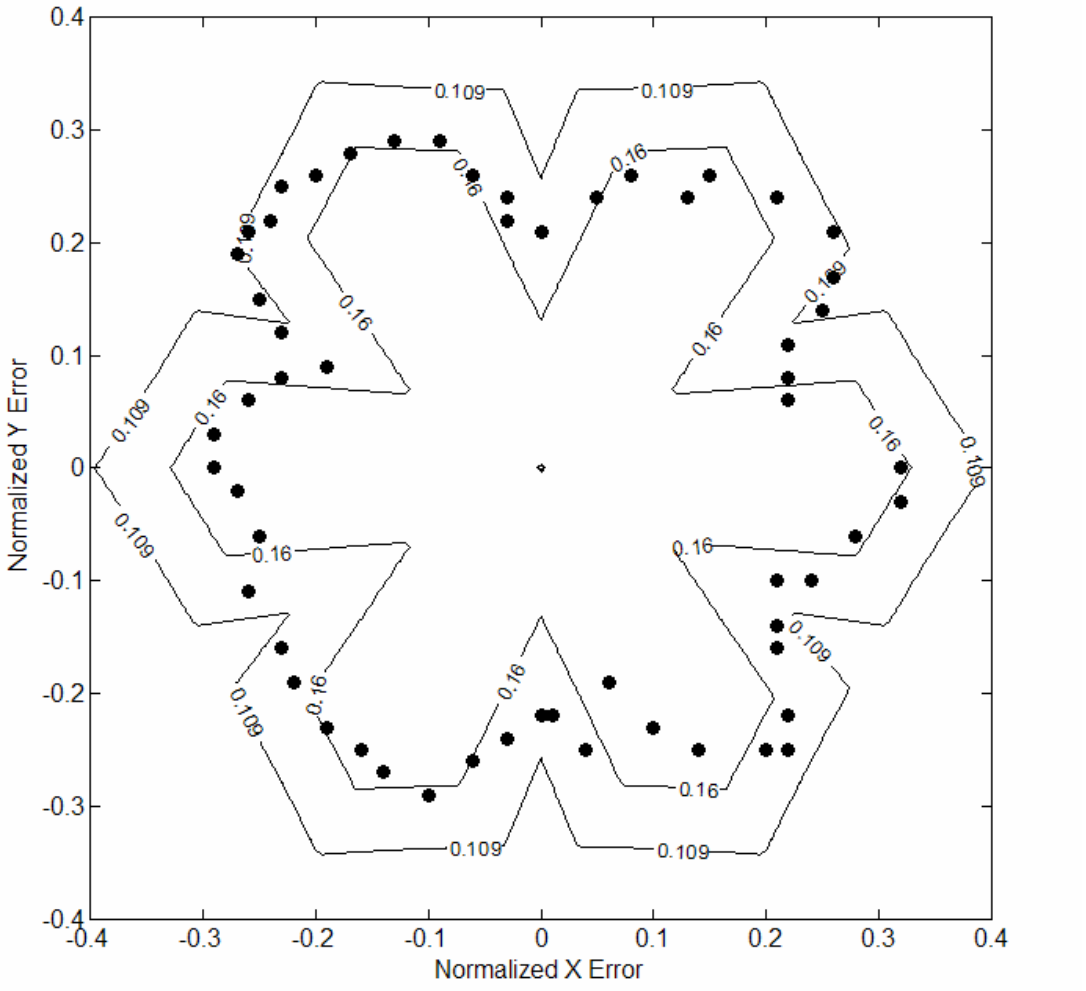

Figure 6.18 Predicted and measured boundary limits for 1018 steel hex part with .400" tall 1" wide head, boundaries for $0.109 < \mu_s < 0.160$

The trend predicted was that the direction directly toward or away from each gripping face would predict the most favorable self-aligning qualities. This is indeed the trend observed in the results, and also the trend that is felt physically when a part is closed in the gripper. During testing, it was very clear that moving the part tip directly toward or away from a gripping face produced the strongest effect of self-alignment. As predicted by the model, between these areas of favorable self-alignment existed areas of less favorable behavior. This can be seen in the results and also could be felt physically when grasping the part. The self-aligning motion in the less favorable areas was not as strong and immediate as that in the most favorable areas. Self-aligning in the center of the predicted region was quite strong regardless of direction.

The size of the self-aligning boundary is of more interest than the shape itself, since this will in general predict the magnitude of part angular error the gripper can tolerate. The experimental results match the predicted boundary quite well, with the largest nodes of the boundary corresponding closely to the maximum tolerable error. The nodal areas of the boundary closest to the origin also reasonably predicted the minimum tolerable error.

It should be noted that the experimental grasping setup was slightly difficult to use with a hex shaped part, due to the fact that the axial orientation of the hex part needed to be maintained for consistent results. For this reason, the experiment was rerun with a round headed part, to eliminate the need to orient the workpiece about its central axis before grasping.

The first round headed part tested was .400" tall and had a 1" diameter head. The part's shape is similar to that shown previously in Figure 6.7. The model was again run and used to predict the self-alignment boundaries for the upper and lower values of the 95% confidence interval for μ_s.

The results can be seen in Figure 6.19. A relatively strong self-aligning effect was predicted, and was also observed in the tests. The data collected matches quite well with the boundary predicted, with the majority of the points falling in the interval predicted.

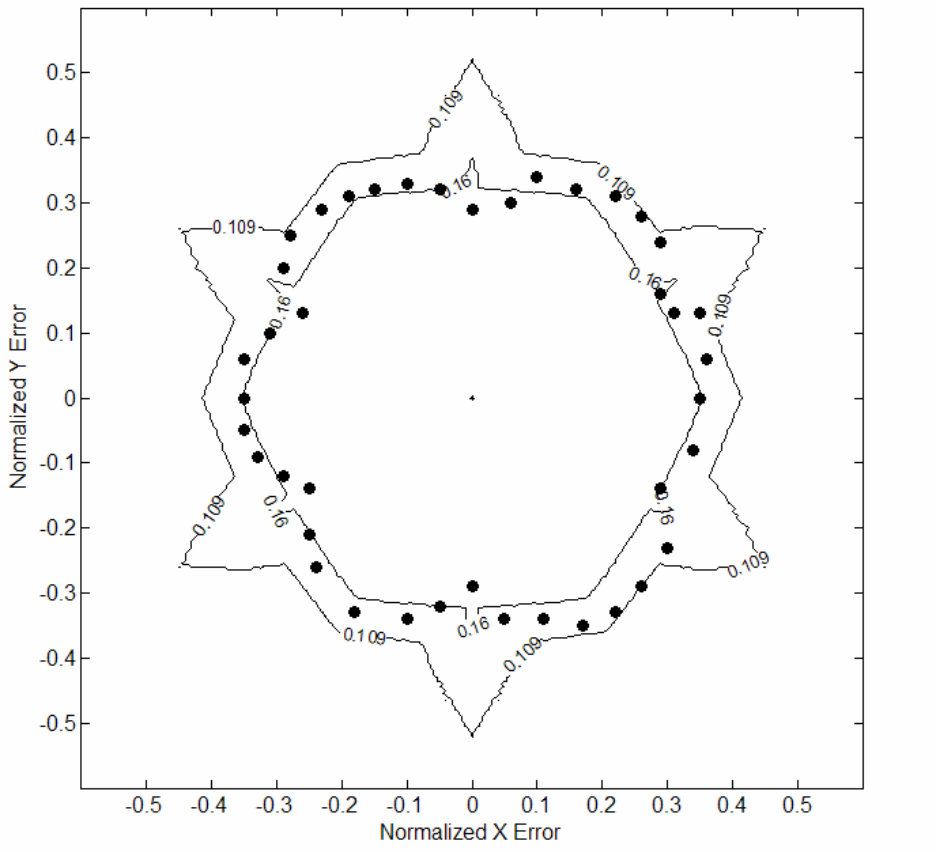

Figure 6.19 Predicted and measured boundary limits for 1018 steel round part with .400" tall 1" dia. head, boundaries for $0.109 < \mu_s < 0.160$

The test piece was then modified to shorten the head height. The diameter was fixed at 1" as in the previous test, however this experiment utilized a 0.300" tall head, 0.100" shorter than before. The model predicted a smaller self-alignment region for this geometry, but nonetheless predicted that a self-aligning effect would occur.

Results of the model prediction and experimental testing can be seen in Figure 6.20. Once again the majority of the collected data falls within the interval predicted, and the part experienced favorable self-alignment qualities. The model predicted quite well that the size of the boundary would not be as large as in the previous test which used a taller part head.

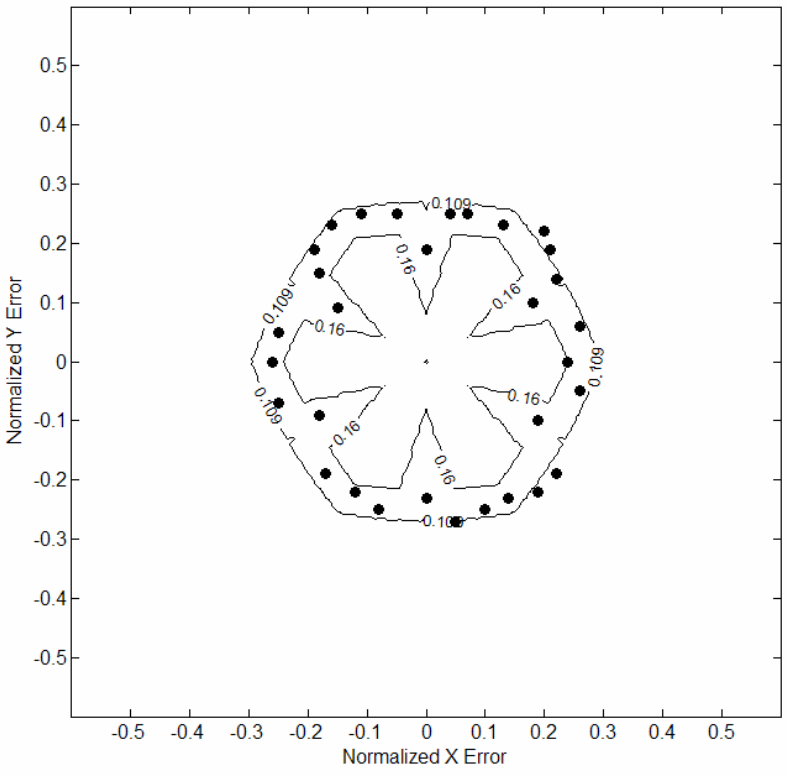

Figure 6.20 Predicted and measured boundary limits for 1018 steel round part with .300" tall 1" dia. head, boundaries for $0.109 < \mu_s < 0.160$

Finally, the test part was modified again to further decrease the head height. This test utilized the same 1" diameter as before, with a 0.200" tall round head. The model predicted a small region of self-alignment region if μ_s were toward the lower bound of the confidence interval, and no self-alignment if μ_s were near the upper limit of the interval.

The predicted boundary and recorded data can be seen in Figure 6.21. The self-aligning effect observed for this geometry was very weak, which was expected from the small to nonexistent boundary predicted by the model.

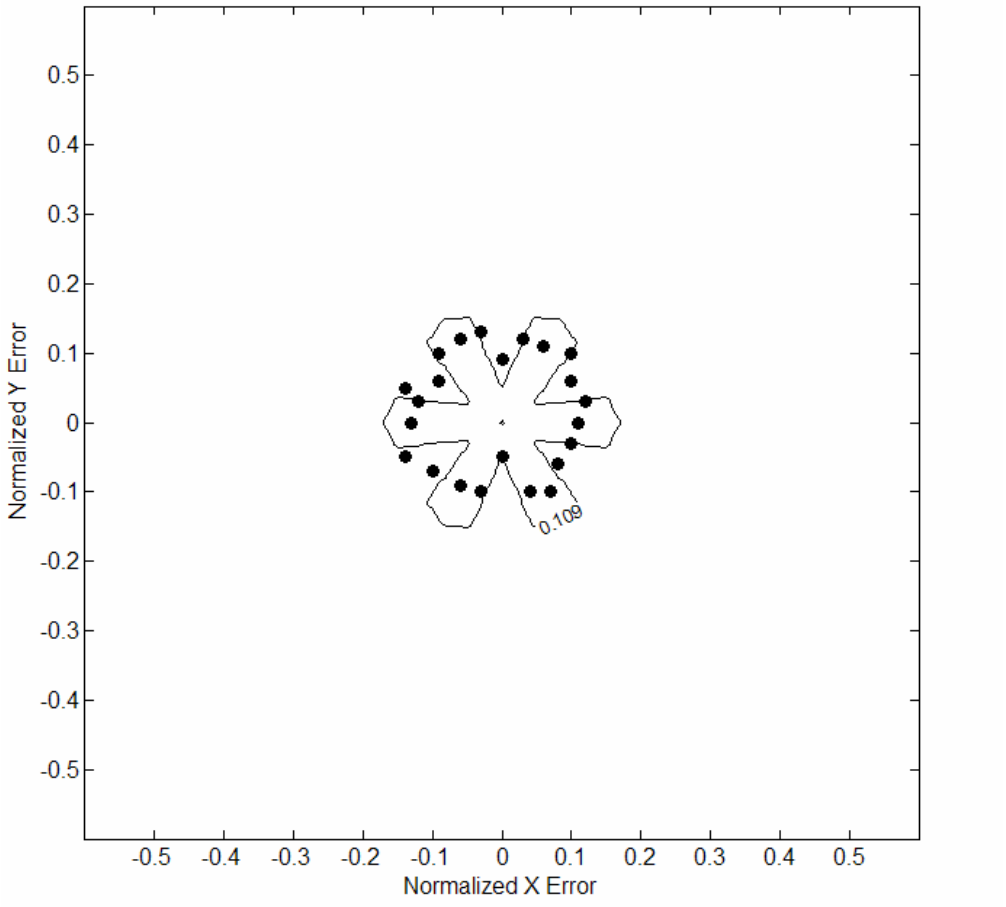

Figure 6.21 Predicted and measured boundary limits for 1018 steel round part with .200" tall 1" dia. head, boundaries for $\mu_s > 0.109$

Testing was difficult for the .200" tall round part, since even when self-alignment did occur it was not as strong as in previous tests. The results match the predicted boundaries in magnitude, although not as well in shape as in the previous tests. This discrepancy can be attributed to difficulty in testing; since the self-alignment effect was so weak in this case it was difficult to determine where the part transitioned from self-alignment to no self-alignment.

These model results would indicate to a designer that self-alignment, if present, would be very weak. This is exactly what was observed, suggesting that a part of this particular geometry would need other means to orient it before presentation to the gripper. Earlier tests with parts of taller head geometry were expected to have good self-aligning qualities, and this effect was observed in the experiment. Parts which were predicted to possess strong self-aligning qualities would require very little outside effort to reach their desired orientation in the gripper.

6.4 Impact on the Automation System Design

The gripper analysis has been validated and shown to reasonably predict the self-aligning qualities of the gripping system developed. Since the tests conducted used parts similar in geometry to those encountered by the automation system developed in Chapter 4, a review of the automation system design should be performed at this time.

From the model results, it was observed that the self-aligning qualities of the gripper are sensitive to coefficient of friction and part geometry. From the design statement of the automation system, it is known that the system will be expected to

process a wide variety of part shapes and part materials. While certain parts encountered by the system may posses strong self-aligning qualities, others may not. Also, over time, the coefficient of friction between the gripper and part may increase from the ideal controlled conditions encountered during experimental testing. For these reasons, the system should not rely on self-alignment exclusively to guarantee placement tolerances will be held.

It should be assumed that at least some parts grasped will retain their angular errors during the pick and place process. To alleviate this problem, the placement tolerance was relaxed as far as possible. This was accomplished by increasing the hole oversize amount to the maximum amount that would still allow the gripper fingers to fit between adjacent parts in each tray layout. The final hole oversize was increased from 1/8" (.125") beyond the bolt shank diameter to .140" beyond the bolt shank diameter. This increase is small, but could mean the difference between a failed and successful placement. Also, the holes on the ceramic heating plate and aluminum post processing rack were chamfered, to enable any slightly off center parts to enter their destination holes.

If the system was expected to handle a small variety of parts which exhibited very strong self-aligning qualities, and coefficient of friction was expected to remain low, a much tighter placement tolerance could be enforced. This is the benefit of the grasping model, it allows the designer to predict what design features will be necessary to achieve proper functionality early in the design process, when changes are still easy to make.

6.5 Summary

This chapter presented the results of the grasping analysis formulated in Chapter 6. The grasping model was run iteratively to assemble a solution space of part angular errors for which the gripper was expected to be able to self-align parts. These errors were visualized by plotting them on a horizontal reference plane a fixed distance from the part. A reference axis through the part's centerline was used to intersect the reference plane, with each combination of angular part errors yielding a location on the reference plane.

Initial model results of model iteration showed an error boundary with a six sided pattern of symmetry. The size of the predicted boundary was found to be heavily dependent on μ_s, and ranged from a very fault tolerant shape to one which predicted no self-alignment even for small errors. The fault tolerance of the gripper was found to be independent of the grasping force, as was concluded earlier from the two dimensional model. The six sided shape of the boundary was found to be a product of the three jaw nature of the gripper. Grasping hex headed parts as well as round parts produced the six lobed fault tolerance region, although the lobe shapes changed with part style.

Part height was varied to examine its effect on model output. As expected, shorter parts were predicted to be less tolerant to part orientation errors in the gripper. Short headed parts were predicted to have almost no self-alignment qualities, while taller parts were expected to self align quite well.

The model was validated by using test parts machined from 1018 Carbon Steel, and the gripper-to-part coefficient of friction was experimentally determined using a three axis dynamometer. A laser mounted in the test piece was used to collect self-alignment data during tests with the prototyped gripping system.

With knowledge of coefficient of friction and with test data collected, the model was compared to experiment for a number of part configurations. In all cases the model predicted the gripper performance quite well. The case of a part with very low height yielded little self-alignment and thus difficulty in testing. However, the model predicted this behavior.

The self-alignment model was shown to be a reliable means of predicting and quantifying gripper performance, and was validated for a number of part geometries. The model is shown to be a useful tool for the design engineer in the early planning stages of a robotic part handling system.

CHAPTER 7

AUTOMATION SYSTEM PROTOTYPE TESTING

Under supervision of CAMotion, the automation system developed in Chapter 4 was prototyped and assembled by the author. The initial phases of assembly, wiring, and programming were performed in CAMotion's facility. After programming and testing, the system was transported to Georgia Tech for interfacing with the thread rolling machine. Overall, the system performed very well, and the gripping system proved to be quite reliable. This chapter will briefly discuss the results.

7.1 Overall System

System assembly went smoothly, and the design for assembly approach developed in Chapter 4 enabled "zeroing" the heating and post processing areas easily under the Y axis. The assembled system with guarding can be seen in Figure 7.1. The layout was found to be ergonomically easy to use, and the guarding scheme enables adequate access for machine setup.

Figure 7.1 Assembled automation system

Figure 7.2 shows the assembled heating subframe, and Figure 7.3 shows the assembled tray drive system. The heating subframe's ceramic plates performed quite well and proved to be resilient to damage, despite the brittle nature of the ceramic material. The trapezoidal screw heating table height adjustment was also shown to be a valuable addition to the system. The ceramic plates in the heating area proved to be prone to impact damage, due to the brittle nature of ceramic materials. Future plans are to machine the same plate design with PEEK plastic, which has acceptable temperature resistance coupled with higher impact strength than ceramic materials.

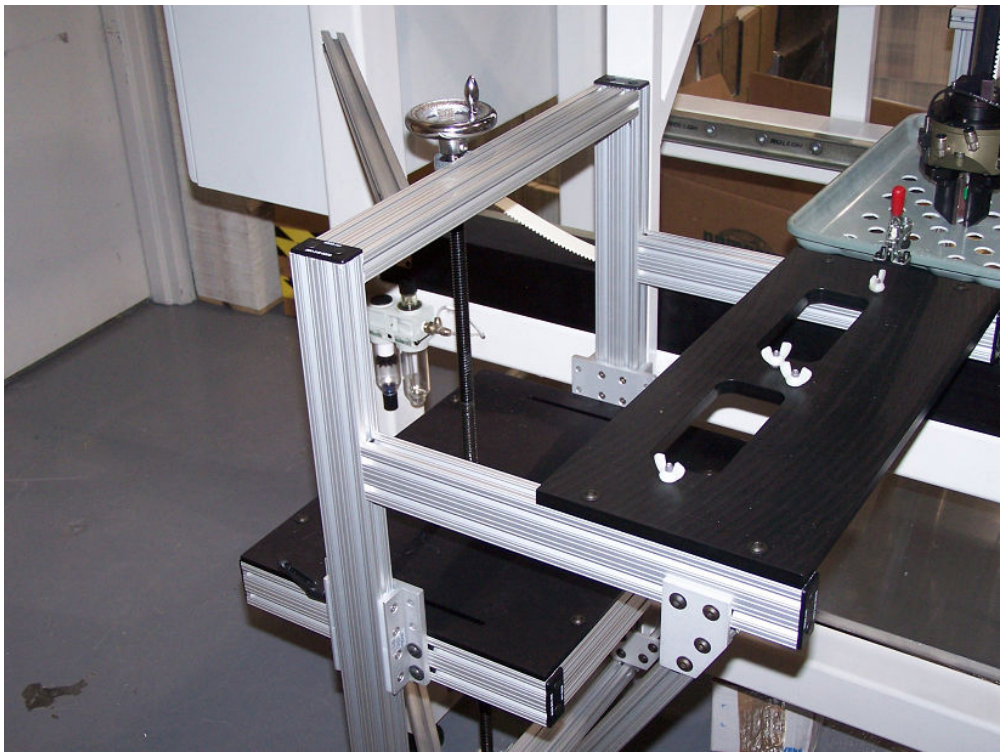

Figure 7.2 Assembled heating area

Figure 7.3 Assembled tray drive system

The system's motions were programmed using CAMotion's CAMGUI programming interface, and made use of a state based system operation. Upon startup, the system has no knowledge of what transport tray locations contain parts. A proximity sensor on the gripper senses whether a part is present upon grasping, the location is recorded as "empty" if a part is not present or if a part is removed from the location. Likewise the system records the state of all points during each operation, locations are marked as "full", "heating", or "empty" based on the performed action. The program analyzes the overall state of the system and then plans its next motion in a main decision loop, allowing realtime motion planning. This results in a robust system which can accommodate any situation an operator might present the machine with.

7.2 System Tuning

As mentioned earlier, CAMotion's strength is in using intelligent motion control to achieve tight placement tolerances even in somewhat compliant structures. This is achieved by command shaping control algorithms, which remove frequency components in the planned trajectory which would serve to excite the natural frequency of the structure.

Without command shaping, the robot was run at moderate speeds with success. However, increasing accelerations and velocities beyond 50% of the robot's maximum began to induce oscillations in the end effector and main frame structure. This not only reduces the longevity of the system, but makes placing long parts difficult due to the oscillation in the part relative to the placement point.

To alleviate this, command shaping was enabled on the horizontal and vertical axes which drive the end effector. The horizontal axis was tuned to remove frequencies which would excite the main welded frame structure. These frequencies were found by attaching an accelerometer to the frame and inducing vibration by running the machine. The vertical axis was tuned to remove oscillations induced by the compliance in the vertical axis extrusion. These frequencies were found by extending the axis to a typical height and attaching an accelerometer to the end effector. The frequencies used are summarized in Table 7.1.

Table 7.1 Command shaping frequencies employed

	Frequency 1	Frequency 2
Y axis (tuned to welded frame structure)	4.5 Hz	8.5Hz
Z axis (tuned to z axis extrusion)	8Hz	9Hz

Command shaping smoothed the motions considerably, and enabled the robot to be run at full speed even with the longest parts dictated by the design requirements. These speeds and tolerances would not have been possible using traditional PID motion control, as was initially attempted.

7.3 Cycle Times

Analysis in Chapter 4 predicted a worst case cycle time of 9.7 seconds, and a best case cycle time of 6.1 seconds. The goal was that the total cycle, including rolling, not exceed 10 seconds. At the time of testing, the system was found to be slightly slower than predicted. The best case cycle time meets the 10 second goal, while the worst case cycle time is approximately 14 seconds. It is planned to modify the programming so the heater's start time is coordinated with the thread roller's motions, so the automation always arrives "just in time" to insert a part in the roller. This will ensure the best case scenario every cycle, thus satisfying the design goals.

The discrepancy in cycle time prediction was a product of the method for motion planning in CAMotion's controls. The analysis assumed straight line, constant acceleration and deceleration moves, while in reality the system takes into account far more constraints when planning a trajectory. Also, command shaping added another level of motion complexity not accounted for in the initial analysis. Despite the discrepancy, the initial analysis reasonably predicted the machine's capabilities, and was a worthwhile design exercise for proving an initial concept.

7.4 Gripping System

The prototyped gripping system performed exceptionally well. The semicircular face design produced a stable grasp on any head style fastener, and the four sets of tooling accommodated the range of sizes dictated by the design guidelines. Hex headed parts were stable in grasp quality regardless of whether each gripping face contacted one

or two tips of the hex feature. 12 point and spline headed fasteners were a natural fit for the semicircular design.

The A-2 gripping faces also performed quite well. Concerns about the faces incurring damage from the corners of hex shaped parts were disproved during testing. After 10,000+ cycles with hex headed parts, the gripping faces showed no noticeable signs of wear or surface degradation. Also, the faces were very resilient to end effector collision, which occurred occasionally during initial programming. Even when a grasped part was forced along the faces under full grasping force, no noticeable gouging or surface marring was observed.

7.5 Summary

This chapter briefly presented the results of the automation system prototype testing. The system was found to perform acceptably and met the design goals planned in Chapter 4. Command shaping control algorithms were used to enable fast system performance and smooth operation. The gripping system was also tested extensively, and produced a reliable grasp on all styles and sizes of fasteners. The gripping faces were found to be durable and resilient to damage.

CHAPTER 8

CONCLUSIONS AND RECOMMENDATIONS

This thesis followed the design process of an automatic part loading and unloading system for a thread rolling machine used in aerospace fastener production from initial concept to prototyping and testing. The design process began with a comprehensive review of the production methods and a desire to develop a workcell concept. This knowledge was used to create a workcell automation plan which was used as the basis for the automation system's development. Within the automation system, a universal gripping system was developed which accommodates grasping of a variety of fastener styles and sizes, and the development of the gripping system led to the development of a model which predicts gripper error tolerance.

8.1 Conclusions

The following topics were covered specifically in the course of this thesis:

- Through discrete time analysis and consideration of design goals, a highly automated workcell was ruled out in favor of a simpler approach for the problem at hand. The simpler approach entails manual operator transport of batches of parts between automation systems. This methodology results in a workcell which is more flexible and conducive to producing small batches of specialized parts.

- A transport tray system was implemented as a method for moving parts between machines equipped with part loading/unloading automation. The transport tray concept was shown to be a viable method of quickly presenting a batch of parts to an automatic loading system, as well as a safe method of transport which eliminates part-to-part contact.
- An automatic part loading and unloading system for a thread rolling machine was designed and prototyped in conjunction with CAMotion, Inc. The robot selected was an adaptation of CAMotion's CRP-1000 pick and place robot. The machine was found to hold adequate placement tolerances to satisfy the peg-in-hole problem of inserting bolts into oversized destination holes.
- A universal fastener gripping system was developed, based on a semicircular gripping face profile which utilizes A-2 tool steel gripping faces. The gripping system was found to reliably grasp a wide variety of fastener styles and sizes, and the gripping faces were found to be resilient to wear after 10,000+ cycles.
- A grasping model was developed to predict what types of errors the proposed gripper can tolerate. The model was designed to predict if the gripper is capable of self-aligning a workpiece with a certain combination of angular errors in its jaws.
- The grasping model was verified by testing the prototyped gripping system with a test workpiece. The grasping model was found to predict the bounds on error tolerance well under a variety of conditions.

8.2 Recommendations

This research presents many areas for future work, both academic and practical. The practical aspect of the system involves manufacturing a large quantity of transport trays to implement the reduced automation workcell concept. However prototyping the trays was expensive, partly due to the small production run manufactured. Traditional machining methods were used, however other alternative methods could be investigated such as water jet cutting. The possibility of machining more than one tray at a time should be considered. The trays can be stacked atop one another and possibly be machined or water jet cut in batches. Lastly, the two steel locating features added cost to each tray. It may be possible to use the trays by solely locating on the tray material.

In regards to the automation aspect of this thesis, initial tests showed the system to perform satisfactorily, and all design goals were achieved. However, more testing time is recommended for the system, as any long term mechanical issues may not emerge during prototype testing. This is also true for the gripping system, while initial wear characteristics were acceptable, a longer term test period would be useful in evaluating the design and material choices.

Academically, the gripping self alignment model presents areas for further work. Only one gripper-workpiece material pair was tested for the model verification. Material pairs with varying coefficients of friction should be tested to verify the model more completely. Also, a greater variety of part head shapes should also be tested for yet further verification.

The grasping model also presents room for expansion. The model as presented only allows for semicircular grasping faces as developed for the gripper in the automation

system. The analysis is developed fairly specifically around this geometry. A more robust method of specifying gripper geometry as a model input could make the analysis more useful to other applications. Also, the model currently allows only for a three jaw gripper. The techniques described could be adapted to more typical two jaw designs.

Another area of the grasping model which merits further investigation is the case of multiple points of contact on each gripping face. The current model only allows for one point of contact on each of the three faces, limited by the number of equations available to solve for unknown forces. More points of contact would require a more complex model, possibly incorporating stiffness analysis to find forces at each point of contact.

The additions described could potentially make the grasping model very general, in which case the gripper geometry and part geometry could be easily entered into the system. These additions could make the model adaptable to nearly any grasping application, and thus very useful in a variety of applications.

APPENDIX A

Here the derivation of the 2-D self alignment model is described in further detail. It was found from a moment sum that to constrain part motion, that A.1 must be satisfied. Simple trigonometry is now used to solve for the relation of moment lengths l_x and l_y, shown in A.2

$$\begin{aligned} \sum M_o &= F_f l_y - F_n l_x \\ Ff &= \mu F_n \\ \therefore l_x &= \mu l_y \end{aligned} \tag{A.1}$$

$$l_x = \tan\left[\tan^{-1}\left(\frac{h}{d}\right) - \alpha\right] l_y \tag{A.2}$$

The relations for l_x and l_y are substituted into the result from A.1, yielding A.3. Cancelling l_y and using a trigonometric relation to eliminate the subtractive tangent angle, then solving for the desired result α results in A.4.

$$\tan\left[\tan^{-1}\left(\frac{h}{d}\right) - \alpha\right] l_y = \mu l_y \tag{A.3}$$

$$\alpha_{\max} = \tan^{-1}\left[\frac{\frac{h}{d} - \mu}{\frac{\mu h}{d} + 1}\right] \tag{A.4}$$

APPENDIX B

These calculations develop an equation to calculate end effector movement times assuming constant acceleration and deceleration. A maximum velocity v_{max} is also assumed. The motion undergoes an initial time of constant acceleration until velocity v_{max} is reached, followed by a period of constant deceleration. t_{accel} represents the time accelerating and, t_{vmax} represents the time spent traveling at maximum velocity.

The total time for the motion (with equal acceleration and deceleration) is given by equation B.1. The acceleration and deceleration times are easily found by B.2.

$$t_{move} = 2t_{accel} + t_{v\max} \tag{B.1}$$

$$t_{accel} = \frac{v_{\max}}{a_{move}} \tag{B.2}$$

If the distance required by the move is d_{move}, the distance is given by B.3. Using the relation for t_{accel} from B.2 in B.3 yields t_{vmax}.

$$d_{move} = \frac{1}{2} a_{move} t_{accel}^{\ 2} + \frac{1}{2} a_{move} t_{accel}^{\ 2} + v_{\max} t_{v\max} \tag{B.3}$$

$$t_{v\max} = \frac{d_{move}}{v_{\max}} - \frac{v_{\max}}{a_{move}} \tag{B.4}$$

Thus the total time for the move is given by substitution into B.1.

$$t_{move} = \frac{v_{\max}}{a} + \frac{d}{v_{\max}} \tag{B.5}$$

REFERENCES

Akella, S., and Mason, M. T. "Parts orienting by push-aligning." Nagoya, Japan, 414-20.

Alcombright, D. S., and Bedwell, W. T. (1999). "Fastener Delivery System." *Proceedings of the Aerospace Automated Fastening Conference and Exposition 1999*, 125-128.

Anon. (1987). "THREAD ROLLING." *Manufacturing Engineering*, 99(1), 51-56.

Asada, H., and By, A. B. (1985). "Kinematic analysis of workpart fixturing for flexible assembly with automatically reconfigurable fixtures." *IEEE Journal of Robotics and Automation*, RA-1(2), 86-94.

Bicchi, A., and Kumar, V. "Robotic grasping and contact: a review." San Francisco, CA, USA, 348-353.

Boivin, E., Sharf, I., and Doyon, M. "Optimum grasp of planar and revolute objects with gripper geometry constraints." New Orleans, LA, USA, 326-32.

Boothroyd, G. (1992). *Assembly Automation and Product Design*, Marcel Dekker, New York.

Bornes, P., and LeCann, R. P. (2000). "The Modular Casette Fastener and Delivery System." *Proceedings of the SAE Aerospace Automated Fastening Conference and Exposition 2000*, 127-131.

Bothwell, J. M. (1989). "Automation - the 'real world'." *Fastener Age*, 3(5), 8.

Cutkosky, M. R., and Wright, P. K. (1986). "Friction, stability and the design of robotic fingers." *International Journal of Robotics Research*, 5(4), 20-37.

Endres, T. E. (1998). "Fastener Feeding Systems." *1998 SAE Aerospace Automated Fastening Conference & Exposition, Long Beach, CA, Proceedings*, 3-9.

Eranov, G. G., and Obukhova, L. N. (1986). "INTRODUCTION OF A FLEXIBLE PRODUCTION SYSTEM OF MACHINING OF SPECIAL FASTENERS." *Chemical and Petroleum Engineering (English translation of Khimicheskoe i Neftyanoe Mashinostroeni*, 22(9-10), 517-520.

Ginsberg, J. H. (1998). *Advanced Engineering Dynamics, Second Edition*, Cambridge University Press, New York.

Harada, K., and Kaneko, M. (2002). "A sufficient condition for manipulation of envelope family." *IEEE Transactions on Robotics and Automation*, 18(4), 597-607.

Kalpakjian, S., and Schmid, S. R. (2003). *Manufacturing Processes for Engineering Materials*, Pearson Education, Upper Saddle River.

Kopka, T., and Schwer, A. (2003). "Thread rolling on the night shift." *Wire Industry*, 70(830), 138-139.

Lee, S. H., and Cutkosky, M. R. (1991). "Fixture planning with friction." *Journal of Engineering for Industry, Transactions of the ASME*, 113(3), 320-327.

Mason, M. T. (1986). "Mechanics and planning of manipulator pushing operations." *International Journal of Robotics Research*, 5(3), 53-71.

Mirtich, B., and Canny, J. "Easily computable optimum grasps in 2-D and 3-D." San Diego, CA, USA, 739-747.

Montana, D. J. (1992). "Contact stability for two-fingered grasps." *IEEE Transactions on Robotics and Automation*, 8(4), 421-30.

Morales, A., Sanz, P. J., del Pobil, A. P., and Fagg, A. H. (2006). "Vision-based three-finger grasp synthesis constrained by hand geometry." *Robotics and Autonomous Systems*, 54(6), 496-512.

Saliger, F. (2006). "Innovations for thread rolling." *Wire*, 56(1), 16-17.

Stancik, B., and Boad, C. (1999). "Flexibility in Fastener Feeding." *Proceedings of the Aerospace Automated Fastening Conference and Exposition 1999*, 147-151.

Tudbury, C. A. (1960). *Basics of Induction Heating*, Pillar Induction, New Rochelle, New York.

Vanderspek, P. G. (1993). *Planning for Factory Automation*, McGraw-Hill, New York.

Wiesenfeld, D. (1998). "Thread and form rolling - planetary (rotary) versus flat die machines." *Wire Industry*, 65(776), 585-587.

Wiesenfeld, Y. (2000). "Trends & developments in thread rolling machines and tooling." *Wire Industry*, 67(802), 697.

Zhang, M. T., and Goldberg, K. (2002). "Gripper point contacts for part alignment." *IEEE Transactions on Robotics and Automation*, 18(6), 902-10.

Zhang, T., Cheung, L., and Goldberg, K. "Shape tolerance for robot gripper jaws." Maui, HI, 1782-1787.

Zhang, T., and Goldberg, K. "Design of robot gripper jaws based on trapezoidal modules." Seoul, 1065-1070.